Deciphering the role of EZH2 in the control of HIF2α signaling and its effects on cellular phenotypes in breast and lung cancer

Inaugural Dissertation
submitted to the Faculty of Medicine
in partial fulfillment of the requirements
for the PhD-Degree
of the Faculties of Veterinary Medicine and Medicine
of the Justus Liebig University Giessen

By
Salisa Kruijning
Of
Blaricum, Netherlands

Giessen 2026

From the Institute of Neuropathology
Director: Prof. Dr. med. Till Acker
of the Faculty of Medicine of the Justus Liebig University Giessen

Supervisor and First Reviewer:

Prof. Dr. med. Till Acker
Institute of Neuropathology
Justus Liebig University Giessen

Second reviewer:

Prof. Dr. Alexander Brehm
Institute of Molecular Biology and Tumor Research
Marburg University

Committee Vice-Chair and Co-Supervisor:

Prof. Dr. Gergana Dobreva
Medical Faculty Mannheim
Heidelberg University

Committee Chair:

Prof. Dr. Martin Diener
Institut für Veterinär-Physiologie und -Biochemie
Justus Liebig University Giessen

Date of Doctoral Defense: February 18, 2026

Ehrenwörtliche Erklärung

Hiermit erkläre ich, dass ich die vorliegende Arbeit selbstständig und ohne unzulässige Hilfe oder Benutzung anderer als der angegebenen Hilfsmitel angefertigt habe. Alle Textstellen, die wörtlich oder sinngemäß aus veröffentlichten oder nichtveröffentlichten Schriften entnommen sind, und alle Angaben, die auf mündlichen Auskünften beruhen, sind als solche kenntlich gemacht. Bei den von mir durchgeführten und in der Dissertation erwähnten Untersuchungen habe ich die Grundsätze guter wissenschaftlicher Praxis, wie sie in der „Satzung der Justus-Liebig-Universität Gießen zur Sicherung guter wissenschaftlicher Praxis“ niedergelegt sind, eingehalten sowie ethische, datenschutzrechtliche und tierschutzrechtliche Grundsätze befolgt. Ich versichere, dass Dritte von mir weder unmittelbar noch mitelbar geldwerte Leistungen für Arbeiten erhalten haben, die im Zusammenhang mit dem Inhalt der vorgelegten Dissertation stehen, und dass die vorgelegte Arbeit weder im Inland noch im Ausland in gleicher oder ähnlicher Form einer anderen Prüfungsbehörde zum Zweck einer Promotion oder eines anderen Prüfungsverfahrens vorgelegt wurde. Alles aus anderen Quellen und von anderen Personen übernommene Material, das in der Arbeit verwendet wurde oder auf welches direkt Bezug genommen wird, wurde als solches kenntlich gemacht. Insbesondere wurden alle Personen genannt, die direkt und indirekt an der Entstehung der vorliegenden Arbeit beteiligt waren. Mit der Überprüfung meiner Arbeit durch eine Plagiatserkennungssoftware bzw. ein internetbasiertes Softwareprogramm erkläre ich mich einverstanden.

Giessen,
Place, Date

Signature (Salisa Kruijning)

Summary

Hypoxia is a hallmark of solid tumors and a critical driver of cancer progression, largely mediated by hypoxia-inducible factors (HIFs). While HIF1α has been extensively studied, the transcriptional regulation of HIF2α, encoded by the endothelial PAS domain protein 1 (EPAS1) gene, remains less well understood. Enhancer of zeste homolog 2 (EZH2), the catalytic subunit of polycomb repressive complex 2 (PRC2), is a known epigenetic regulator with canonical roles in gene repression via H3K27 tri-methylation and emerging non-canonical functions, including transcriptional activation. The interplay between EZH2 and HIF signaling, particularly regarding HIF2α, is largely unexplored.

In this study, the role of EZH2 as a potential regulator of HIF2α in breast and lung cancer model systems was investigated. EZH2 knockdown decreased HIF2α protein under hypoxic conditions and EPAS1 mRNA levels under normoxic and hypoxic conditions in MDA-MB-231 and PC-9 cell lines. Restoration of EZH2 rescued EPAS1 expression. Mechanistic studies revealed that this regulation occurs independently of PRC2, EZH2's methyltransferase activity, EZH1, Notch1 signaling, and transcriptional elongation. Chromatin immunoprecipitation demonstrated direct binding of EZH2 to a region approximately 1.7 kb downstream of the EPAS1 transcription start site, without enrichment of H3K27me3, supporting a non-canonical transcriptional activator function for EZH2. These findings indicate that EZH2 directly maintains EPAS1 transcription independent of chromatin repression and contributes to sustaining transcriptional activity within a globally repressive hypoxic environment.

Functionally, EZH2 depletion impaired the expression of HIF2α target genes, including GLUT1 and PGK1, and reduced invasion capacity in MDA-MB-231 cells under hypoxia. In PC-9 cells, EZH2 knockdown decreased proliferation, which was partially rescued by transient HIF2α restoration, and anchorage-independent growth. These findings indicate that EZH2 promotes tumorigenicity at least in part through HIF2α. Clinical analyses revealed that high EZH2 and EPAS1 expression correlate with poor prognosis in breast cancer patients, underscoring the potential clinical relevance of this regulatory axis.

Overall, this study establishes EZH2 as a novel non-canonical transcriptional activator of EPAS1, linking an epigenetic regulator to hypoxia signaling. These findings extend

our understanding of EZH2 beyond its canonical repressive role and suggest that the EZH2-HIF2α regulatory axis may contribute to malignant phenotypes such as proliferation and invasion under hypoxic conditions. Future studies utilizing RNA-seq, *in vivo* models, and pharmacological inhibitors targeting EZH2 and HIF2α could provide further insight into the mechanistic and therapeutic potential of this regulatory pathway in cancer.

Zusammenfassung

Hypoxie ist ein Kennzeichen solider Tumoren und ein entscheidender Faktor für das Fortschreiten von Krebserkrankungen, der weitgehend durch Hypoxie-induzierbare Faktoren (HIFs) vermittelt wird. Während HIF1α bereits umfassend untersucht wurde, ist die Transkriptionsregulation von HIF2α, das vom Endothelial PAS Domain Protein 1 (EPAS1)-Gen kodiert wird, noch weniger gut verstanden. Enhancer of zeste homolog 2 (EZH2), die katalytische Untereinheit des Polycomb-Repressivkomplexes 2 (PRC2), ist ein bekannter epigenetischer Regulator mit kanonischen Funktionen bei der Genrepression über H3K27-Tri-Methylierung und neuen nicht-kanonischen Funktionen, einschließlich der Transkriptionsaktivierung. Die Wechselwirkung zwischen EZH2 und HIF-Signalwegen, insbesondere in Bezug auf HIF2α, ist weitgehend unerforscht.

In dieser Arbeit wurde die Rolle von EZH2 als potenzieller Regulator von HIF2α in Brust- und Lungenkrebs-Modellsystemen untersucht. Der Knockdown von EZH2 verringerte das HIF2α-Protein unter hypoxischen Bedingungen und die EPAS1-mRNA-Spiegel unter normoxischen und hypoxischen Bedingungen in den Zelllinien MDA-MB-231 und PC-9. Durch eine Reaktivierung von EZH2 konnte die EPAS1-Expression wieder zurückgewonnen werden. Mechanistische Studien zeigten, dass diese Regulation unabhängig von PRC2, der Methyltransferaseaktivität von EZH2, EZH1, Notch1-Signalübertragung und Transkriptionselongation erfolgt. Chromatin-Immunpräzipitation zeigte eine direkte Bindung von EZH2 an eine Region etwa 1,7 kb stromabwärts der EPAS1-Transkriptionsstartstelle ohne Anreicherung von H3K27me3, was eine nicht-kanonische Transkriptionsaktivatorfunktion für EZH2 unterstützt. Diese Ergebnisse deuten darauf hin, dass EZH2 die EPAS1-Transkription unabhängig von der Chromatin-Repression direkt kontrolliert und somit dazu beiträgt, die Transkriptionsaktivität in einer insgesamt repressiven hypoxischen Umgebung aufrechtzuerhalten.

Funktionell beeinträchtigte die EZH2-Depletion die Expression von HIF2α-Zielgenen, darunter GLUT1 und PGK1, und reduzierte die Invasionsfähigkeit in MDA-MB-231-Zellen unter Hypoxie. In PC-9-Zellen verringerte der EZH2-Knockdown die Proliferation, die durch eine vorübergehende Wiederherstellung von HIF2α teilweise wiederhergestellt wurde, sowie das anchorage-unabhängige Wachstum. Diese

Ergebnisse deuten darauf hin, dass EZH2 zumindest teilweise über HIF2α zur Tumorigenität beiträgt. Klinische Analysen zeigten, dass eine hohe EZH2- und EPAS1-Expression mit einer schlechten Prognose bei Brustkrebspatientinnen korreliert, was die potenzielle klinische Relevanz dieser regulatorischen Achse unterstreicht.

Insgesamt etabliert diese Arbeit EZH2 als einen neuartigen nicht-kanonischen Transkriptionsaktivator von EPAS1, der einen epigenetischen Regulator mit der Hypoxiesignalgebung verbindet. Diese Ergebnisse erweitern unser Verständnis von EZH2 über seine kanonischen repressiven Funktionen hinaus und legen nahe, dass die EZH2-HIF2α-Regulationsachse unter hypoxischen Bedingungen zu malignen Phänotypen wie Proliferation und Invasion beitragen könnte. Zukünftige Studien unter Verwendung von RNA-Seq, In-vivo-Modellen und pharmakologischen Inhibitoren, die auf EZH2 und HIF2α abzielen, könnten weitere Einblicke in das mechanistische und therapeutische Potenzial dieses Regulationsweges bei Krebs liefern.

List of Figures

1. Introduction

2. Results

3. Discussion

List of Tables

1. Introduction

4. Materials and methods

Abbreviations

ACTB	actin beta
AR	androgen receptor
BAM	β-addition motif
bHLH-PAS	basic helix-loop-helix-PER/ARNT/SIM
BM	brain metastasis
CD	cluster of differentiation
CHIP	carboxyl terminus of Hsc70-interaction protein
ChIP-qPCR	chromatin immunoprecipitation followed by quantitative polymerase chain reaction
ChIP-seq	chromatin immunoprecipitation followed by sequencing
DAPI	4′,6-diamidino-2-phenylindole
DNMT	DNA-methyltransferase
E2F1	E2F transcription factor 1
EBD	EED-binding domain
EED	embryonic ectoderm development
EGFR	epidermal growth factor
EMT	epithelial-mesenchymal transition
enChIP-MS	engineered DNA-binding molecule-mediated chromatin immunoprecipitation followed by mass spectrometry
EPAS1	endothelial PAS domain protein 1
ER	estrogen receptor
EZH	enhancer or zeste homolog
FDA	Food and Drug Administration
Fe2+	ferrous iron
FIH	factor inhibiting HIF
FOXK2	forkhead box K2
FoxM1	forkhead box M1
GFP	green fluorescent protein
GLUT1	glucose transporter type 1
H3K27me3	tri-methylated histone H3 lysine 27
H3K4me3	tri-methylated histone H3 lysine 4
HER2	human epidermal growth factor receptor 2
HES1	hairy and enhancer of split 1
HIF	hypoxia-inducible factor
HK2	hexokinase 2
HPRT1	hypoxanthine phosphoribosyltransferase 1
HRE	hypoxia response element
Hsp70	heat shock protein 70
JMJD	Jumonji domain
KDM	histone lysine demethylases
MCSS	motif connecting SANT1 and SANT2
mRNA	messenger RNA
MYT1	myelin transcription factor 1

NFκB	nuclear factor kappa B
NICD	Notch intracellular domain
Notch	neurogenic locus notch homolog protein
NSCLC	non-small lung cancer
OCT4	octamer-binding transcription factor 4
ODD	oxygen-dependent degradation
PGK1	phosphoglycerate kinase 1
PHD	prolyl hydroxylase domain
PI3K	phosphoinositide 3-kinase
POR	pLenti6-CMVp-ODD/FLuc-SV40p-Rluc
pO2	oxygen tension
PR	progesterone receptor
PRC	polycomb repressive complex
PROTAC	proteolysis-targeting chimera
RBBP	retinoblastoma-binding protein
RBPJ	immunoglobulin kappa J region
RNA Pol II	RNA polymerase II
RNA-seq	RNA sequencing
RPL30	ribosomal protein L30
RT-qPCR	quantitative reverse transcription polymerase chain reaction
S21	serine 21
SAH	S-adenosylhomocysteine
SAL	SET activation loop
SAM	S-adenosylmethionine
SBD	SANT1 binding domain
SCLC	small lung cancer
SET	su(var), enhancer of zeste, trithorax
sgRNA	single guide RNA
shRNA	short hairpin RNA
Siah2	siah E3 ubiquitin protein ligase 2
siRNA	small interfering RNA
SND1	tudor domain containing 1
SOX	SRY-box transcription factor
Src	proto-oncogene tyrosine-protein kinase Src
SRM	stimulation-responsive motif
STAT3	activator of transcription 3
SUZ12	suppressor of zeste 12 homolog
TAD	transactivation domain
TET	ten eleven translocation
TNBC	triple-negative breast cancer
UTR	untranslated region
VEGF	vascular endothelial growth factor
VHL	von Hippel-Lindau
Y244	tyrosine 244
Y696	tyrosine 696

Table of Contents

1. Introduction

1.1. Hypoxia

Oxygen sensing is an evolutionarily conserved fundamental process that enables cells and tissues to detect and adapt to changes in oxygen availability (1). Oxygen is required for cellular energy production by the mitochondria and survival of all aerobe organisms. Hence, oxygen sensing plays a crucial role in development, normal tissue homeostasis, and several pathological conditions, including cancer (2,3).

1.1.1. The hypoxic tumor microenvironment

Low oxygen availability, known as hypoxia, is a feature occurring in 50-60% of solid tumors (3). It is a driver for several hallmarks of cancer, including deregulating cellular metabolism and epigenetic reprogramming (4,5). As a result, hypoxia induces cancer progression and metastatic potential (3).

Hypoxia occurs as a consequence of an imbalance between oxygen delivery and consumption (6). This imbalance is caused by the rapid proliferation of cancer cells and a deficiency in vascularization (3,7). In response to hypoxia, energy conservation processes are activated in order to survive. These processes include a metabolism shift from oxidative phosphorylation to glycolysis, epigenetic changes that primarily contribute to gene repression, and messenger RNA (mRNA) translation inhibition (8–11). In addition, angiogenesis is induced to enhance oxygen supply to hypoxic regions (12). Many of these processes are regulated by an evolutionarily conserved, hypoxia-induced signaling pathway mediated by hypoxia-inducible factors (HIFs) (13).

1.1.2. The HIF signaling pathway and its regulation

HIFs are heterodimeric transcription factors composed of bHLH-PAS (basic helix-loop-helix-PER/ARNT/SIM) domains, including an unstable oxygen-dependent alpha subunit (HIF1α, HIF2α, HIF3α) or a stable beta subunit (HIF1β) (13). HIF1α was first described by Semenza and his colleagues in 1995 (14). HIF2α was discovered two years later by different groups and was therefore given different names, including endothelial PAS domain protein 1 (EPAS1), which is still the most commonly used name for the gene encoding HIF2α (15–17). Although three HIFα subunits exist, HIF1α

and HIF2α seem to be responsible for the majority of HIF-dependent effects on cancer progression (18).

HIFs are essentially regulated through posttranslational modifications. When oxygen levels are sufficient, from now on referred to as normoxia, proline residues in oxygen-dependent degradation (ODD) domains become hydroxylated by members of the prolyl hydroxylase domain 1-3 (PHD 1-3) family (19,20). Upon hydroxylation, a binding site for the von Hippel-Lindau (VHL) tumor suppressor protein is generated. VHL is part of a ubiquitin ligase complex and targets HIFα for ubiquitination-induced proteasomal degradation (21–23). PHDs are oxygen as well as α-ketoglutarate and ferrous iron (Fe^{2+}) dependent. Thus, the PHDs are unable to hydroxylate HIFα under hypoxic conditions, resulting in the stabilization of HIFs. Upon stabilization, HIFα dimerizes with HIF1β, followed by translocation to the nucleus where it binds and induces the expression of genes harboring hypoxia response elements (HREs) containing a conserved 5`-RCGTG-3` core sequence (2,13,14,18) (Fig. 1.1).

Although proline hydroxylation-dependent regulation is the most studied posttranslational regulatory mechanism of HIFα proteins, it is not the only one. An additional oxygen, α-ketoglutarate, and Fe^{2+}-dependent regulator of HIFα is factor inhibiting HIF (FIH) (13). Under normoxic conditions, FIH hydroxylates asparagine residues 803 and 851 in the C-terminus transactivation domain (TAD) of HIF1α and HIF2α, respectively (24,25). This blocks the association with the transcription factor and coactivator p300 required for the activation of the HIF target genes (26). However, HIF2α is less prone to FIH-mediated inactivation (27,28).

1.1.3. Regulatory and functional differences between HIF1α and HIF2α

Even though HIF1α and HIF2α are structurally similar and both sensitive to PHD-dependent regulation, they do differ in expression patterns and function. HIF1α is expressed in nearly all mammalian tissues (18). HIF2α expression is more restricted and was originally believed to be mainly expressed in endothelial cells (15), but in later years, many more tissue types were added to the list, indicating that HIF1α and HIF2α are often co-expressed (18,29).

Besides expression differences between tissues, HIF1α and HIF2α also respond differently to oxygen levels. HIF1α and HIF2α are both upregulated at 1% O_2. However,

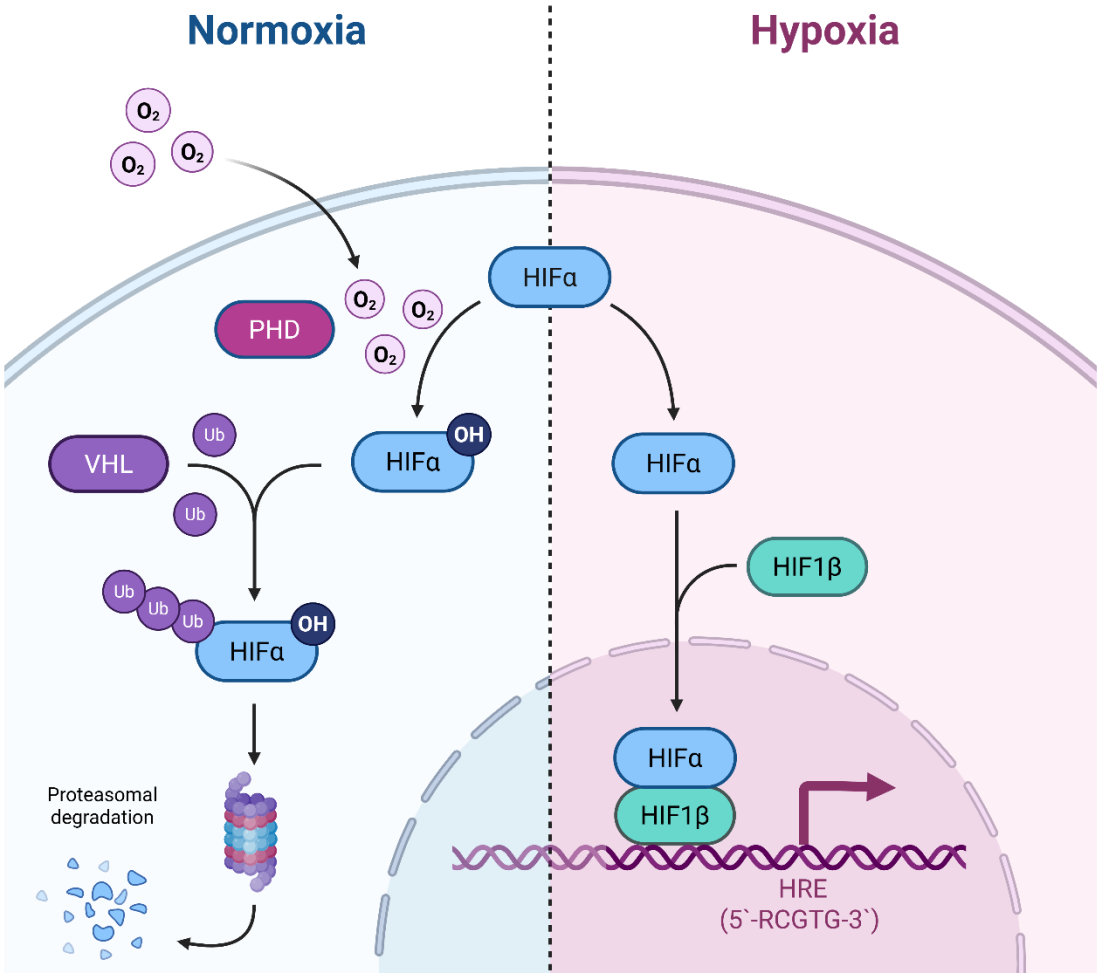

Figure 1.1: A schematic overview of the HIF signaling pathway.

Under normoxia, HIFα proteins are hydroxylated by PHD enzymes. Hydroxylated HIFα is recognized by the VHL tumor suppressor protein, leading to ubiquitination and proteasomal degradation. Under hypoxic conditions, PHDs are inactive, allowing HIFα to dimerize with HIF1β and translocate to the nucleus, where the complex binds hypoxia response elements (HREs) inducing gene expression. Created with BioRender.com.

from 2%, HIF1α protein levels were not detectable in glioma cells (30), while HIF2α levels were still detectable at 5% O_2 in neuroblastoma cells (31). They also show a distinct temporal pattern. HIF1α levels rise quickly under hypoxic conditions and remain detectable for a shorter amount of time, making it the acute responder (30–32). HIF2α levels rise a bit later, but remain stable for a longer period of time, making it a marker of chronic hypoxia (30–33). This phenomenon is also known as the HIF switch, which could be caused by several factors. One cause could be that HIF1α mRNA has a shorter halve-life and is thus less stable than HIF2α (33,34), which could cause the decrease in protein levels under hypoxia. In addition, two other E3 ubiquitin ligases besides VHL have been described to regulate HIFs and have been implicated as potent regulators of the HIF switch. HIF-associated factor (HAF) degrades HIF1α in an

oxygen-independent manner, while it induces HIF2α transactivation. Of note, HAF protein levels are decreased under acute hypoxia and rise under chronic hypoxia (35). The other E3 ubiquitin ligase complex is carboxyl terminus of Hsc70-interaction protein (CHIP), which, after recruitment by heat shock protein 70 (Hsp70), also degrades HIF1α but not HIF2α in an oxygen independent manner (36). More potential regulators of the HIF switch have been described, however, their role is less well defined (18,29,37). In addition, the protein levels of the key HIF-regulators PHD2 and PHD3 have been shown to be upregulated under hypoxic conditions (38,39). They affect HIFα levels even under hypoxia and act as protective negative feedback regulators of HIFs. Henze *et al*. found that PHD2 knockdown affected the stability of both HIF1α and HIF2α protein levels in glioblastoma cells upon 6 hours of hypoxia. In contrast, PHD3 knockdown partially stabilized HIF1α protein levels upon 24 hours of hypoxia, and no effect was found on HIF2α. When both PHD2 and PHD3 were knocked down, partial stabilization of both HIF1α and HIF2α was observed upon 24 hours of hypoxia, resulting in attenuation of the HIF switch (38). These results suggest a complex regulatory network of HIFα protein levels, in which the activities and levels of PHD2 and PHD3 act together with other factors and are themselves subject to regulation.

Besides differential expression, HIF1α and HIF2 also have functionally different roles. Even though they bind to the same consensus sequence and have many common target genes, they also have isoform specific target genes, involved in different processes. Interestingly, two independent papers showed that HIF1α binds mostly at the proximal promoter, whereas HIF2α binds mostly at the distal promoter, suggesting that HIF2α in many cases might function more as an enhancer than a core promoter-activating transcription factor (40,41).

1.1.4. The role of HIFs in cancer progression

HIF1α and/or HIF2α protein levels have been shown to be increased in many different cancer types including breast and lung cancer compared to healthy tissue based on immunohistochemistry analyses (42,43). In breast cancer, elevated HIF1α protein level or mRNA expression has been consistently associated with poor prognosis for a long time (42,44–46). HIF2α, while less studied, has been described as a potential negative prognostic marker as well, reflecting its role in regulating genes promoting tumor progression, angiogenesis, and metastatic potential (43,47–49). In lung cancer, HIF1α overexpression is associated with shorter overall and recurrence-free survival, serving

as a significant prognostic indicator (42,50,51). However, HIF2α is also considered a potential prognostic factor in lung cancer and, notably, only HIF2α overexpression has been correlated with poor clinical outcome in two independent studies (52,53). Given the prognostic value of HIFs, research has focused on developing drugs inhibiting HIFs. Three HIF targeting drugs have been approved by the Food and Drug Administration (FDA). However, only the HIF2α-specific inhibitor Belzutifan has been approved for cancer patients with VHL-related disease, such as renal cell carcinoma (54). The other two are not inhibitors, but HIFα stabilizers and are not approved for cancer treatment (55,56). This further supports the importance of HIFs, specifically HIF2α, in cancer progression. Nevertheless, its role in tumor progression must be viewed with caution, as there is genetic evidence of its tumor suppressor activity (57).

HIFs promote cancer progression through multiple mechanisms, influencing several hallmarks of cancer as illustrated in Figure 1.2.

Enabling replicative immortality: Normal cells undergo a limited number of cell divisions known as the “Hayflick limit” (58), while cancer cells overcome this control of cell proliferation. This is in part due to telomere maintenance that occurs by transcriptional activation of telomerase reverse transcriptase by HIF1α under hypoxia, resulting in cell immortalization (59).

Deregulating cellular metabolism: HIF1α regulates target genes that rapidly induce glycolytic enzymes and glucose transporters to boost glycolysis and lactate production (29,60). In contrast, HIF2α has a smaller effect on glucose metabolism than HIF1α, and broader effects on lipid and amino acid metabolism as well as energy homeostasis (29,61–63).

Inducing vascular remodeling: HIFs are central regulators of angiogenesis, controlling blood vessel formation, remodeling, and stabilization under hypoxia. HIF1α drives early vessel formation by inducing vascular endothelial growth factor (VEGF) and other pro-angiogenic factors, and supports vessel stabilization. HIF2α plays a key role in vessel maturation, strengthening endothelial junctions, and remodeling the extracellular matrix, while also activating VEGF (29,64). Both isoforms cooperate in extracellular matrix degradation to facilitate endothelial migration. Although partially compensatory, their distinct roles ensure the formation of a functional, stable

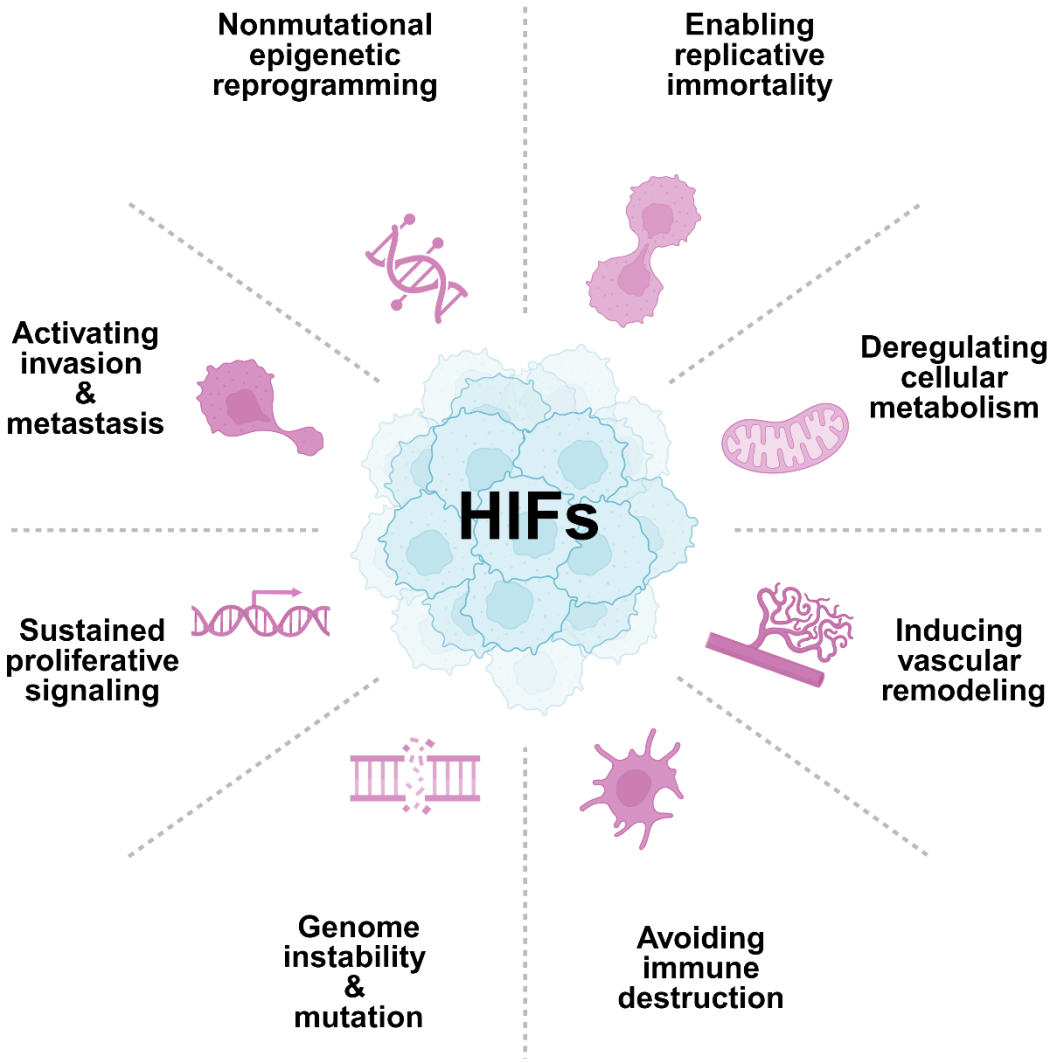

Figure 1.2: An overview of the roles of HIFs in the hallmarks of cancer.
Hypoxia inducible factors (HIFs) play an important role in cancer progression by affecting several hallmarks of cancer. See details in the text. Adapted from Hanahan *et al.* (5). Created with Biorender.com.

vasculature in tumors (29).

Avoiding immune destruction: Hypoxia and HIF signaling create a profoundly immunosuppressive tumor microenvironment that allows cancer cells to evade immune destruction. HIF1α regulates the expression of cluster of differentiation (CD) 39 and CD73, which generate extracellular adenosine that binds A2 receptors on T cells, suppressing receptor signaling and cytotoxic activity. HIF1α also drives CCL28 production, which recruits regulatory T cells, while simultaneously enabling tumor-associated macrophages and myeloid-derived suppressor cells to inhibit T cell proliferation and interferon-γ release in a HIF1α dependent manner. In addition, HIF

induced VEGF not only supports angiogenesis but also impairs dendritic cell function and increases PD-L1 expression, reducing T cell–mediated killing (2).

Genome instability & mutation: Hypoxia and HIF signaling can reduce DNA repair capacity by downregulating mismatch repair and homologous recombination genes. This fosters an accumulation of mutations and chromosomal aberrations. HIFs also promote survival of genetically unstable cells by regulating cell cycle checkpoints and DNA repair (65).

Sustaining proliferative signaling: HIFs upregulate growth factors, which stimulate tumor cell proliferation. HIF1α is also phosphorylated by mitogen-activated protein kinase, enhancing transcription of target genes that support cell growth. Under hypoxia, HIFs promote VEGF expression, stimulating endothelial cell proliferation. In parallel, loss of tumor suppressors like PTEN removes inhibition of the phosphoinositide 3-kinase (PI3K)/Akt pathway, further enhancing HIF activity and proliferative responses (64–66).

Activating invasion & metastasis: HIF1α predominantly promotes extracellular matrix remodeling by inducing PLOD2 and lysyl oxidase family members, leading to collagen cross-linking, which facilitates local invasion and metastasis (2). In parallel, HIF2α regulates genes that sustain the metastatic phenotype, including those involved in VEGF signaling and stemness (64)**,** thereby complementing HIF1α in supporting vascular permeability, intravasation, and colonization of distant organs. Epithelial-mesenchymal transition (EMT) is another key step for metastasis formation, during which epithelial cells lose their rigid structure and cell-cell contacts and acquire a motile, mesenchymal phenotype. HIFs contribute to EMT by regulating target genes that control cytoskeletal remodeling, cell adhesion, and remodeling of the extracellular matrix (67).

Nonmutational epigenetic reprogramming: This hallmark is one of the last ones added to the list by Hanahan *et al.* in 2022 and plays an important role in cancer progression (5). HIFs not only regulate transcriptional responses to hypoxia but also modulate the expression and activity of epigenetic regulators, linking oxygen sensing to chromatin remodeling. For example, HIF1α and HIF2α can upregulate ten eleven translocation 1 (TET1), a 5-methylcytosine hydroxylase that initiates DNA demethylation, Jumonji domain (JMJD) lysine demethylases (KDMs), and DNA-methyltransferases (DNMTs), resulting in alteration of DNA and histone methylation

patterns at specific genomic loci (68). In parallel, HIFs drive changes in metabolite levels, including α-ketoglutarate (69,70), which is required for JMJD lysine demethylase and TET function. Thus, by influencing the activity of histone and DNA-modifying enzymes, HIFs link cellular metabolism to chromatin state (68).

Conversely, epigenetic mechanisms also contribute to the regulation of HIFα levels and to the transcriptional regulatory functions of HIFs. DNA methylation of promoters, such as VHL, increases the transcriptional activator function of HIF1α and promotes HIF1α target gene activation (71). Also, lysine-specific demethylase 1 can stabilize HIF1α by preventing proteasomal degradation (72). Non-coding RNAs, as well as microRNAs, can also modulate HIFα stability through interactions with epigenetic regulators (73). In addition, DNMT3a has been shown to silence EPAS1 by methylating the promoter and thus transcriptionally regulating EPAS1 levels (74).

Hypoxia-induced transcriptome changes are not necessarily driven by HIFs. Several studies have reported increased histone methylation under hypoxia, including the repressive marks tri-methylated histone H3 lysine 27 (H3K27me3) and H3K9me3, which may result from HIF-independent loss of function of oxygen-dependent KDMs and contribute to the energy-conservation response described earlier (75,76). At the same time, the active chromatin mark tri-methylated histone H3 lysine 4 (H3K4me3) has also been shown to increase under hypoxic conditions (76). Interestingly, Batie *et al.* found that most genes bound by H3K4me3 were downregulated under hypoxia (76), which could be explained by bivalent epigenetic marks, where H3K4me3 and H3K27me3 coexist at the same promoters (77,78), or by the recruitment of repressive complexes, such as ING2–mSin3a–HDAC1, to H3K4me3-bound promoters, thereby inhibiting transcription (79). Yet, despite this global, genome-scale shift toward a more repressive chromatin state, HIFs are still transcribed, translated, and able to activate their target genes.

Given the importance of hypoxia and HIFs in epigenetic regulation of gene expression, and the oxygen-, Fe^{2+}-, and α-ketoglutarate-dependency of KDMs (like the PHDs) (80,81), we hypothesized that JMJD family KDMs or other factors of the histone lysine methylation system might act in concert with PHDs and could be involved in HIF regulation. In a small-scale short hairpin RNA (shRNA) screen of several KDMs and the methyltransferase enhancer of zeste homolog 2 (EZH2), we found a reduction in HIF2α levels upon knockdown of EZH2, prompting further investigation into its role in

HIF2α regulation.

1.2. Enhancer of zeste homolog 2 (EZH2)

The importance of EZH2 in cancer is related to various functions of this protein. These include its canonical role as the catalytic subunit of the polycomb repressive complex 2 (PRC2) as well as non-canonical activities.

1.2.1. The canonical function of EZH2

PRCs are epigenetic regulators that control gene expression by modifying chromatin structure to maintain genes in a repressed state (82). The PRC2 is an essential chromatin modifier that is conserved across organisms ranging from plants to flies and humans (83,84). The complex contains four core subunits: EZH2 (or its paralog EZH1), embryonic ectoderm development (EED), suppressor of zeste 12 homolog (SUZ12), and retinoblastoma-binding protein (RBBP) 4 or 7 (85). EZH2 is the catalytic subunit of the PRC2. It contains a su(var), enhancer of zeste, trithorax (SET) domain, which transfers the methyl group from the methyl donor S-adenosylmethionine (SAM) to H3K27, and successively mono-, di-, and tri-methylates its target (86–90). H3K27me3 marks the chromatin for PRC1-mediated compaction, restricting access for the transcriptional machinery, such as RNA polymerase II (RNA Pol II) to the genes in that region, resulting in gene repression (88,89,91,92) (Fig. 1.2).

Although EZH2 is best known for its role within the PRC2, its diverse domain architecture suggests a broader functional repertoire.

1.2.2. The structure of EZH2

Besides the SET domain, EZH2 is composed of several other domains with various functions. EZH2 is divided into two main functional domains, the regulatory domain (start at the N-terminus) and the catalytic domain, each of which can be subdivided into smaller conserved structural protein domains/motifs (Fig. 1.3). The N-terminus contains a SANT1 binding domain (SBD), which is required for the EZH2-EED interaction (93,94). Next to the SBD, the EED-binding domain (EBD) is found, which is required for the direct interaction with EED (94). Next to the EBD, there is a β-addition motif (BAM), which is also involved in the maintenance of the EZH2-EED connection, though the exact function is unknown (93,94). Following the BAM, the SET activation loop (SAL) and the stimulation-responsive motif (SRM) link one side of the SET domain

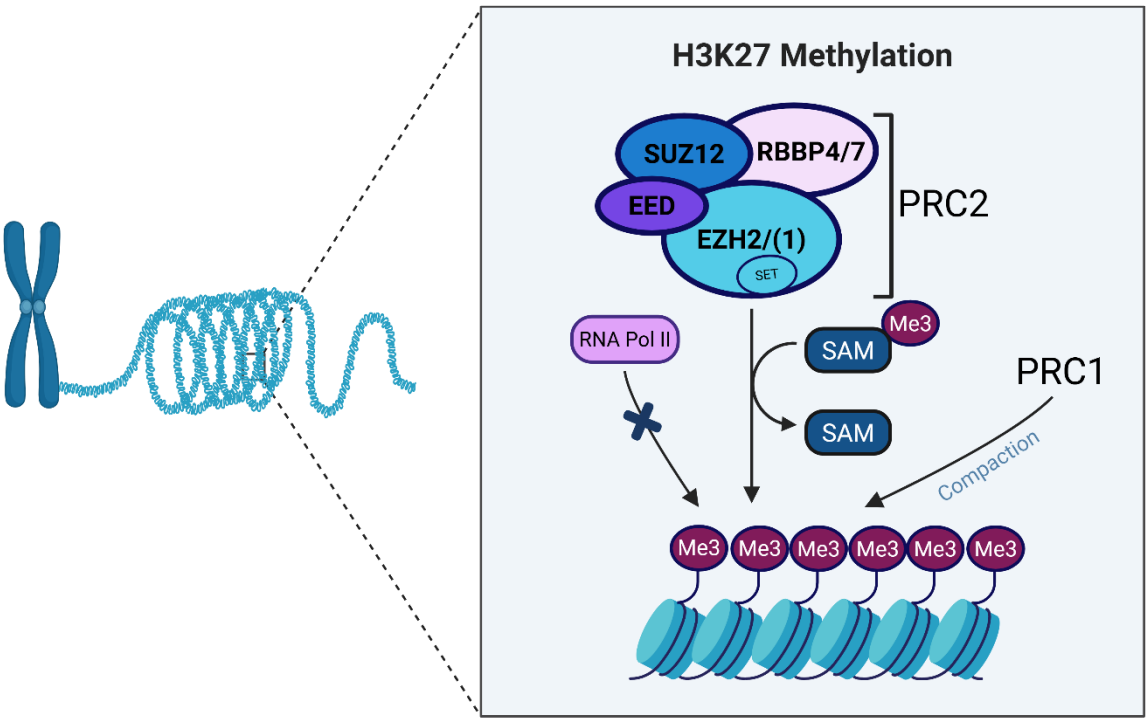

Figure 1.3: The canonical function of EZH2.

The PRC2 consists of four core subunits: EZH2, or its paralog EZH1, EED, SUZ12, and RBBP4/7. EZH2 contains a SET domain that transfers methyl groups from the methyl donor SAM to H3K27, generating tri-methylated H3K27. The repressive H3K27me3 mark promotes chromatin compaction by PRC1, restricting access of transcriptional machinery, including RNA Pol II, and thereby silencing gene expression. Created with BioRender.com.

to the EED subunit, forming a sandwich-like assembly with EED and H3K27me3 that transmits tri-methylation signals to the catalytic center, stimulating EZH2 activity (93,94). The last domain of the regulatory part of EZH2 is the SANT1 domain, which binds to the SBD and forms a belt-like structure maintaining the EZH2-EED connection (94). The catalytic domain starts with the motif connecting SANT1 and SANT2 (MCSS), followed by the SANT2 domain where SUZ12 interacts with EZH2 (94). Following the SANT2 domain is the CXC domain, which interacts with DNA and nucleosomes, and the C-terminus contains the SET domain (94,95). In 2020, Jiao *et al*. found a partially distorted TAD in EZH2 and EZH1 (96). Phosphorylation of EZH2 at serine 21 (S21) or tyrosine 244 (Y244) could unlock this TAD. The TAD plays an important role in the non-canonical functions of EZH2 (96–99), which will be addressed later. An overview of the domains and the structure of EZH2 in the PRC2 are presented in Figure 1.3 (93,94,96).

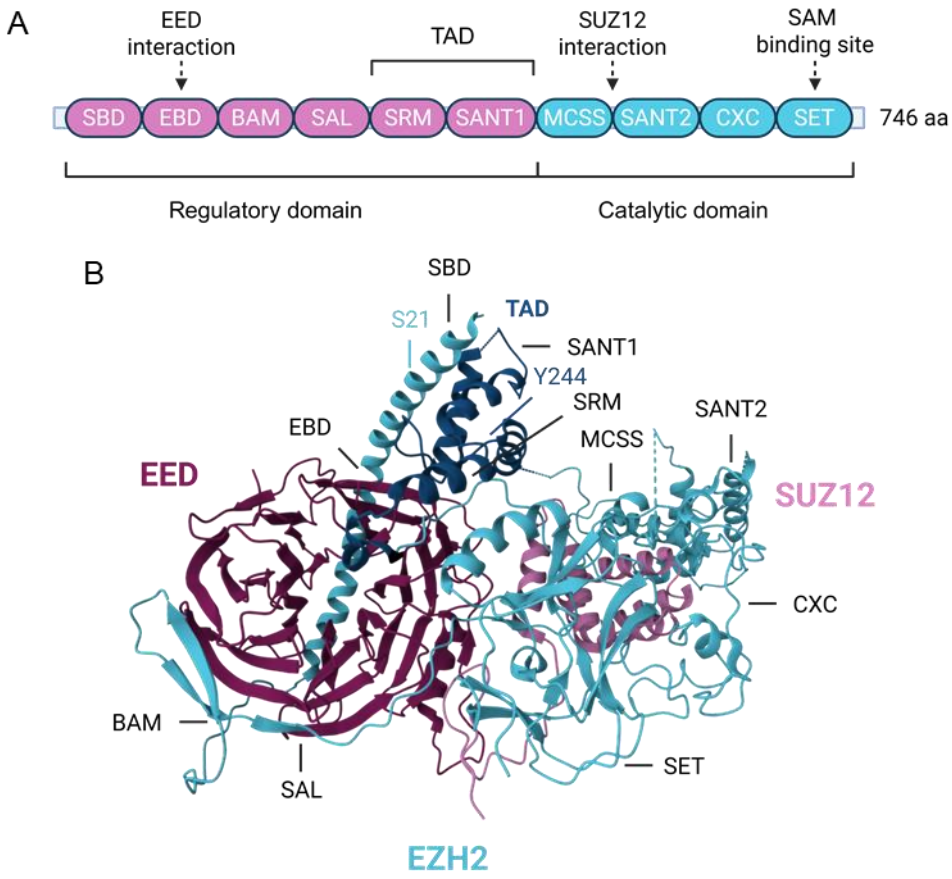

Figure 1.4: The structure of EZH2.

A) The regulatory domain's main function is forming the EZH2-EED complex. It also contains the partially distorted transactivation domain (TAD), which can be unlocked by S21 or Y244 phosphorylation. The catalytic domain contains the interaction sites with SUZ12 and the catalytic SET domain, which is the binding site for the methyl donor SAM. **B)** The structure of EZH2 (cyan) with its TAD domain (dark blue) in the PRC2 with EED (magenta) and SUZ12 (pink). *BAM: β-addition motif;* EBD: EED-binding domain; MCSS: motif connecting SANT1 and SANT2; SAL: SET activation loop; SBD: SANT1 binding domain; SET: su(var), enhancer of zeste, trithorax; SRM: stimulation-responsive motif. Created with BioRender.com.

1.2.3. The role of EZH2 in cancer progression

In the context of cancer, EZH2 is most often considered to be an oncogene. Hyperactivation of EZH2 by overexpression or gain-of-function point mutations at tyrosine 641 is a phenomenon found in many different malignancies. This hyperactivation correlates with tumor growth, metastasis, and poor prognosis, and was first found in prostate cancer (100,101), followed in many other cancers such as breast cancer (101–106), lung cancer (107–109), colorectal cancer (110), neuroblastoma (107), glioblastoma (111), melanoma (112,113), and lymphoma (113). Although there is overwhelming evidence of EZH2 functioning as an oncogene, some have also

described it as a tumor repressor (114,115). Wang *et al.* found heterozygous deletion and inactivation mutations in EZH2 in 33 out of 230 lung adenocarcinoma patients, of which 5% also had KRAS mutations. They studied the effect of both in mice and found amplified Akt and ERK activation and an increased inflammatory response, resulting in tumor progression in mice (114). A tumor suppressor function was also found in T-cell acute lymphoblastic leukemia by Ntziachristos *et al.* (115). They found increased cell growth and tumor growth upon EZH2 knockdown. This shows that EZH2's function in cancer is context specific (115).

EZH2 was initially believed to promote cancer progression solely through its methyltransferase activity, mainly by repressing tumor suppressor genes. Despite the development of inhibitors targeting this catalytic function, their clinical efficacy has been limited, leading to increasing interest in the non-canonical roles of EZH2, which remains an active area of investigation (116,117).

1.2.4. Non-canonical functions of EZH2

Over the last few years, several non-canonical functions of EZH2 have been discovered. Besides methylating histones, EZH2 can methylate non-histone targets in a methyltransferase-dependent manner. In 2005, Cha *et al.* observed that phosphorylation of serine 21 by Akt reduces H3K27me3 levels, while not compromising the PRC2 composition. They speculated that it could shift its affinity from H3K27 to non-histone targets (118). Kim *et al.* demonstrated that EZH2 can methylate signal transducer and activator of transcription 3 (STAT3) at lysine 180 in glioblastoma, which activates the function of STAT3 and promotes tumorigenicity. Also, for this activation, the previously discovered phosphorylation of S21 is required, potentially occurring within the context of the PRC2 (119). STAT3 activation through methylation by EZH2 was also found in breast cancer a few years later, in which case blocking STAT3 methylation reduced cell proliferation and migration (120). Among several other proteins (121), β-catenin is also a target for the methyltransferase function of EZH2 (122,123). β-catenin can be tri-methylated by EZH2 at lysine 49, which enhances its binding to chromatin in both embryonic stem cells and colorectal cancer, requiring S21 phosphorylation of EZH2 (122,123). In colorectal cancer, the functional consequences of this modification remain unclear (123). However, in embryonic stem cells, EZH2-mediated lysine 49 tri-methylation of β-catenin confers a repressor function (122). In addition, EZH2 can form a complex with β-catenin which promotes transactivation of

Wnt target genes (124,125), inducing cell cycle progression in breast cancer cells (124) and intestinal tumorigenesis (125).

EZH2 can also affect protein stability in a methyltransferase-independent manner. Wang *et al*. showed that EZH2 can bind to and stabilize MYC and NMYC in neuroblastoma and small cell carcinoma by competing with the SCF^{FBW7} ubiquitin ligase, which would otherwise mark MYC and NMYC for degradation. In agreement with this, the authors also showed that EZH2 depletion inhibits tumor growth (107).

Besides stabilizing MYC family proteins, EZH2 can also regulate the stability of p53 mRNA in a methyltransferase-independent manner. EZH2 can directly bind to p53 mRNA and induces its translation. Conversely, EZH2 knockdown reduces p53 mRNA levels and shortens the mRNA half-life (126). EZH2-dependent induction of mutant p53 promotes tumor growth and metastasis in various cancer models (126).

In 2011, Lee *at al.* published a pioneering report describing EZH2 as a methyltransferase-independent transcriptional activator. They found that EZH2 binds to and induces the expression of nuclear factor kappa B (NFκB) target genes IL-6 and TNF with RelA and RelB as co-regulators in estrogen receptor (ER)-negative breast cancer cells, correlating with poor disease outcome, while they found the opposite in ER-positive cells (127). This co-regulation of NFκB target genes by EZH2 and RelA and RelB was also found in triple-negative breast cancer (TNBC) cells by Dardis *et al.* (128). Besides co-regulating transcriptional activation, EZH2 also binds to the RELB (128,129) and NFKB promoters, activating their transcription (128). Neurogenic locus notch homolog protein 1 (NOTCH1) has also been shown to be a direct target gene of EZH2's transcriptional activator function in breast cancer and glioblastoma inducing stemness (130,131). Androgen receptor (AR) gene expression is also directly induced by EZH2 binding independent of its methyltransferase function in prostate cancer (132). Moreover, Xu *et al*. found that AR and EZH2 are co-recruited to specific genomic sites and cooperate to activate target gene transcription in prostate cancer, and that EZH2's methyltransferase function and S21 phosphorylation, but not the PRC2, is necessary for this cooperation (133). Wang *et al.* also found the cooperation of AR with EZH2 for transcriptional activation. However, they found this to be independent of EZH2's methyltransferase function (97). In addition, Liu *et al.* found a methyltransferase-independent cooperation between EZH2-EED and AR for transactivation. However, whether or not the EZH2-EED interaction is required for this

is questionable, since EED knockdown decreases EZH2 levels and the used EZH2 targeting drug, Astemizole, degrades both EED and EZH2 proteins (134). The EZH2 and AR connection was generally associated with prostate cancer progression (97,134,135). Furthermore, E2F transcription factor 1 (E2F1) has been described as an EZH2 target gene in prostate cancer by Yi *et al.* They found binding of EZH2 and not H3K27me3 at the E2F1 promoter and together with E2F1 regulated itself independent of the methyltransferase function of EZH2, inducing tumorigenesis (136). This cooperation was also described by Tabbal *et al.*, which suggested that EZH2 and E2F1 co-regulate E2F1 target genes in adrenocortical carcinoma (137). Interestingly, EZH2 has also been sown to be target gene of E2F1 (138). Zhang *et al*. further showed that EZH2 is also a transcriptional regulator of c-JUN in breast cancer inducing brain metastasis. To function as a transcriptional activator in this context, phosphorylation of EZH2 at tyrosine 696 (Y696) by proto-oncogene tyrosine-protein kinase Src (Src) was required (106).

A methyltransferase-independent transcriptional activator function of EZH2 has also been described in hypoxia stimulating breast cancer invasion. In this context, EZH2 forms a complex with forkhead box M1 (FoxM1) and promotes the expression of its target genes, including FOXM1 itself. Mahara *et al.* observed that when HIF1α levels were increased, EED, SUZ12, and H3K27me3 levels were reduced, while EZH2 levels were unaltered or increased, and that HIF1α, but not HIF2α, knockdown restored these levels, but abolished FoxM1 induction (139). In addition, the EZH2 promoter contains an HRE, to which HIF1α can bind (HIF2α was not tested), thus inducing the transcription of EZH2 (140). Together, these data showed that HIF1α induces a functional switch of EZH2 (139). These and the various previously described functions of EZH2 are summarized in Figure 1.4.

Besides RelA/RelB, AR, E2F1, and FoxM1, other proteins were also found to interact with EZH2 to induce transactivation. EZH2 also interacts with RNA Pol II in breast cancer (103,106) and in natural killer/T-cell lymphoma, in which JAK3 mediated phosphorylation of EZH2 at Y244 is required for this interaction, which also unlocks the TAD (141). The acetyltransferase transcription activator protein p300 has also been described to be an interaction partner of EZH2 in prostate cancer (96,99) and leukemia (98). In addition, c-MYC in leukemia (98) and multiple myeloma (142), NMYC in T-cell lymphoma (143), and YY1 in prostate cancer (144) have been reported as

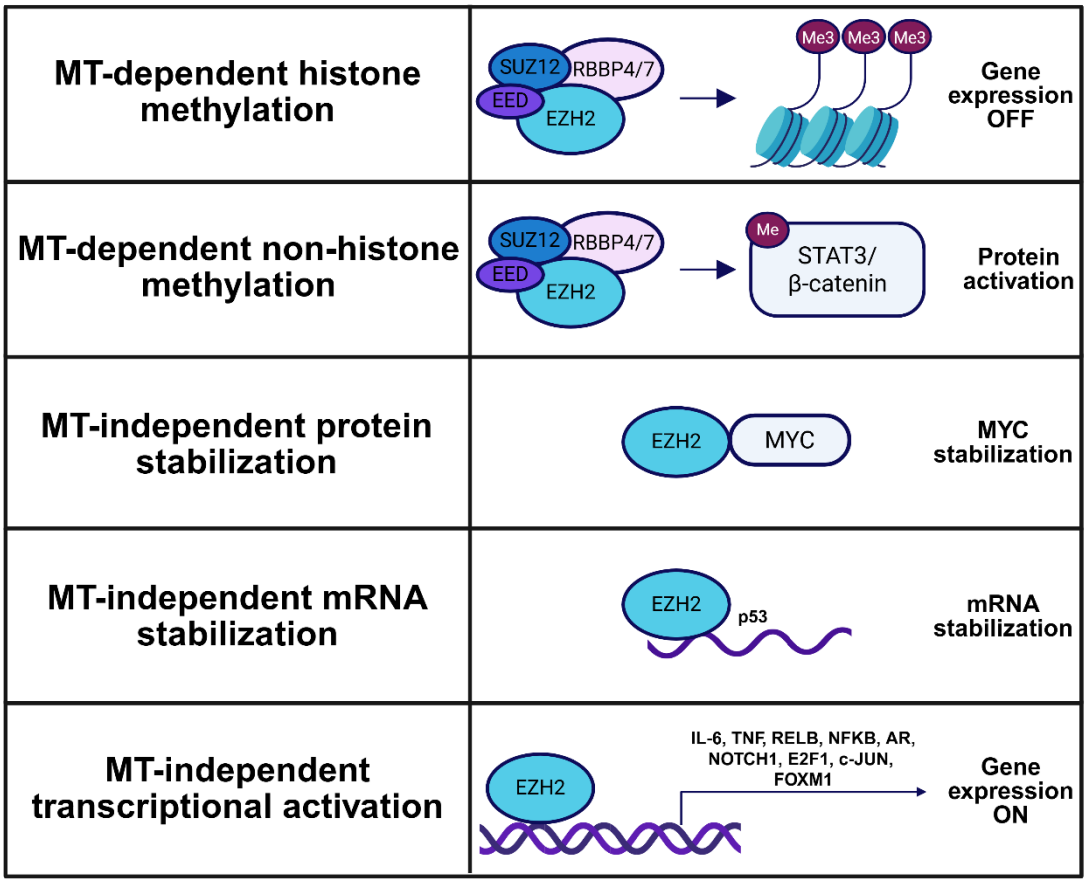

Figure 1.5: An overview of the functions of EZH2.

EZH2 regulates gene expression via its methyltransferase (MT) activity within the PRC2. In a methyltransferase-dependent manner, EZH2 can also activate proteins, whereas in a methyltransferase-independent manner, it stabilizes MYC family proteins and p53 mRNA and activates the transcription of multiple genes. Created with BioRender.com.

EZH2 partners for the transcriptional activator function of EZH2.

1.2.5. Targeting EZH2 in cancer therapy

Since EZH2 is often overexpressed or mutated in cancer, it is an attractive target for pharmacological interventions. The first EZH2 inhibitors targeted the methyltransferase function of EZH2, since the non-canonical functions were discovered later by Lee *et al.* in 2011. EZH2 methyltransferase targeting compounds inhibit EZH2's function by accumulating S-adenosylhomocysteine (SAH) or competing with the methyl donor SAM. One of the first potent EZH2 inhibitors is DZNep, which was discovered in 2007 by Tan *et al.* (145). DZNep was tested in breast and colon cancer cell lines, and it was shown to induce apoptosis in the breast cancer cell line MCF-7 (145). It inhibits EZH2 by accumulating SAH, which represses the activity of SAM (146). This inhibition also leads to the depletion of the PRC2 proteins (145). It is important to note that the

inhibitor is not EZH2 specific, as global SAM levels are affected by DZNep.

Another group of EZH2 methyltransferase inhibitors competes with SAM binding within the SET domain of EZH2 and acts more selectively. By preventing the transfer of the methyl groups to H3K27, they efficiently block the methyltransferase function of EZH2. The first SAM competitor, EPZ005687, was discovered in 2012 by Knutson *et al.,* and it was followed by the development of the experimentally widely used GSK126 (147) and EPZ-6438 (Tazemetostat) (148). Tazemetostat is the only EZH2 inhibitor that has been FDA approved for cancer treatment, specifically for epithelioid sarcoma (149) and follicular lymphoma (150). The most recent EZH2 methyltransferase inhibitors are CPI-0209 (Tulmimetostat) (151) and HH2853 (152), which target both EZH2 and EZH1.

Recently, several novel dual inhibitors and PRC2 disruptive inhibitors have also been developed. Dual inhibitors target both EZH2 and another target of interest, such as PARP1. This increases inhibitory activity in TNBC cells, but the efficacy depends on BRCA mutation status (153,154). The heat shock protein 90 was also co-targeted with EZH2 in a recent dual inhibitor approach, which showed potent anti-glioblastoma activity (155). PRC2-disruptive inhibitors commonly target EED because of its scaffolding role in the complex (121,156). For example, Astemizole targets the EZH2-EED interaction and could arrest proliferation in lymphoma cells (157).

Given the limited efficacy of most EZH2 methyltransferase inhibitors in clinical trials, perhaps also because these do not affect the non-canonical functions, there has been a greater focus on EZH2 degraders in the last years. Three modes of action have been used to create these degraders (121).

1. Degradation by CHIP, which senses inappropriate folding when the inhibitor binds to the SET domain, thereby triggering degradation.
2. Hydrophobic tags, which activate the unfolded protein response, marking EZH2 for degradation.
3. Proteolysis-targeting chimeras (PROTACs). These PROTACs contain a specific ligand for a distinct E3 ubiquitin ligase, another ligand specific for a target protein, and an optimized chemical linker connecting the two (158).

EZH2 degraders currently being investigated for the development of novel therapeutic strategies are summarized in Table 1.1 (121).

Table 1.1: EZH2 degrader overview.

Compound	Mode of degradation	Tumor samples	Reference
GNA002	CHIP	Head and neck cancer, breast cancer, hepatocellular carcinoma cell lines & head and neck mouse xenografts	Wang *et al.* 2017 (159)
IHMT-337	CHIP	TNBC, lymphoma cell lines & lymphoma mouse models	Mei *et al.* 2023 (160)
MS1943	Hydrophobic tag	Breast cancer cell lines & breast cancer mouse xenografts	Ma *et al*. 2020 (161)
YM181 YM281	PROTAC	Prostate, colon, DLBCL cancer cell lines & mouse xenografts	Tu *et al.* 2021 (162)
MS8815	PROTAC	TNBC cell lines & mouse xenografts	Dale *et al.* 2022 (163)
MS8847	PROTAC	Leukemia, AML, TNBC cell lines	Valez *et al.* 2024(164)
E7	PROTAC	Prostate cancer, Ovarian cancer, NSCLC, TNBC, and DLBCL cell lines	Liu *et al.* 2021 (165)
U3i	PROTAC	TNBC and leukemia cell lines	Wang *et al*. 2022 (166)
MS177	PROTAC	Leukemia, lymphoma, neuroblastoma, and cervical cancer cell lines & multiple myeloma cell lines	Wang *et al.* 2022 (98) Yu *et al.* 2023 (142)

Information derived from Wozniak *et al.* (121). *AML: Acute myeloid leukemia; DLBCL: Diffuse large B-cell lymphoma; NSCLC: non-small lung cancer; PROTAC: proteolysis-targeting chimera; TNBC: triple-negative breast cancer.*

1.3. Breast and lung cancer as model systems

Breast and lung cancers represent two of the most prevalent malignancies in the Western world, accounting for a major proportion of cancer incidence and mortality, with lung cancer and breast cancer causing most mortalities in men and women, with

20% (167,168) and 7% (167), respectively. Despite advances in early detection and targeted therapies, both tumor types are characterized by high rates of relapse and therapeutic resistance (169–172). Metastasis, and especially brain metastasis (BM), are very common in both cancers, with lung cancer being the most common cause of BM, followed by breast cancer. About 10 to 20% of lung cancer patients have BM at the time of diagnosis, and about 40% will develop it over time (173). In breast cancer patients, BM were found in 7.2% of the patients at the time of diagnosis, and 17.5% developed over time (174). Even though advances in therapies have been made, lung BM patients have a median survival of 9 to 15 months (175), whereas breast BM patients have a median survival ranging from 4.4 to 18.9 months, depending on the subtype (174). A major contributing factor is the hypoxic tumor microenvironment, which drives aggressive phenotypes (176–181). In addition, epigenetic regulators such as EZH2 have emerged as important players in breast and lung cancer progression, as discussed in previous sections. Together, these features make breast and lung cancers highly relevant model systems to study the interplay between EZH2 and HIFs.

1.3.1. Breast cancer classification

Breast cancer can be divided into four main subtypes: luminal A, luminal B, human epidermal growth factor receptor 2 (HER2)-positive, and TNBC. The classification is based on the presence of several biomarkers and is important in the determination of treatment strategies (171). Key biomarkers include the hormone receptors ER and the progesterone receptor (PR), as well as the non-hormone receptor HER2 and the proliferation marker Ki-67. ER is a ligand-activated transcription factor for genes associated with cell survival and proliferation. PR is also a ligand-activated transcription factor regulating genes involved in cell cycle, differentiation, and proliferation. HER2 is a tyrosine kinase receptor and part of the epidermal growth factor (EGFR) family, which unlike ER and PR, typically does not act as a transcription factor. Upon ligand binding, this receptor forms heterodimers or homodimers with other EGFR members and thus becomes activated (171). The activated receptor initiates signaling pathways such as the RAS, PI3K, and STAT3 pathways, which influence gene expression (182). The EGFRs regulate genes involved in proliferation, survival, differentiation, angiogenesis, and invasion and metastasis, resulting in a worse clinical outcome (183). Ki-67 is a protein involved in chromosome organization and it is a widely used general proliferation marker (171).

Luminal A cancer occurs in 50-60% of breast cancer patients, which makes it the most common subtype. Patients with this subtype also have the best prognosis. The luminal A subtype is characterized by being ER-positive, high PR levels, a low or no expression of HER2, and low expression of Ki-67. The luminal B subtype is characterized by being ER-positive and HER2-negative or HER2-positive. When luminal B cancer is HER2-negative, PR expression is low, but Ki-67 expression is high. In luminal B HER2-positive cancer, PR and Ki-67 expression vary. High Ki-67 expression accelerates tumor growth, resulting in a worse prognosis. HER2-positive cancer is characterized by high HER2 and Ki-67 expression and no or low expression of ER and PR levels, which has a worse prognosis than the luminal cancers. TNBC expresses low to no hormone receptors or HER2, but has very high Ki-67 levels, and is often driven by BRCA mutations. TNBC patients have the biggest risk for developing metastasis, often in the brain and lung, resulting in a higher mortality rate with a median overall survival rate of 4.4 months in patients with BM (174,184–186). The subtypes are summarized in Table 1.2. The Table also shows which group the cell lines used in this study belong to.

1.3.2. The hypoxic tumor microenvironment of breast cancer

Hypoxia is a common feature of breast tumors. Oxygen levels in the breast were studied by Vaupel *et al.,* and they found that normal breast tissue has a median oxygen tension (pO_2) of 65mm Hg, whereas the median pO_2 is 28mm Hg in breast tumors (187). They also found that about 60% of the investigated breast tumors has pO_2 values below 2.5mm Hg (187). Many research projects have focused on HIF1α and its role in breast cancer progression (140,176,188–191), but HIF2α also plays an important role in breast cancer development and metastasis and has been shown to be a potential prognostic marker (43,47–49,192–196). HIF2α is often linked to regulating stemness, by regulating signaling pathways like β-catenin/Wnt, Notch, and mTOR, thereby contributing to cancer progression (196–199).

1.3.3. Lung cancer classification

Lung cancer can be divided into two main types, non-small cell lung cancer (NSCLC) and small cell lung cancer (SCLC), based on morphology as the gold standard. NSCLC occurs in about 85% of lung cancer patients and SCLC in 15%, with SCLC being the most aggressive type of lung cancer (200,201). NSCLC can be subdivided into three

Table 1.2: Breast cancer subtype overview.

Subtype	**Key Features** (171)	**Occurrence** (171,202)	**Prognosis Summary** (171)	**Cell lines used**
Luminal A	ER+/PR+/ HER2-/ Ki-67-	50-60%	Best	MCF-7
Luminal B	ER+/PR-/HER2- /Ki-67+ or HR+ /HER2+	15%	Intermediate	MDA-MB-361
HER2-positive	ER-/PR-/HER2+/ Ki-67+	10-15%	Worse	
TNBC	ER-/PR-/HER2-/ Ki-67+	10%	Worst	MDA-MB-231 MD-MB-157 BT-549

TNBC: Triple-negative breast cancer.

subtypes: lung adenocarcinoma, lung squamous cell carcinoma, and large cell lung carcinoma. Table 1.3 summarizes the different lung cancer types and shows the cell lines used in this study.

1.3.4. The hypoxic tumor microenvironment of lung cancer

Like in breast cancer, hypoxia is a common problem in lung cancer (179). Le *et al.* found that normal lung tissue has a median pO_2 of 42.8 mm Hg and lung cancer tissue has a median pO_2 of 16.6 mm Hg (203). Also in lung cancer, more research has focused on the role of HIF1α in lung cancer progression (191,204–208). However, there have also been several studies demonstrating that HIF2α plays an important role in cancer progression and as previously mentioned is considered a potential prognostic marker (52,53,209–213). This could be partially explained by inducing stemness though β-catenin/Wnt signaling (209,212,213).

Table 1.3: Lung cancer subtypes overview.

Subtype	Occurrence (201)	Cell lines used
NSCLC Lung adenocarcinoma	44%	PC-9, A549, H2030, H441
NSCLC Lung squamous cell carcinoma	22%	
NSCLC Large cell lung carcinoma	1%	
NSCLC other	16%	
SCLC	15%	

NSCLC: non-small lung cancer; SCLC: small lung cancer.

1.4. The links between HIFs and EZH2

Both HIFs and EZH2 have been implicated in cancer progression, and in the last years, relationships between them have been discovered. These relationships are not one-directional and have been found in several tumor types including breast cancer (139,189,190,214), lung cancer (206–208,215), and colorectal cancer (110). A HRE within the EZH2 gene was discovered in 2011 by Chang *et al*. and validated for HIF1α binding in breast tumor-initiating cells using chromatin immunoprecipitation followed by quantitative polymerase chain reaction (ChIP-qPCR), demonstrating that hypoxia increased EZH2 transcription (140). Unfortunately, as mentioned before, HIF2α binding was not tested. This transcriptional activity of HIF1α at the EZH2 promoter can be induced by staphylococcal nuclease and tudor domain containing 1 (SND1) (189). SND1 is also a co-activator for E2F1 (216), which transcriptionally regulates EZH2 and HIF2α (138,217). Forkhead box K2 (FOXK2) counteracts this HIF1α-EZH2 axis by repressing HIF1β and EZH2 (190). However FOXK2 is transactivated by ER and repressed by EZH2, and thus downregulated in TNBC, thereby the HIF1α-EZH2 axis is maintained and worsens ER-negative breast cancer clinical outcome, which highlights the complexity of the HIF1α-EZH2 axis in breast cancer (139,190,214). HIF1α-dependent regulation of EZH2 has also been described A549 lung cancer cells by Zhou *et al.* (215). They also demonstrated HIF1α binding to the EZH2 promoter using ChIP-qPCR and a luciferase reporter assay.

HIF1α can also affect EZH2 function, as was previously discussed in breast cancer, by negative regulation of EED and SUZ12 (139). HIF1α directly binds to the EED and SUZ12 promoter, resulting in loss of the active chromatin mark H3K27ac, while not affecting EZH2. This negative regulation causes the functional switch from a repressor to a transcriptional activator (139). In lung cancer cells, something very similar was observed. Wang *et al.* showed that HIF1α inhibition or knockdown does not affect EZH2 levels, but does increase H3K27me3 levels and SUZ12 protein and mRNA levels, suggesting a HIF1α dependent negative regulation of PRC2 activity in this context as well (206). They also suggested that this upregulation of PRC2 activity upon HIF1α inhibition contributes to drug resistance. For this reason they developed a dual inhibitor, DYB-03, which simultaneously targets HIF1α and EZH2 and demonstrated potent antitumor activity. (206). Taken together, these studies suggest diverse and likely context-dependent roles for HIF1α-mediated PRC2 regulation, in which HIF1α can activate EZH2 expression and/or suppress SUZ12 and EED expression. The timing and context-dependence of these regulatory events, as well as their effects on chromatin state and genome-wide transcription, remain to be fully elucidated.

Conversely, Wang *et al.* showed that EZH2 negatively regulates HIF1α in a methyltransferase-dependent manner. Upon EZH2 knockdown in the lung cancer cell lines A549 and H460, HIF1α protein levels were increased, which was reversed upon EZH2 rescue (206). They found no effect of EZH2 knockdown on HIF2α and HIF1β protein levels (206). Zhao *et al.* also found reduced HIF1A mRNA levels upon EZH2 knockdown in Lewis lung carcinoma cells (207). However, under glucose deprivation, a positive regulation of HIF1α by EZH2 was observed by Saggese *et al.* They showed that, upon glucose deprivation and EZH2 knockdown, HIF1α protein and HIF1A mRNA levels were reduced in A549 cells (208). These findings suggest that additional factors or mechanisms may influence the final outcome of EZH2-dependent regulation of HIF1α, which may increase or decrease depending on the specific cellular context.

These studies demonstrate a complex and clinically relevant link between HIF1α and EZH2, highlighting their potential as therapeutic targets. Yet, most investigations have largely focused on HIF1α, with limited attention to HIF2α, despite its important role in cancer as discussed earlier. In recent years, however, more research has begun to uncover the mechanisms regulating HIF2α as well.

HIF2α can be regulated at DNA, mRNA, and protein level (218). Several promoter-associated proteins have been found for EPAS1 such as c-Myc (219), E2F1 (217), and p52 (220) as positive regulators based on ChIP-qPCR data, and HDX, which was identified as a negative regulator of EPAS1 in an engineered DNA-binding molecule mediated chromatin immunoprecipitation followed by mass spectrometry (enChIP-MS) screening study (221). At the mRNA level, several microRNAs can negatively regulate EPAS1, including miR-185 (222), miR-145 (223), miR-17, and miR-20A (224). In addition, iron regulatory proteins bind to a conserved iron response element in the 5′ untranslated region (UTR) of EPAS1 mRNA, blocking its translation under iron-deficient conditions (225,226). At the protein level, non-coding RNA ZFAS1 was found to bind and upregulate HIF2α protein levels under hypoxic and normoxic conditions, while reducing HIF1α levels (227). Furthermore, as discussed in section 1.1.2, HIF2α gets hydroxylated by PHDs and FIH, but it can also be phosphorylated, acetylated, and methylated (218). When looking at EZH2's function, its regulatory activity occurs at the same levels at which EPAS1/HIF2α can be regulated, as shown in Figure 1.4. Figure 1.5 depicts how HIF2α can be regulated and how EZH2 could play a role.

There are, however, more indirect pathways through which EZH2 could influence HIF2α levels. For example, siah E3 ubiquitin protein ligase 2 (Siah2) regulates the stability of PHDs (228), and EZH2 has been reported to repress SIAH2 in a PRC2-dependent manner (229), in which it could indirectly affect HIF2α stability. These multiple layers of regulation make investigating the dependency of HIF2α on EZH2 more challenging.

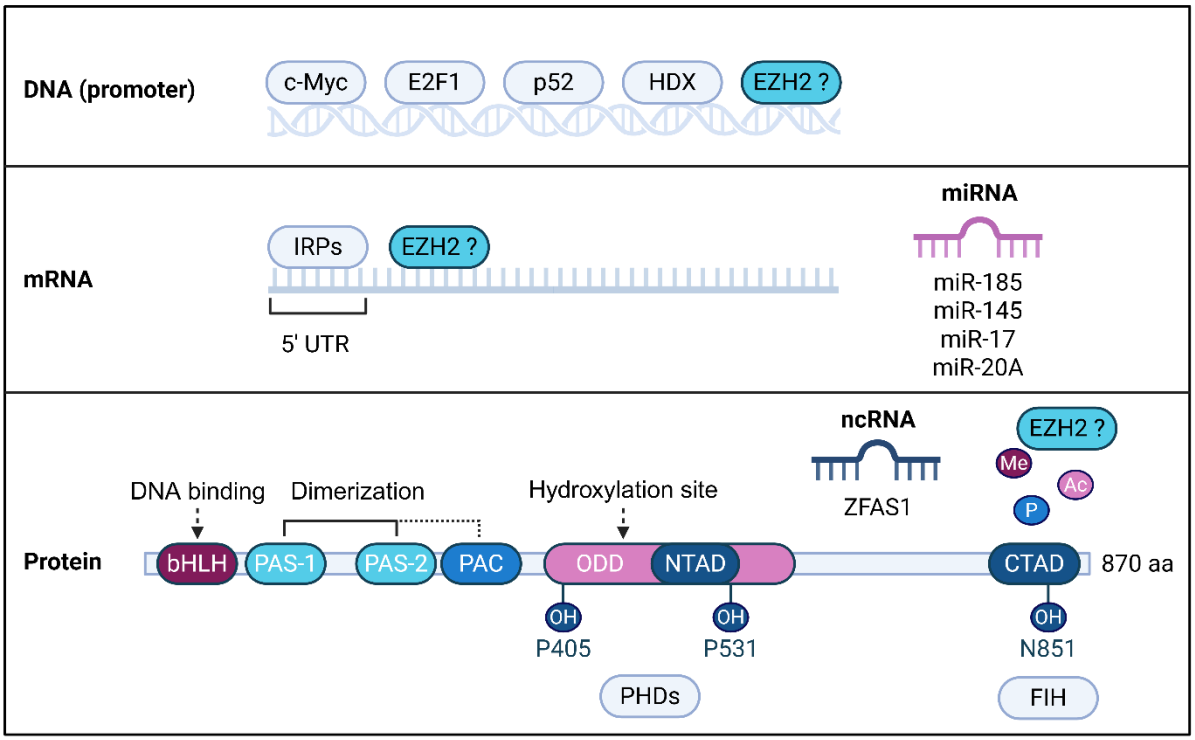

Figure 1.6: An overview of HIF2α regulation.

HIF2α is regulated at multiple levels: at the DNA level by transcriptional activators such as c-Myc, E2F1, and p52, and the repressor HDX; at the mRNA level by miRNAs and iron regulatory proteins, which negatively regulate EPAS1; and at the protein level through posttranslational modifications and binding of the non-coding RNA ZFAS1, affecting its function and stability. EZH2 may influence HIF2α regulation at all of these levels. Created with BioRender.com.

1.5. Aims of the thesis project

Hypoxia is a key driver of cancer progression, largely mediated by HIFs (230). The mechanisms behind HIFα stability have been widely studied, but its transcriptional regulation is less well understood, especially for HIF2α. Given the pivotal role of HIF2α in cancer progression, one focus of our lab is to discover regulatory pathways specifically for HIF2α. Among other investigations, a small-scale loss of function screening was conducted in our laboratory using shRNAs. Since we hypothesized that KDMs might cooperate with PHDs due to their shared cofactor requirements, the screening focused on KDMs and on EZH2, which counteracts H3K27 demethylases and is a known regulator of tumor progression and a therapeutic target in various types of cancer (100–108,111–113,146,149,150). The results of this screening suggested a role for EZH2 as a novel regulator of HIF2α, as HIF2α protein levels were decreased upon EZH2 knockdown in a single cell clone from genetically engineered MDA-MB-231 cells (MDA-POR) under intermittent hypoxic conditions.

As afore mentioned, links between EZH2 and HIF1α have been described in several studies and a recent review summarizes the main findings on the relation between EZH2 and HIF1α (191). However, no regulatory relationship between EZH2 and HIF2α has yet been reported.

The aims of this study were therefore:

1) to validate the previous findings in parental MDA-MB-231 cells,
2) to evaluate whether the observed regulation is tumor-type independent,
3) to decipher the molecular mechanisms by which EZH2 regulates HIF2α,
4) to uncover the functional consequences of this regulation,
5) to evaluate its relevance and potential implications in various tumor models.

With these aims in mind, this study sought to uncover a novel regulatory interaction between a druggable epigenetic modifier and the hypoxia signaling pathway, with the potential to inform the development of new therapeutic strategies as well as the refinement of existing ones.

2. Results

2.1. HIF dynamics and the effect of EZH2 knockdown on HIFs

2.1.1. HIF dynamics in MDA-MB-231 and PC-9 cells

Given the inconsistency in defining acute and chronic hypoxia in the literature and the kinetics of cellular HIF1α and HIF2α levels, I first sought to establish how my experimental models respond to hypoxia treatments of different durations. This was also important to specify the conditions for later experiments.

The two models used in most of the experiments, MDA-MB-231 and PC-9 cells, were subjected to hypoxic conditions for increasing durations (Fig. 2.1). In both cell lines, HIF1α levels rose within the first few hours of hypoxia and remained high for 8 hours, after which HIF1α levels declined, consistent with its role as an early responder. In contrast, HIF2α accumulated more gradually in MDA-MB-231 cells and was maintained for longer periods, peaking at 48 hours. In PC-9 cells HIF2α accumulated with a similar pattern to HIF1α levels, peaking at 8 hours, but remained detectable up to 48 hours. In both cell lines this reflected its function in sustaining the hypoxic response.

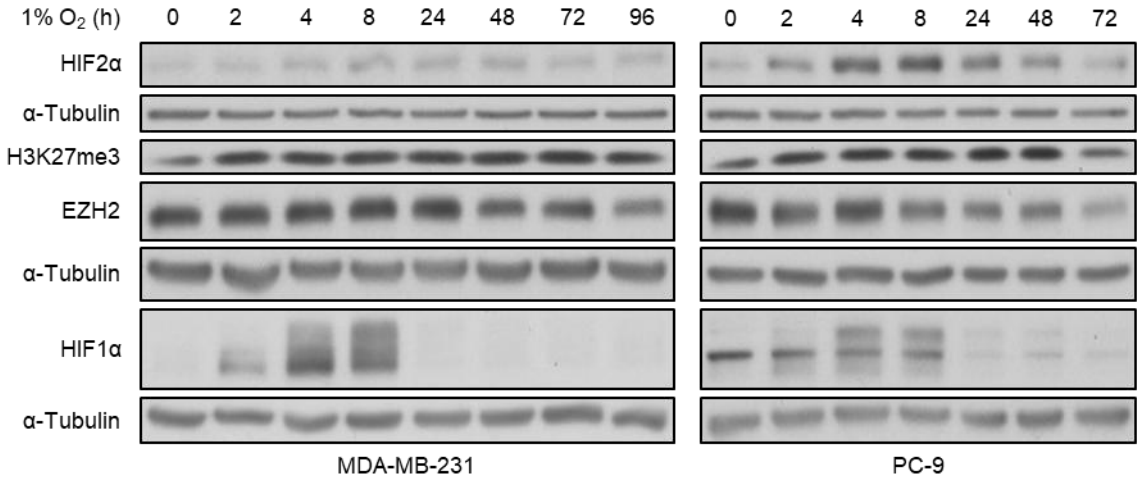

Figure 2.1: Dynamics of HIFs, EZH2, and H3K27me3 during hypoxic exposure.

Western blots showing the protein changes in MDA-MB-231 and PC-9 upon hypoxic exposure (1% O_2) at different time points (n=1).

Additional western blot analyses were performed to monitor the effect of the same treatments on EZH2 and the main product of its enzymatic activity, H3K27me3. EZH2 levels appear to decrease with longer hypoxia exposure in both cell lines, whereas H3K27me3 levels increase initially and then decrease at the latest time points in both cell lines, suggesting a repressive state under hypoxic conditions up to 72 hours in MDA-MB-231 and 48 hours in PC-9 cells, as has been described in the literature (75,76).

These observations confirm that both cell lines possess a functional HIF signaling pathway and that EZH2 levels decrease only slightly up to 48 hours, providing a solid reference point for the mechanistic studies described in the following sections.

2.1.2. EZH2 knockdown reduces HIF2α protein and EPAS1 mRNA levels in a subset of breast and lung cancer cell lines

To confirm the previously observed effect of EZH2 knockdown on HIF2α protein levels in MDA-POR cells, I generated parental MDA-MB-231 knockdown cells using two different shRNA's (Fig. 2.2A,B). Additionally, EZH2 was knocked down in PC-9 cells using shRNA #2 (Fig. 2.2A,B). EZH2 protein and mRNA levels and H3K27me3 levels confirmed efficient knockdown of EZH2 in both cell lines. HIF2α levels were decreased in both cell lines upon EZH2 knockdown under hypoxia, consistent with the results from the preliminary knockdown screen. HIF1α levels were decreased in PC-9 cells, although the results were inconsistent between independent repeats.

After confirming HIF2α protein levels decrease upon EZH2 knockdown in both MDA-MB-231 and PC-9 cells subjected to hypoxia, the aim was to determine whether HIF2α is also regulated at the mRNA level. EPAS1 mRNA levels were significantly reduced in MDA-MB-231 EZH2 knockdown cells under normoxic and hypoxic conditions transduced with shEZH2 #2 ($p < 0.0001$), while HIF1A mRNA levels were unchanged ($p = 0.1093$, $p = 0.7057$, respectively). HIF1A mRNA levels were significantly reduced under normoxic and hypoxic conditions in the cells transduced with shEZH2 #1 ($p = 0.0021$, $p = 0.0096$, respectively), although the decrease under hypoxia was relatively small (Fig. 2.2B). EZH2 knockdown in PC-9 cells showed a non-significant decreasing trend under both normoxic and hypoxic conditions ($p = 0.0525$ and $p = 0.1746$, respectively), but the observed differences were small. HIF1α mRNA levels were not

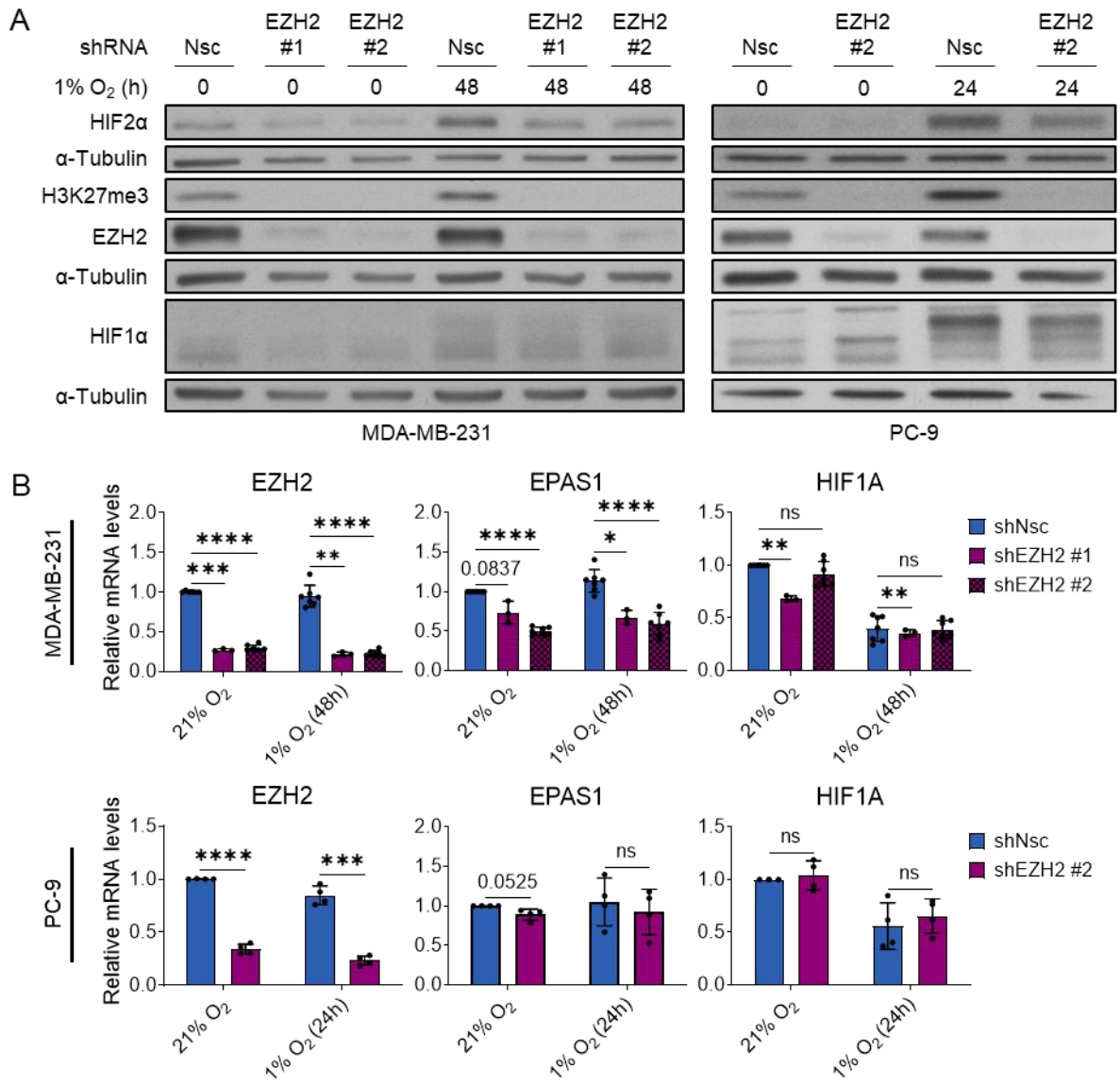

Figure 2.2: shRNA-mediated knockdown of EZH2 and its effect on HIF1α/HIF2α protein and HIF1A/EPAS1 mRNA levels.

MDA-MB-231 (n=7) and PC-9 (n=4) cells were exposed to normoxic (21% O_2) or hypoxic (1% O_2) conditions for 48 or 24 hours, respectively. **A)** Western blots showing EZH2 knockdown efficiency and its effect on HIF levels. **B)** RT-qPCR analysis showing corresponding mRNA levels relative to HPRT1. The data are presented as mean ± SD. Statistical significance was determined using a two-tailed paired t-test. ns $p > 0.05$; * $p < 0.05$; ** $p < 0.01$; *** $p < 0.001$; **** $p < 0.0001$. *Nsc: non-silencing control.*

affected by EZH2 knockdown in PC-9 cells (p = 0.6276, p = 0.5054, respectively) (Fig. (Fig. 2.2B).

To further validate these findings and rule out shRNA specific effects, I used small interfering RNA (siRNA)-mediated knockdown in both cell lines. In both cell lines the EZH2 knockdown was efficient, confirmed by reduced levels of EZH2 protein and mRNA, and H3K27me3 levels (Fig. 2.3A,B). In both cell lines HIF2α protein levels were

notably reduced upon EZH2 knockdown under hypoxia. At the mRNA level, HIF2α was significantly reduced under normoxic conditions in MDA-MB-231 cells (p = 0.0258), although the reduction was minor. Under hypoxic conditions, there was also a minor decrease, but it was not significant (p = 0.1732) (Fig. 2.3B). However, in PC-9 cells there was a large significant reduction of EPAS1 mRNA levels upon EZH2 knockdown under normoxic and hypoxic conditions (p = 0.0038, p = 0.0010, respectively) (Fig. 2.3B). Together, these results show that HIF2α is dependent on EZH2 availability and is at least in part regulated at the mRNA level. This is also supported by microarray data from Yu *et al*. showing a significant reduction in EPAS1 mRNA levels upon EZH2 knockdown in H16N2 human mammary epithelial cells and RWPE prostate epithelial cells (p = 0.0024, p = 0.0099, respectively) (Fig. 2.3C) (GSE8145) (231).

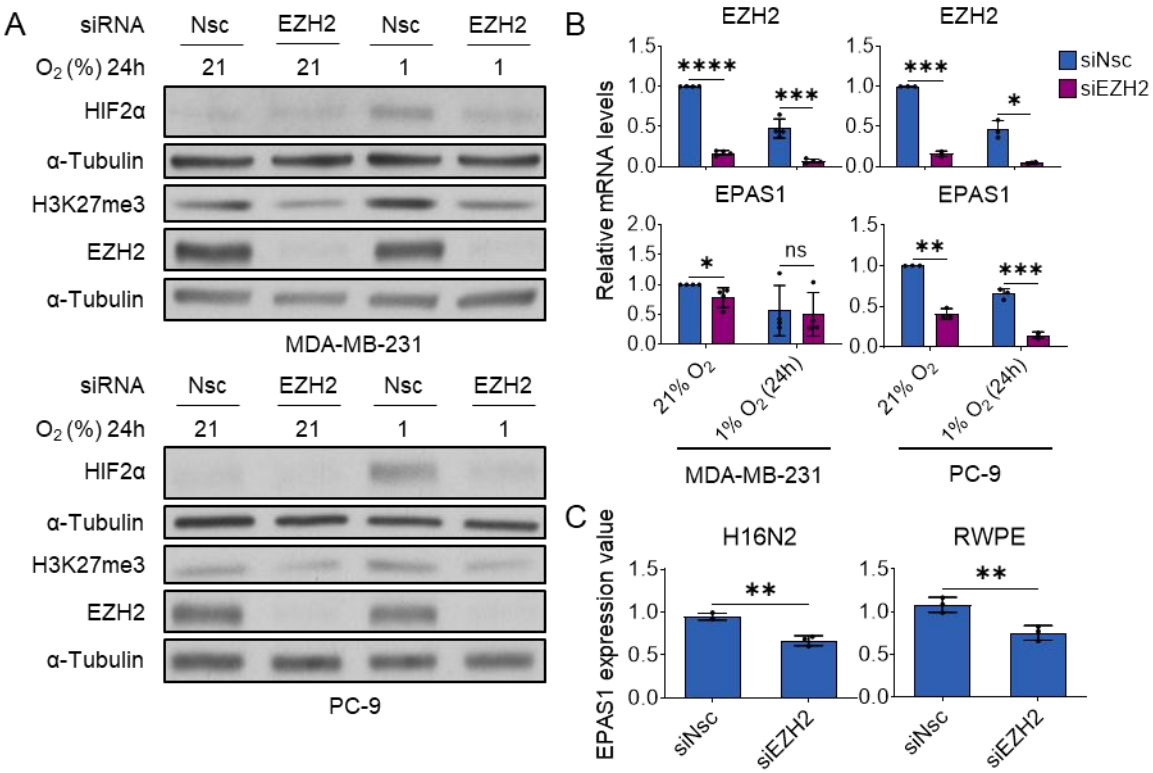

Figure 2.3: siRNA-mediated knockdown of EZH2 and its effect on HIF2α protein and EPAS1 mRNA levels.

MDA-MB-231 (n=4) and PC-9 (n=3) cells were transfected with siEZH2 for 48 hours and exposed to normoxic (21% O_2) or hypoxic (1% O_2) conditions for 24 hours. **A)** Western blots showing EZH2 knockdown efficiency and its effect on HIF2α levels. **B)** RT-qPCR analysis showing corresponding mRNA levels relative to ACTB. **C)** Microarray data from Yu *et al.* (n=3) (231). The data are presented as mean ± SD. Statistical significance was determined using a two-tailed paired t-test for **B** and a two-tailed student's t-test for **C**. ns p > 0.05; * p < 0.05; ** p < 0.01; *** p < 0.001; **** p < 0.0001. *Nsc: non-silencing control.*

To address if the observed HIF2α dependency on EZH2 is specific to these cell lines or present across other breast and lung cancer cell lines and other cancers such as glioblastoma, EZH2 was knocked down in several other cell lines.

As shown in Fig. 2.4A, EZH2 knockdown in another TNBC cell line BT-549 and non-TNBC cell lines MDA-MB-361 and MCF-7 did not reduce HIF2α protein levels. In the TNBC cell line MDA-MB-157, however, a small reduction in HIF2α protein levels was observed under normoxia and hypoxia, and a reduction in EPAS1 mRNA levels was observed, especially under normoxic conditions (Fig. 2.4B). However, since the decrease was small and HIF2α protein levels did not respond to the hypoxia treatment, the cell line was excluded from further analysis. In BT-549 cells, a slight increase was found in EPAS1 mRNA levels and an approximate two-fold increase was found in MCF-7 cells (Fig. 2.4B). These findings clearly demonstrate that HIF2α dependence on EZH2 is not a general feature in breast cancer cells.

EZH2 was also knocked down in the lung adenocarcinoma cell lines A549, H441, and H2030. No decrease in HIF2α protein levels was observed in the three cell lines (Fig. 2.5A) and mRNA levels were unchanged or slightly increased upon EZH2 knockdown (Fig. 2.5B). This shows that HIF2α dependency on EZH2 is also not universal across lung adenocarcinoma cell lines.

EZH2 was additionally knocked down in the glioblastoma cell lines G55 and U87. HIF2α protein levels were inconsistent under normoxic conditions in G55 cells (Fig. 2.6A). Under hypoxic conditions, no reduction of HIF2α protein levels was observed in both G55 and U87 cells (Fig. 2.6A). EPAS1 mRNA levels were also not decreased upon EZH2 knockdown in U87 cells (Fig. 2.6B). Together, these results show that HIF2α dependency on EZH2 is cell line dependent.

2.1.3. EZH2 restoration partially reverses the reduction of EPAS1 mRNA levels

The next aim was to investigate if the reduction in HIF2α levels following EZH2 depletion is reversible upon restoration of EZH2 levels. For this purpose, a long-term experiment with transient siRNA knockdown under normoxia was performed. MDA-MB-231 and PC-9 cells were transfected with siRNA targeting EZH2 for 48 hours, representing day 4 in Figure 2.7. Cells were further cultured and harvested again at day 8, day 11, and 15.

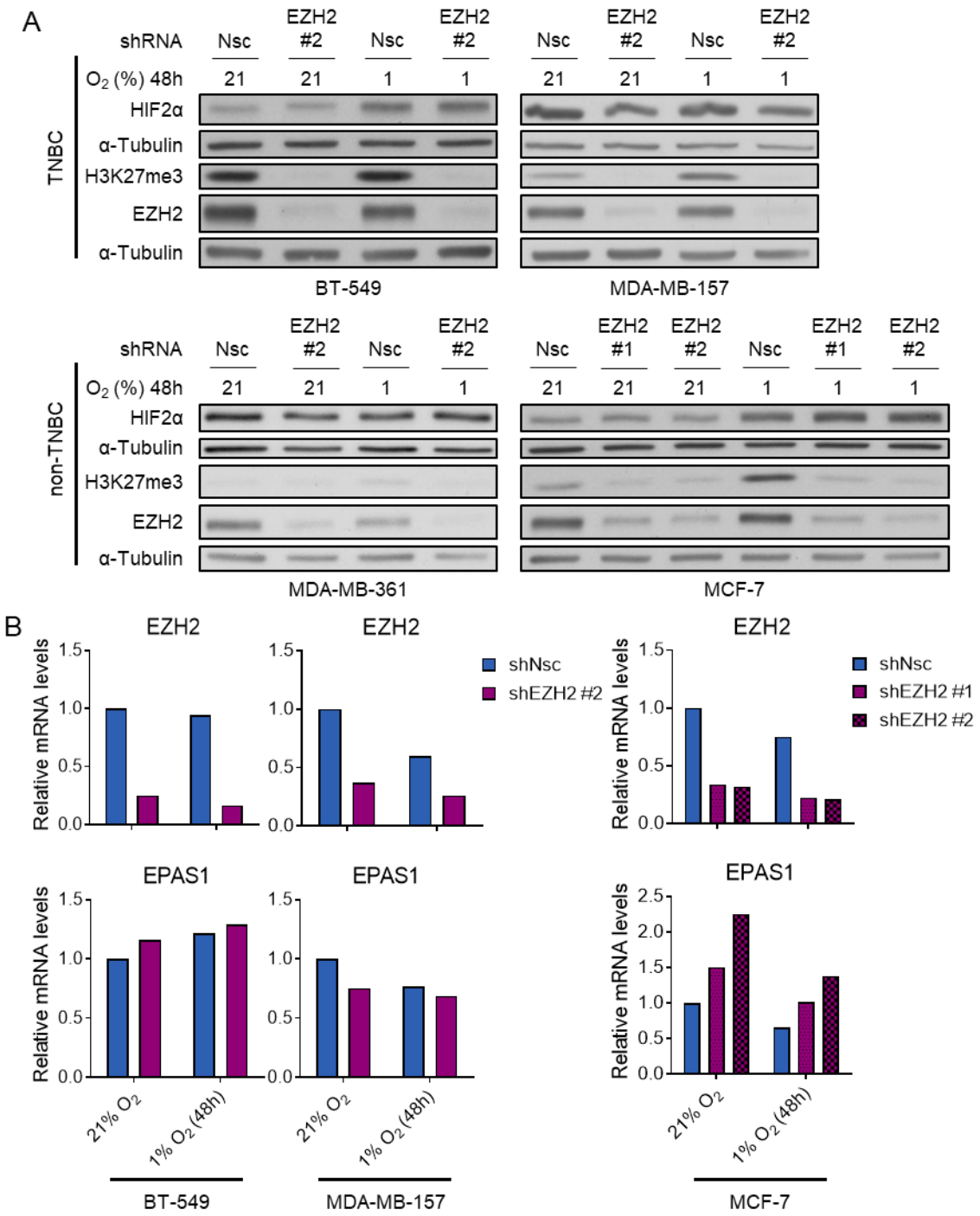

Figure 2.4: shRNA-mediated knockdown of EZH2 in other breast cancer cell lines and its effect on HIF2α protein and EPAS1 mRNA levels.

BT-549, MDA-MB-157, MDA-MB-361, and MCF-7 cells were exposed to normoxic (21% O_2) or hypoxic (1% O_2) conditions for 48 hours (n=1). **A)** Western blots showing EZH2 knockdown efficiency and its effect on HIF2α levels. **B)** RT-qPCR analysis showing corresponding mean mRNA levels relative to HPRT1. *Nsc: non-silencing control*; *TNBC: Triple-negative breast cancer.*

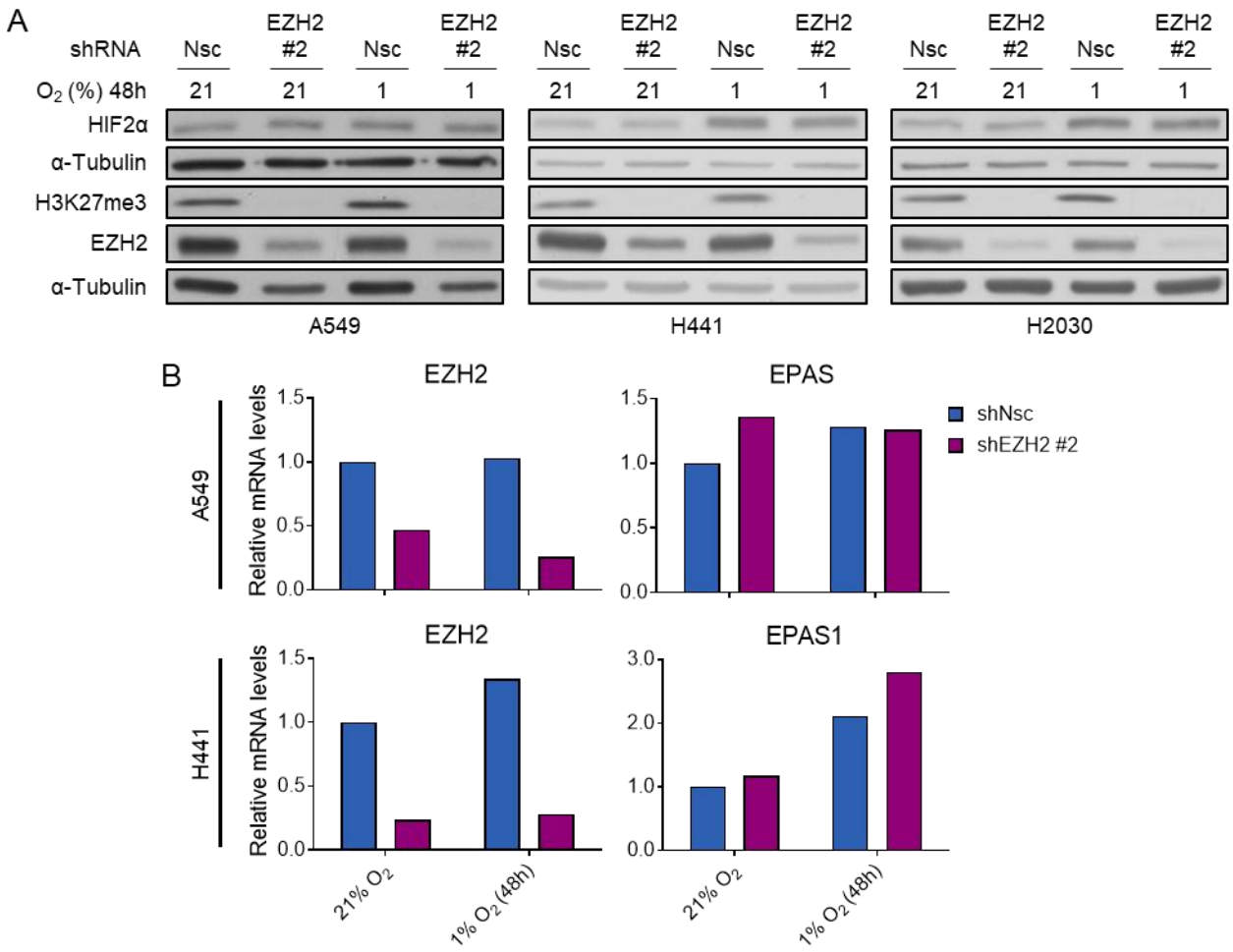

Figure 2.5: shRNA-mediated knockdown of EZH2 in other lung adenocarcinoma cell lines and its effect on HIF2α protein and EPAS1 mRNA levels.

A549, H441, and H2030 cells were exposed to normoxic (21% O_2) or hypoxic (1% O_2) conditions for 48 hours (n=1). **A)** Western blots showing EZH2 knockdown efficiency and its effect on HIF2α levels. **B)** RT-qPCR analysis showing corresponding mean mRNA levels relative to HPRT1. *Nsc: non-silencing control.*

In both cell lines, EZH2 and EPAS1 mRNA levels were significantly reduced at day 4 (MDA-MB-231 p = 0.0040, p = 0.0341; PC-9 p = 0.0050, p = 0.0026, respectively) (Fig. 2.7A). At day 8, EZH2 was still significantly reduced in MDA-MB-231 cells (p = 0.0170), but the difference was visibly smaller (Fig. 2.7A). In two out of three experiments a reduction of HIF2α levels of approximately two-fold was observed. HIF2α levels were slightly higher in the third experiment, resulting in a non-significant difference (p = 0.3280) (Fig. 2.7A). In both cell lines EZH2 levels were still significantly reduced at day 11 (MDA-MB-231: p = 0.0123; PC-9: p = 0.0194), but visibly higher compared to day 4. HIF2α levels in MDA-MB-231 cells were no longer decreased in siEZH2 cells (p = 0.4322), but remained significantly lower in PC-9 cells (p = 0.0249) (Fig. 2.7A). At day 15, EZH2 levels were largely restored in both cell lines, and HIF2α levels in PC-9 cells

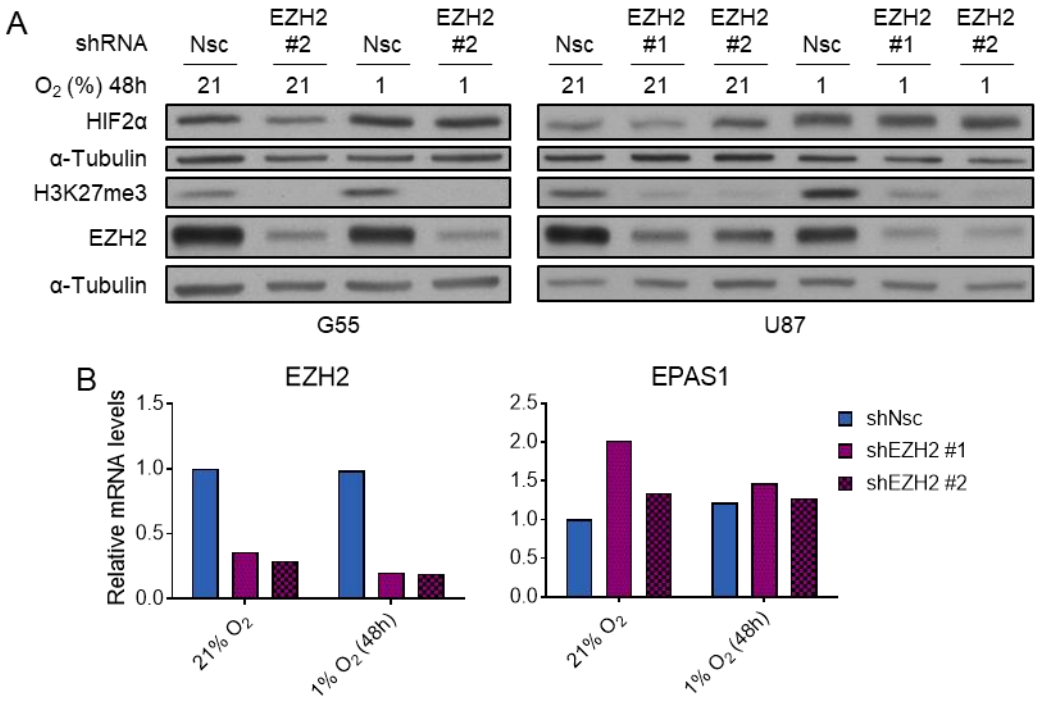

Figure 2.6: shRNA-mediated knockdown of EZH2 in glioblastoma cell lines and its effect on HIF2α protein and EPAS1 mRNA levels.

G55 (n=4) and U87 (n=1) cells were exposed to normoxic (21% O_2) or hypoxic (1% O_2) conditions for 48 hours. **A)** Western blots showing EZH2 knockdown efficiency and its effect on HIF2α levels. **B)** RT-qPCR analysis showing corresponding mean mRNA levels relative to HPRT1. *Nsc: non-silencing control.*

also returned toward baseline.

To determine whether the difference between siNsc (non-silencing control) and siEZH2 cells in EPAS mRNA levels was significantly reduced over time in PC-9 cells, the siNsc/siEZH2 ratio was calculated and compared at the different time points. This ratio was significantly smaller at day 11 compared to day 4 ($p = 0.0019$). In addition, the siNsc/siEZH2 ratio was substantially reduced on day 15 compared to the ratios on days 4 and 11. As two biological replicate samples were analyzed on day 15, no statistical tests were performed using the day 15 data.

Together, these findings show that HIF2α protein/EPAS1 mRNA expression recovers in parallel with EZH2 re-expression, consistent with a direct, reversible dependency of HIF2α transcription on EZH2 availability.

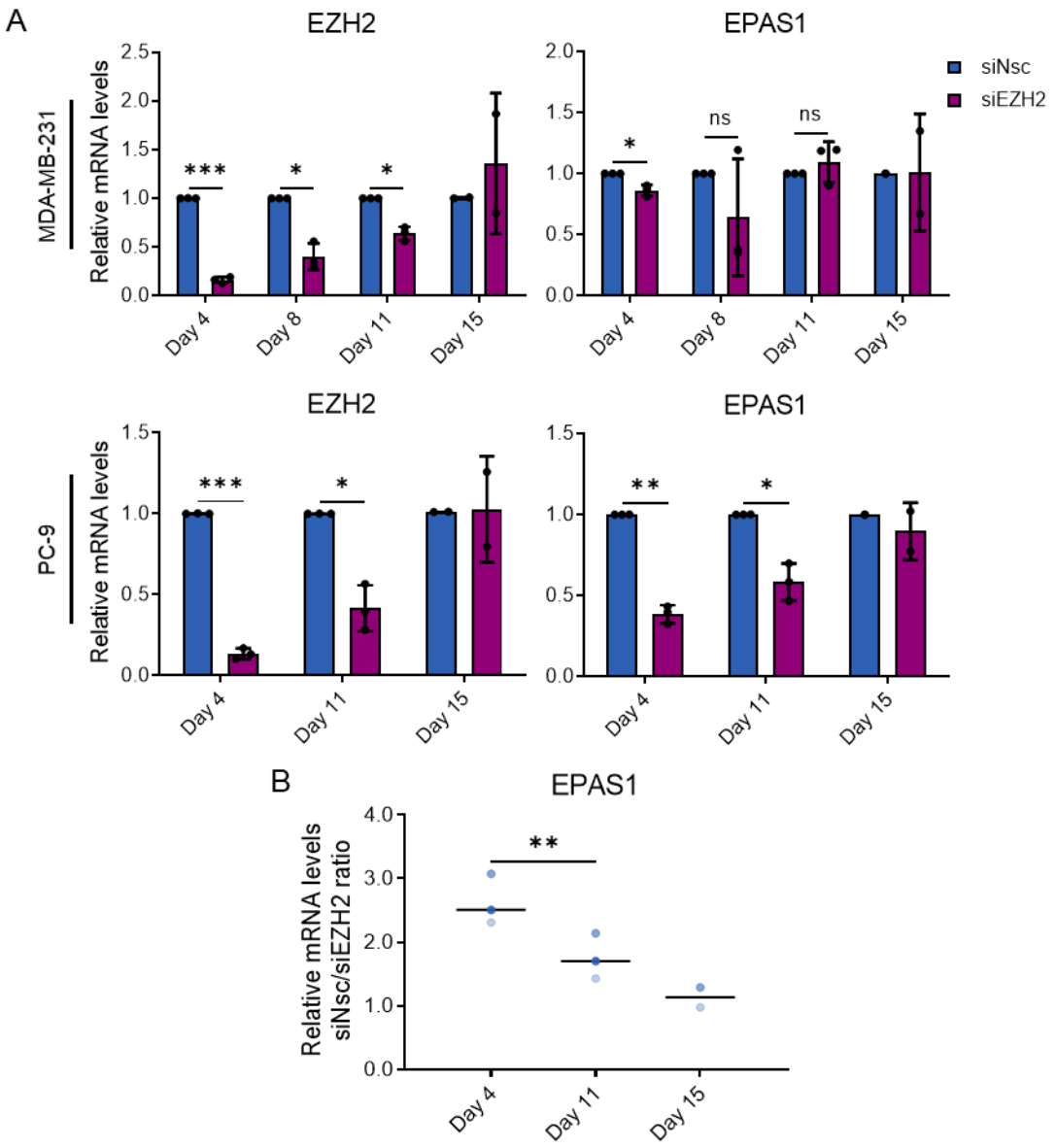

Figure 2.7: The effect of EZH2 restoration on EPAS1 levels after transient EZH2 knockdown. MDA-MB-231 and PC-9 cells were transfected with siEZH2 for 48 hours and kept under normoxic (21% O_2) conditions (day 4) (n=3). The cells were cultured and harvested again on day 8 (n=3), 11 (n=3), and day 15 (n=2) **A)** RT-qPCR analysis showing EZH2 and EPAS1 mRNA levels relative to ACTB at the different time points. **B)** The ratio of the siNsc and siEZH2 relative mRNA levels of EPAS1 at the different time points in PC-9 cells. The data are presented as mean ± SD. Statistical significance was determined using a two-tailed paired t-test. ns $p > 0.05$; * $p < 0.05$; ** $p < 0.01$; *** $p < 0.001$. *Nsc: non-silencing control.*

2.2. Mechanisms of HIF2α regulation by EZH2

2.2.1. HIF2α reduction upon EZH2 knockdown is independent of the PRC2 and EZH2's methyltransferase function

The previous experiments demonstrated that HIF2α expression depends on EZH2 and could be restored upon EZH2 re-expression. To elucidate the underlying mechanisms, I aimed to investigate the potential involvement of the PRC2 in the regulation of HIF2α. To this end, I depleted the other PRC2 subunits EED and SUZ12 in MDA-MB-231 cells by using shRNA-mediated knockdown, creating stably transduced cells.

EZH2, SUZ12, and EED were effectively knocked down, and in all cases, this resulted in the depletion of H3K27me3 levels (Fig. 2.8A). Interestingly, EZH2 protein levels were decreased upon EED and SUZ12 knockdown, while mRNA levels remained stable (Fig. 2.8A,B). SUZ12 protein levels were decreased upon EZH2 knockdown. Under normoxic conditions, SUZ12 mRNA levels were also significantly reduced ($p = 0.0221$), whereas, under hypoxic conditions, this reduction was not significant ($p = 0.1380$) (Fig. 2.8A,B). These results suggest the existence of a bi-directional regulatory system among the subunits.

Most importantly, HIF2α protein levels under hypoxic conditions and EPAS1 mRNA levels under normoxic and hypoxic conditions were exclusively reduced in EZH2 knockdown cells ($p = 0.0360$, $p = 0.0149$, respectively) (Fig. 2.8A,B).

These results show that EZH2 regulates HIF2α independent of the PRC2. However, the regulation may still depend on its catalytic, methyltransferase function. To test if the regulation of HIF2α by EZH2 is methyltransferase-dependent, I treated MDA-MB-231 and PC-9 cells with different concentrations of the EZH2 inhibitor GSK126 under normoxic or hypoxic conditions. GSK126 is a SAM-competitive inhibitor that binds to the SAM binding site within the SET domain of EZH2. By preventing the transfer of the methyl groups to H3K27, it efficiently blocks the methyltransferase function of EZH2 in a highly selective manner (147,232). Thus, it inhibits only the methyltransferase function while leaving EZH2 protein levels intact. In both cell lines, GSK126 indeed only reduced H3K27me3 levels and barely changed EZH2 levels (Fig 2.9A).

More importantly, HIF2α levels remained largely unchanged and only a slight decrease was observed with 1 μM GSK126, the highest concentration used, in PC-9 cells (Fig

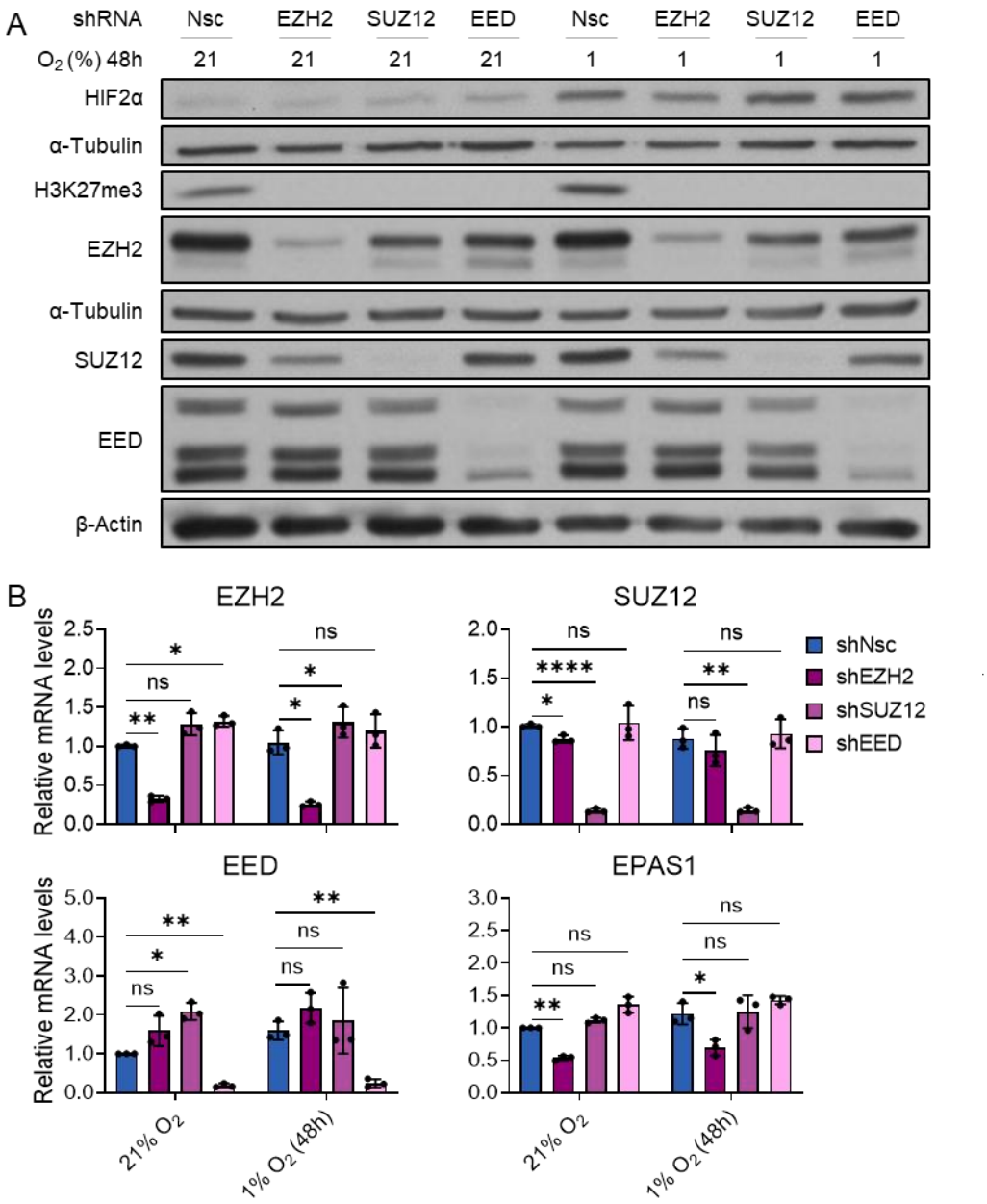

Figure 2.8: shRNA-mediated knockdowns of PRC2 subunits and their effect on HIF2α protein and EPAS1 mRNA levels.

MDA-MB-231 cells were kept under normoxic (21% O_2) or hypoxic (1% O_2) conditions for 48 hours (n=3). **A)** Western blot showing EZH2, SUZ12, and EED knockdown efficiency and its effect on HIF2α levels. **B)** RT-qPCR analysis showing corresponding mRNA levels relative to HPRT1. The data are presented as mean ± SD. Statistical significance was determined using repeated-measures one-way ANOVA with Dunnett's post-hoc test. ns $p > 0.05$; * $p < 0.05$; ** $p < 0.01$; **** $p < 0.0001$. *Nsc: non-silencing control*.

2.9A). In MDA-MB-231 cells treated with 0.2 μM GSK126 under normoxic conditions, a small but significant increase in EZH2 mRNA levels was observed ($p = 0.0439$). In all other conditions in MDA-MB-231 and PC-9 cells, no significant differences were detected (Fig. 2.9B). These results suggest a function of EZH2 in the regulation of

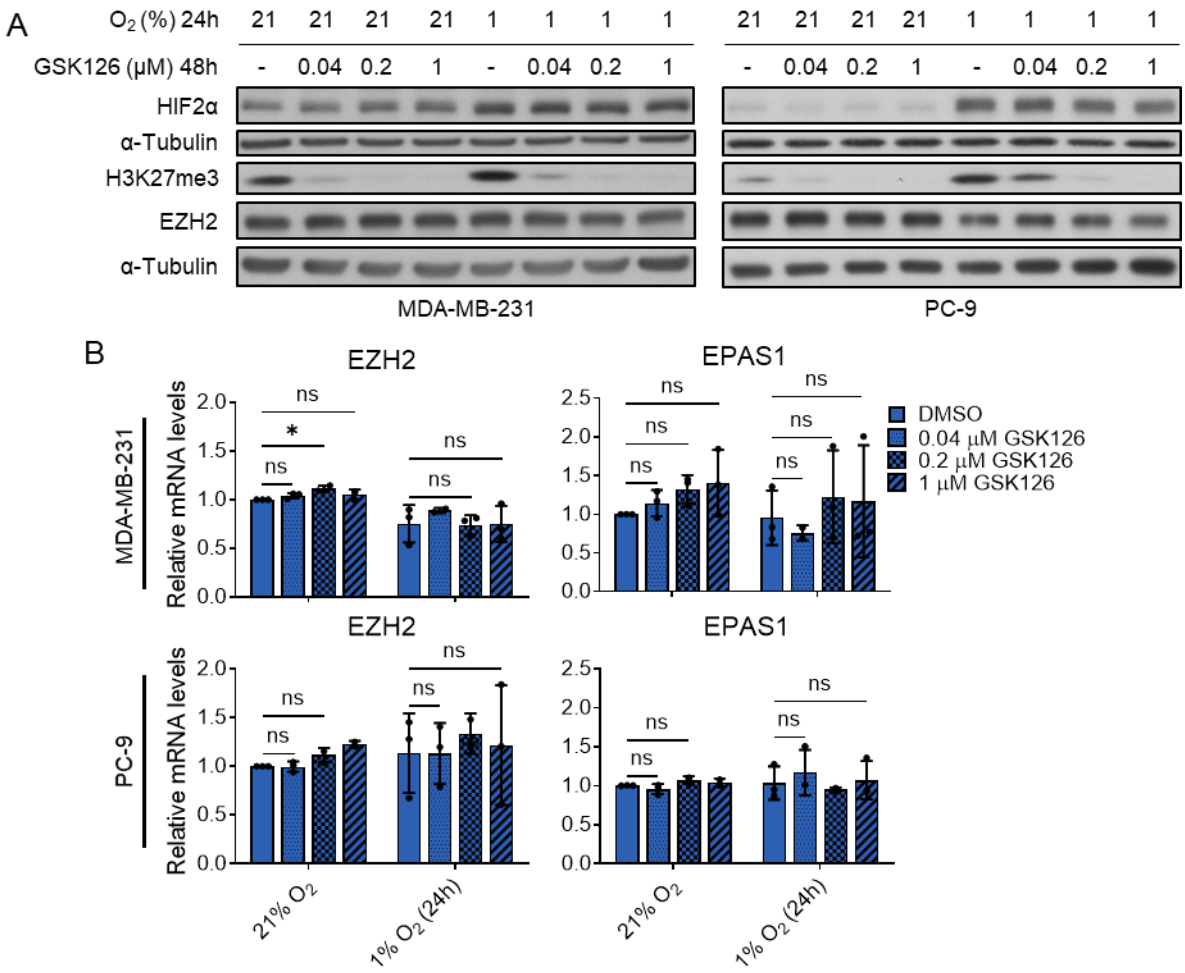

Figure 2.9: Pharmacological inhibition of the methyltransferase function of EZH2 and its effect on HIF2α protein and EPAS1 mRNA levels.

MDA-MB-231 and PC-9 cells were treated with different concentrations of GSK126 for 48 hours and were kept under normoxic (21% O_2) or hypoxic (1% O_2) conditions for 24 hours (where statistical results are shown n=3, otherwise n=2). **A)** Western blots showing GSK126 treatment efficiency and its effect on HIF2α levels. **B)** RT-qPCR analysis showing corresponding mRNA levels relative to HPRT1. The data are presented as mean ± SD. Statistical significance was determined using repeated measures one-way ANOVA with Dunnett's post-hoc test. ns $p > 0.05$; * $p < 0.05$; ** $p < 0.01$; *** $p < 0.001$. *Nsc: non-silencing control.*

HIF2α that is independent of the methyltransferase activity of EZH2.

Together, these results indicate that EZH2 does not require its methyltransferase function and that the other PRC2 subunits are dispensable for EZH2-dependent regulation of HIF2α.

2.2.2. The EZH2 depletion-induced downregulation of HIF2α does not depend on EZH1

The previous results show a PRC2-and methyltransferase-independent regulation of HIF2α by EZH2. However, since EZH1, the paralog of EZH2, may replace EZH2's functions (233,234), EZH1 levels were also investigated.

EZH2 knockdown in MDA-MB-231 cells led to a strong increase in EZH1 protein levels (Fig. 2.10A), prompting further investigation of a potential repressive role for EZH1 in HIF2α regulation.

To test this hypothesis, I knocked down EZH1 using siRNA in MDA-MB-231 shNsc (non-silencing control) and shEZH2 cells. EZH1 knockdown did not affect HIF2α protein levels in shNsc and shEZH2 cells (Fig. 2.10B). However, a surprising decrease in EPAS1 mRNA levels was found in shNsc and shEZH2 cells, while only a small decrease was observed in HIF1A mRNA levels (Fig. 2.10C).

Although the role of EZH1 in HIF regulation warrants further investigation, the results exclude the possibility that HIF2α downregulation upon EZH2 depletion is accomplished by EZH1 induction.

2.2.3. EZH2 does not regulate HIF2α through Notch1 signaling

Upon establishing that EZH2 does not require the PRC2 components or its methyltransferase function, I investigated another potential regulator of HIF2α. Notch1 is one of four cell-surface receptors regulating the Notch signaling pathway. Upon ligand binding, Notch1 undergoes cleavage by γ-secretase, releasing the Notch1 intracellular domain (NICD), which translocates to the nucleus where it interacts with DNA-binding proteins such as recombination signal binding protein for immunoglobulin kappa J region (RBPJ), and induces gene expression (235). NOTCH1 is a target gene of the transcriptional activator function of EZH2 (130,131) and has been shown to be involved in HIF2α regulation (236). In addition, a research group at JLU found occupancy of RBPJ at the EPAS1 promoter. This information makes Notch1 a plausible component of the EZH2-HIF2α regulatory axis.

Since EZH2 has been shown to bind to the NOTCH1 promoter in MDA-MB-231 cells and regulate Notch signaling (130), it is to be expected that NOTCH1 mRNA levels decrease upon EZH2 knockdown. Unexpectedly, NOTCH1 mRNA levels were

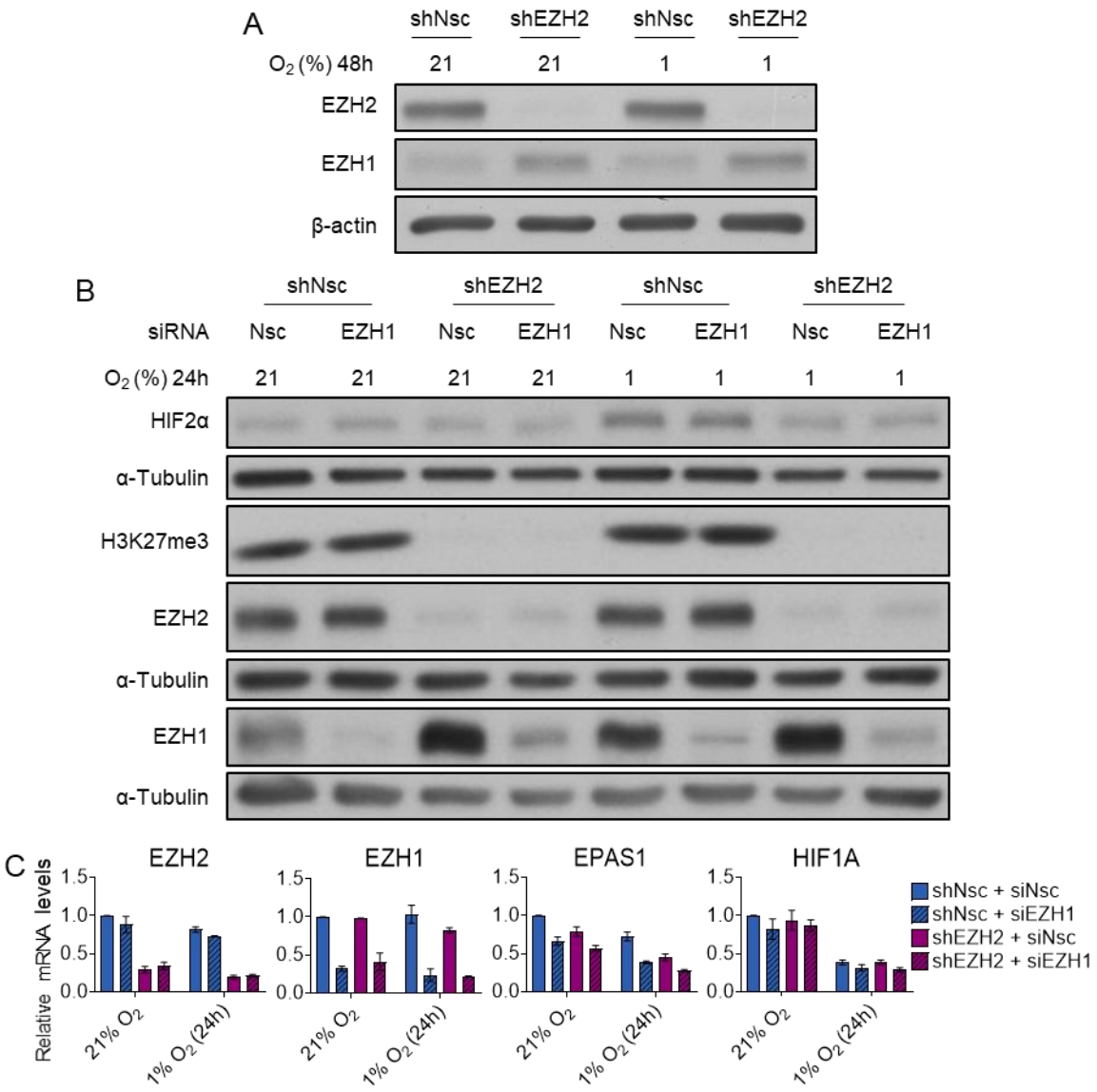

Figure 2.10: EZH1 upregulation upon EZH2 knockdown and siRNA-mediated knockdown of EZH2 and its effect on HIF2α protein and EPAS1 mRNA levels.

A) Western blot showing EZH1 levels upon EZH2 knockdown in MDA-MB-231 cells kept normoxic (21% O_2) or hypoxic (1% O_2) conditions for 24 hours (n=3). **B)** Western blot showing EZH1/2 knockdown efficiency and its effect on HIF2α (n=2). **C)** RT-qPCR analysis showing corresponding mRNA levels relative to HPRT1 (n=2). The data are presented as mean ± SD. *Nsc: non-silencing control.*

unchanged upon EZH2 knockdown under normoxic and hypoxic conditions in my experiments (Fig. 2.11A).

To further test the potential role of Notch1 in the regulation of HIF2α, I pharmacologically blocked Notch signaling by using the γ-secretase inhibitor DAPT (237). Cleaved Notch1 (active) protein levels and hairy and enhancer of split 1 (HES1) mRNA levels, a Notch1 target gene (238), were downregulated upon DAPT treatment, confirming efficient inhibition (Fig. 2.11B,C). EZH2 levels were unresponsive to DAPT

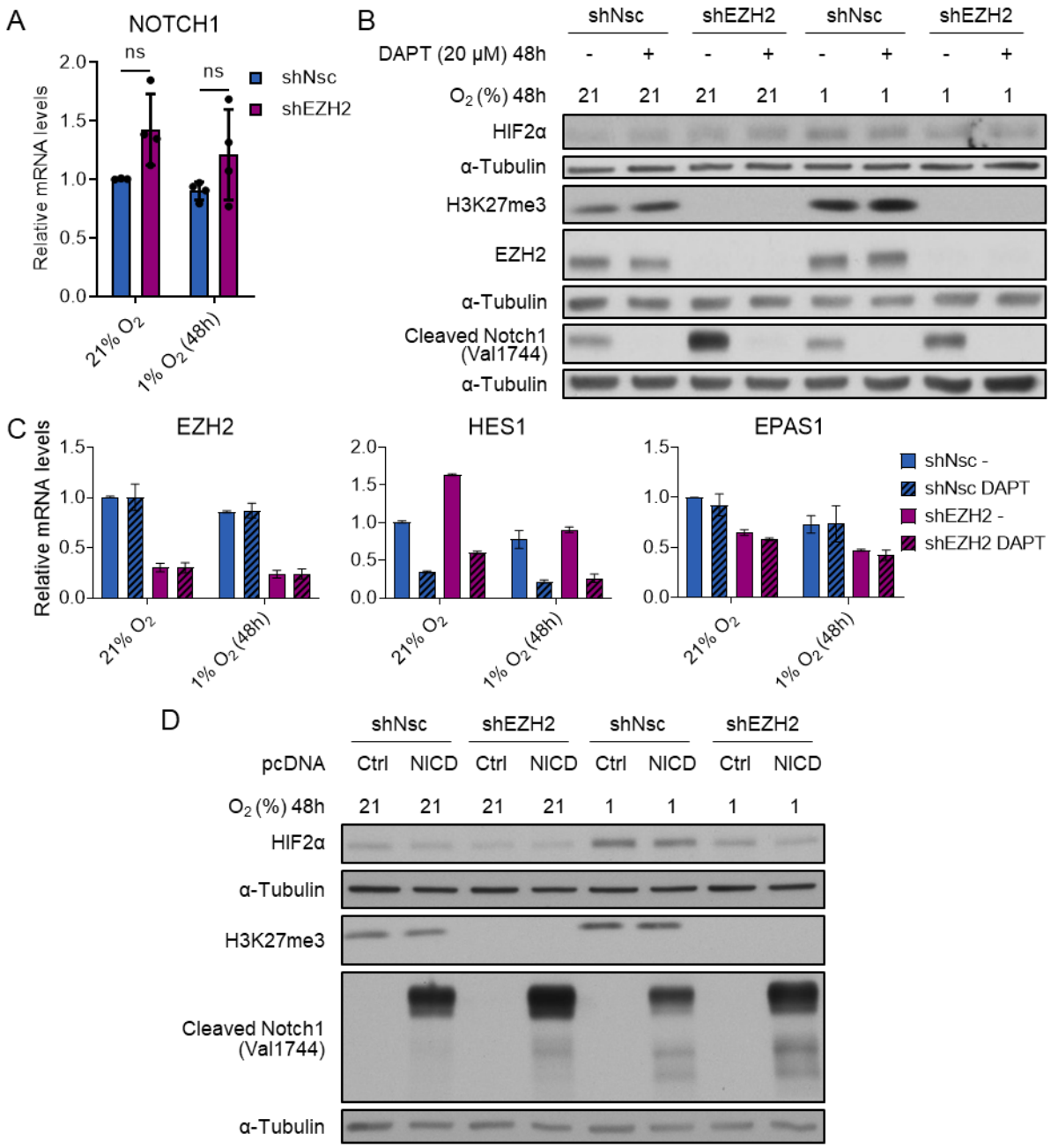

Figure 2.11: The role of Notch1 in HIF2α regulation.

MDA-MB-231 were kept under normoxic (21% O_2) or hypoxic (1% O_2) conditions for 48 hours. **A)** RT-qPCR showing NOTCH1 levels in MDA-MB-231 shNsc and shEZH2 cells (n=3). **B)** Western blot showing the efficiency of 48-hour DAPT (20 μM) treatment and its effect on HIF2α levels (n=2). **C)** RT-qPCR analysis showing corresponding mRNA levels relative to HPRT1 (n=2). **D)** Western blot showing Notch intracellular domain (NICD) overexpression efficiency and its effect on HIF2α levels (n=1). The data are presented as mean ± SD. ns $p > 0.05$. *Nsc: non-silencing control.*

treatment. HIF2α protein levels were also not affected by DAPT treatment, while EPAS1 mRNA levels showed only a very minor decrease (Fig. 2.11B,C). Additionally, Notch1 NICD protein levels were induced upon EZH2 knockdown (Fig. 2.11B). These results suggest that Notch1 is not a regulator of HIF2α in MDA-MB-231 cells.

To further exclude Notch1 as a HIF2α regulator, I transiently overexpressed the Notch1 ICD in MDA-MB-231 cells. Western blot analyses of the cell lysates showed that while overexpression was efficient, HIF2α levels remained unchanged (Fig. 2.11D), confirming that EZH2 does not regulate HIF2α via or with Notch1.

2.2.4. EZH2 does not regulate HIF2α by affecting the elongation

EZH2 has been implicated in transcriptional elongation through indirectly affecting RNA Pol II transcription under heat shock responses (239). To test whether EZH2 similarly regulates EPAS1 transcription, I examined RNA Pol II occupancy across the gene.

To this end, I designed and tested four primer pairs within exon 1 and intron 1, which span up to 28 kb of the EPAS1 gene (Fig. 2.12A), and analyzed the occupancy of RNA Pol II at these loci using ChIP-qPCR. Figure 2.12B shows a significant difference in RNA Pol II occupancy at locus #1 between MDA-MB-231 shNsc and shEZH2 cells ($p = 0.0347$), supporting the hypothesis that EZH2 could regulate EPAS1 as a transcriptional regulator. As expected, the occupancy at the other loci (#2-4) was reduced compared to #1 (Fig. 2.12B). To determine whether EZH2 truly affects elongation, I compared the occupancy between MDA-MB-231 shNsc and shEZH2 cells at loci #2, #3, and #4 relative to locus #1. No significant differences were observed, suggesting that EZH2 does not affect the elongation of EPAS1 in MDA-MB-231 cells.

2.2.5. EZH2 binds to the EPAS1 promoter region

The previous results already suggested a role for EZH2 in transcriptional control of EPAS1. However, these results do not address the direct interaction of EZH2 with EPAS1. To study if EZH2 regulates EPAS1 in a direct manner by binding to the promoter region, another round of ChIP experiments was performed.

Sixty-five primer pairs covering different loci divided around the EPAS1 promoter region were designed and tested. The four primer pairs that worked efficiently ($R^2 > 0.95$ and efficiency between 90 and 110%) were employed in subsequent experiments (Fig. 2.13A). The occupancy of EZH2 (main target), RNA Pol II and H3K4me3 (active chromatin markers), and H3K27me3 (repressive chromatin and canonical EZH2 function marker) was investigated at the four genomic loci and the control genes myelin transcription factor 1 (MYT1), ribosomal protein L30 (RPL30), and NOTCH1 (Fig. 2.13B).

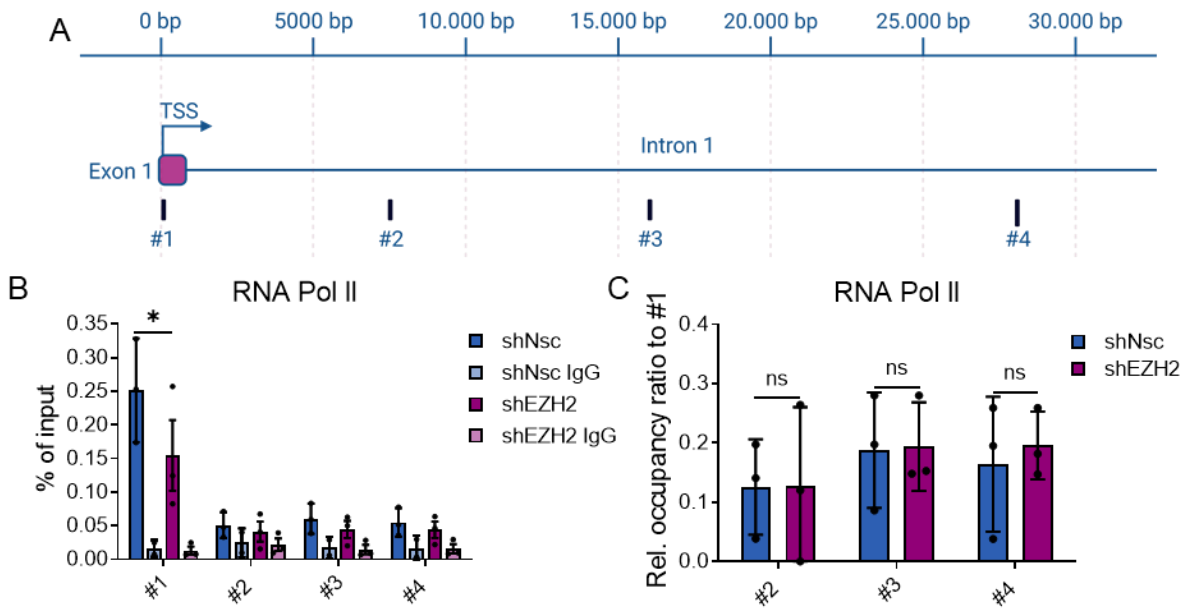

Figure 2.12: The role of EZH2 in EPAS1 elongation.

A) An overview of the four chosen loci within the EPAS1 gene. **B)** Uncorrected % of input of RNA Pol II binding in MDA-MB-231 shNsc and shEZH2 cells. % of input corrected for IgG (relative occupancy) was used for statistical testing (n=3). **C)** Relative occupancy ratio between locus #2, 3, and 4 compared to #1 (n=3). **Note:** One IgG measurement was missing for shNsc. The average from the other two experiments was taken to calculate the relative occupancy. The data are presented as mean ± SD. Statistical significance was determined using a two-tailed paired t-test. ns $p > 0.05$; * $p < 0.05$. *Nsc: non-silencing control.*

EZH2 occupancy in MDA-MB-231 shNsc cells at MYT1 (positive control for PRC2) was significantly higher than at RPL30 (negative control) ($p < 0.0001$), which corresponded with H3K27me3 occupancy ($p < 0.0001$), while RNA Pol II and H3K4me3 ChIP-qPCR signals were very low, near to the background. The EZH2 and H3K27me3 occupancies at MYT1 were abolished upon EZH2 knockdown ($p < 0.0001$). In accordance with the results from the Gonzalez *et al.*, study (130), a significantly higher ChIP-qPCR signal of EZH2 at the NOTCH1 promoter was detected in MDA-MB-231 shNsc cells compared to shEZH2 cells ($p < 0.0001$), which corresponded with RNA Pol II ($p = 0.0312$) and H3K4me3 ($p = 0.0038$), but not with H3K27me3 occupancy ($p < 0.0001$; data not shown in graph). These results confirmed that the antibodies and shRNA-mediated depletion of EZH2 are suitable experimental tools to obtain interpretable data from ChIP analyses.

From the four EPAS1 loci, significant EZH2 occupancy over RPL30 was exclusively found at the EPAS1 #4 locus ($p = 0.0175$), 1,723 bp upstream of the transcription start site (TSS). H3K4me3 occupancy corresponded with this finding ($p = 0.0009$). Although

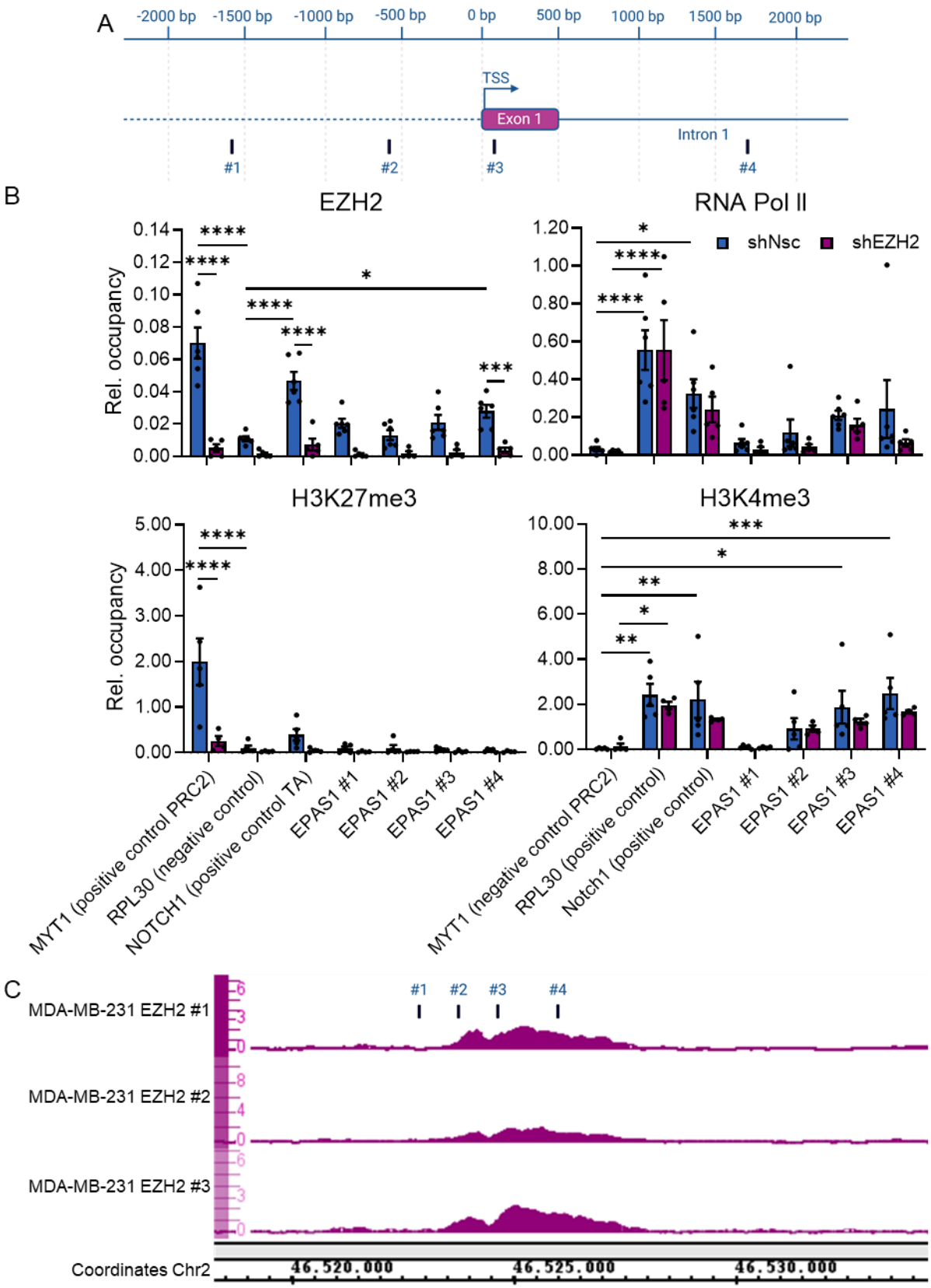

Figure 2.13: The occupancy of EZH2 at the EPAS1 promoter region.

A) An overview of the four selected loci within the EPAS1 gene. **B)** ChIP-qPCR data showing relative occupancies in MDA-MB-231 shNsc and shEZH2 cells of EZH2 (n=6, n=5, respectively), RNA Pol II (n=6, n=5, respectively), H3K27me3 (n=5, n=4, respectively), and H3K4me3 (n=5, n=4, respectively) under normoxic (21% O_2) conditions. **C)** ChIP-seq data showing EZH2 occupancy (enrichment relative

Figure 2.13: continued

to input) at the EPAS1 gene in biological triplicates derived from Dardis *et al.* (GSE223959) (128). The data in B are presented as mean ± SD. Statistical significance was determined using two-way ANOVA with Dunnet's or Sidak's post-hoc tests. ns $p > 0.05$; * $p < 0.05$; ** $p < 0.01$; *** $p < 0.001$; **** $p < 0.0001$. *Nsc: non-silencing control.*

RNA Pol II signal was detected at EPAS1 #4, the signal was not significantly higher compared to MYT1 (negative control) ($p = 0.1916$). H3K27me3 occupancy was near the background at all four EPAS1 loci tested, demonstrating PRC2-independent binding. In addition, the decrease of EZH2 occupancy upon EZH2 knockdown at EPAS1 #4 was significant ($p = 0.0008$). These findings suggest that EZH2 regulates EPAS1 in a direct manner as a transcriptional activator.

The possibility of EZH2 functioning as a transcriptional activator of EPAS1 is further supported by chromatin immunoprecipitation followed by sequencing (ChIP-seq) data from Dardis *et al.* (128). Their data show EZH2 occupancy at the EPAS1 promoter region, including EPAS1 #4, in MDA-MB-231 cells (Fig. 2.13C), as well as HIF2α downregulation upon siRNA-mediated EZH2 knockdown (GSE223959).

2.2.6. Src inhibition reduces EZH2 levels but does not consistently affect HIF2α

Upon establishing that EZH2 likely directly regulates EPAS1 as a transcriptional activator, the aim was to elucidate what causes EZH2 to switch from its canonical PRC2 and methyltransferase-dependent transcriptional repressor function to a transcriptional activator. Zhang *et al.* found that phosphorylation of EZH2 at Y696 by Src induces a transcriptional activator function of EZH2, which controls c-JUN gene expression in MDA-MB-231 BM cells (106). To test whether a Src-dependent switch in EZH2 function may play a similar role in EPAS1 gene expression, I blocked Src using Saracatinib, an ATP-competitive Src inhibitor (240), in MDA-MB-231 and PC-9 cells.

Both cell lines received Saracatinib treatment for 24 or 48 hours, and active Src (p-Src Tyr416) was reduced at both time-points, confirming efficient inhibition of Src activity under normoxic and hypoxic conditions (Fig. 2.14A). Surprisingly, EZH2 protein levels were also reduced in both cell lines (Fig. 2.14A). However, the EZH2 protein levels were inconsistent between experiments in MDA-MB-231 cells. In both cell lines, EZH2 mRNA levels were also reduced. The strongest decrease was observed in PC-9 cells, with levels dropping to 10-20% under normoxic conditions, whereas in MDA-MB-231

cells, levels were only reduced to 60-75% under both normoxic and hypoxic conditions. Interestingly, hypoxia also reduced EZH2 mRNA levels in PC-9 cells down to about 25% compared to normoxic conditions (Fig. 2.14B).

HIF2α protein levels were not decreased in MDA-MB-231 cells upon Saracatinib treatment and mRNA levels were, surprisingly, even increased (Fig. 2.14A,B). However, in PC-9 cells, HIF2α levels were visibly reduced upon Saracatinib treatment under hypoxic conditions and mRNA levels were also reduced down to approximately 20% under normoxic conditions and under hypoxic conditions down to 30-40% (Fig. 2.14A,B). In summary, although pharmacological inactivation of Src reduced EZH2 levels, this effect correlated with decreased HIF2α protein and EPAS1 mRNA levels only in PC-9 cells. Thus, while Src-mediated phosphorylation of EZH2 at Y696 might enhance its transcriptional activator function, pharmacological Src inhibition with Saracatinib cannot be used to test the reverse effect experimentally, as it concurrently decreases EZH2 levels. Of note, the pronounced decrease in EZH2 protein and EPAS1 mRNA in PC-9 cells is consistent with the impact of genetic EZH2 depletion on HIF2α protein and EPAS1 mRNA levels in both PC-9 and MDA-MB-231 cells.

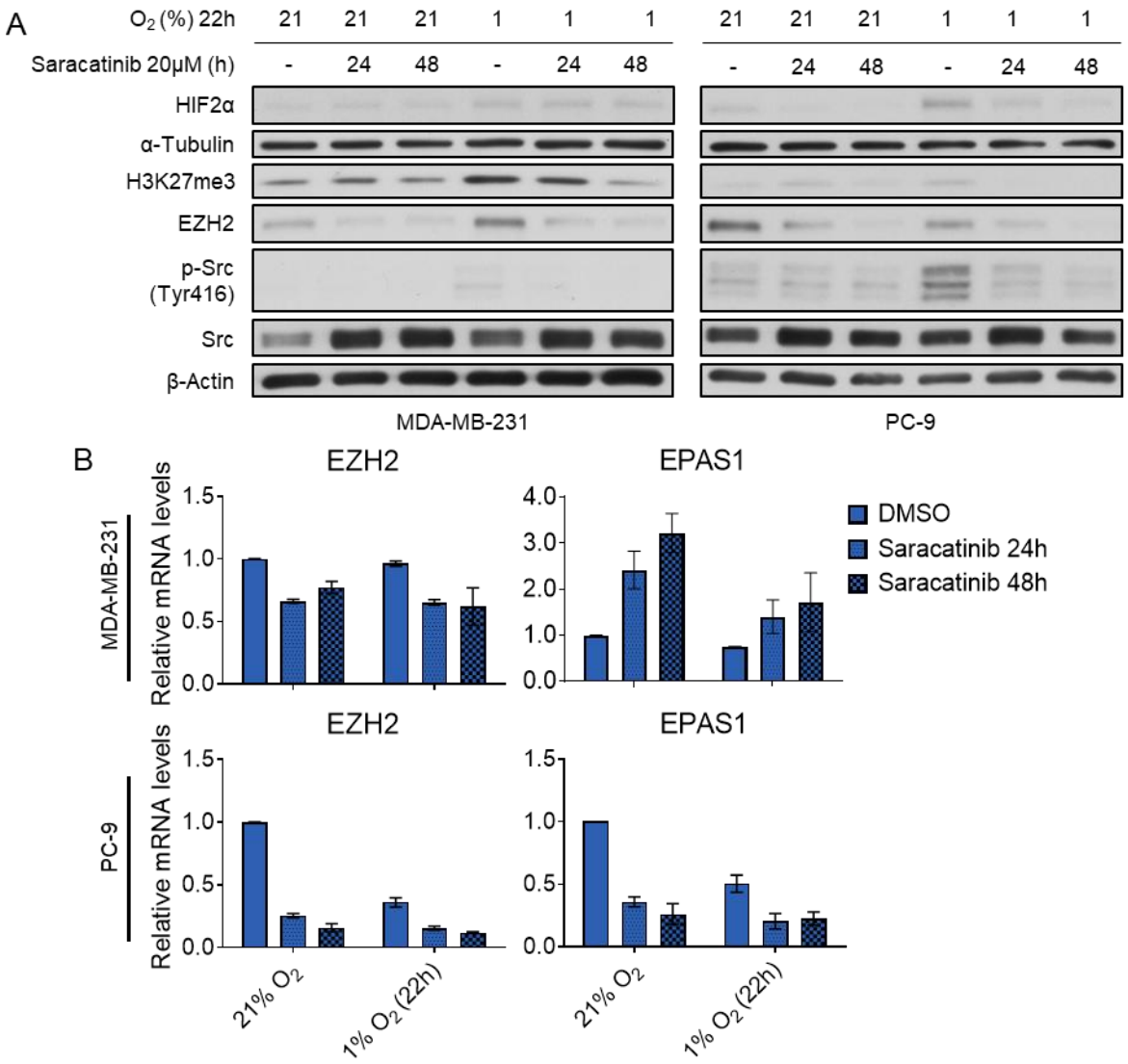

Figure 2.14: Pharmacological inhibition of Src and its effect on HIF2α protein and EPAS1 mRNA levels.

MDA-MB-231 and PC-9 cells were treated with 20 μM Saracatinib for 24 or 48 hours and cells were exposed to normoxic (21% O_2) or hypoxic (1% O_2) conditions for 22 hours (n=2). **A)** Western blots showing the treatment efficiency and its effect on HIF2α levels (n=2). **B)** RT-qPCR analysis showing corresponding mRNA levels relative to HPRT1 (MDA-MB-231) or ACTB (PC-9) (n=2). The data are presented as mean ± SD.

2.3. Biological consequences of EZH2 knockdown under chronic hypoxia and clinical significance

2.3.1. HIF2α target genes are downregulated upon EZH2 knockdown in MDA-MB-231 cells

To determine whether the reduced HIF2α protein levels affect the HIF signaling pathway, EPAS1 was knocked down in MDA-MB-231 and PC-9 cells using shRNA. mRNA levels of HIF1A and several HIF target genes were monitored by quantitative reverse transcription polymerase chain reaction (RT-qPCR), and HIF1α protein levels were assessed by western blotting.

In both cell lines, HIF2α protein and EPAS1 mRNA levels were reduced upon EPAS1 knockdown (Fig. 2.15A). In MDA-MB-231 cells, EPAS1 knockdown did not have an effect on HIF1A and hexokinase 2 (HK2) mRNA levels. Phosphoglycerate kinase 1 (PGK1), glucose transporter type 1 (GLUT1), VEGFA, and PHD3 levels were reduced (Fig. 2.15B). PGK1 and GLUT1 were considered as the most sensitive responders to EPAS1 depletion in the MDA-MB-231 experimental setups used, due to their increased expression under hypoxic conditions and the fact that changes in their mRNA levels were consistent across experiments.

In PC-9 cells, all potential target genes showed decreased levels upon EPAS1 knockdown, as well as HIF1A. However, the decrease was only large for PHD3. In addition, PHD3 levels showed a large increase under hypoxic conditions in PC-9 shNsc cells (Fig. 2.15B). Thus, PHD3 was considered as the most sensitive responder to EPAS1 depletion in PC-9 cells.

The next step was to analyze whether these HIF2α target genes were downregulated upon EZH2 knockdown in MDA-MB-231 and PC-9 cells.

In MDA-MB-231 shRNA-mediated knockdown of EZH2 was utilized and both GLUT1 and PGK1 were significantly downregulated upon EZH2 knockdown under normoxia ($p = 0.0007$, $p = 0.007$, respectively) and hypoxia ($p = 0.0004$, $p = 0.0398$, respectively) (Fig. 2.16A). Both targets were also significantly increased under hypoxic conditions in shNsc cells ($p = 0.0074$, $p = 0.0007$, respectively; data not shown in graph). These results suggest that EZH2 knockdown affects HIF2α downstream target gene expression.

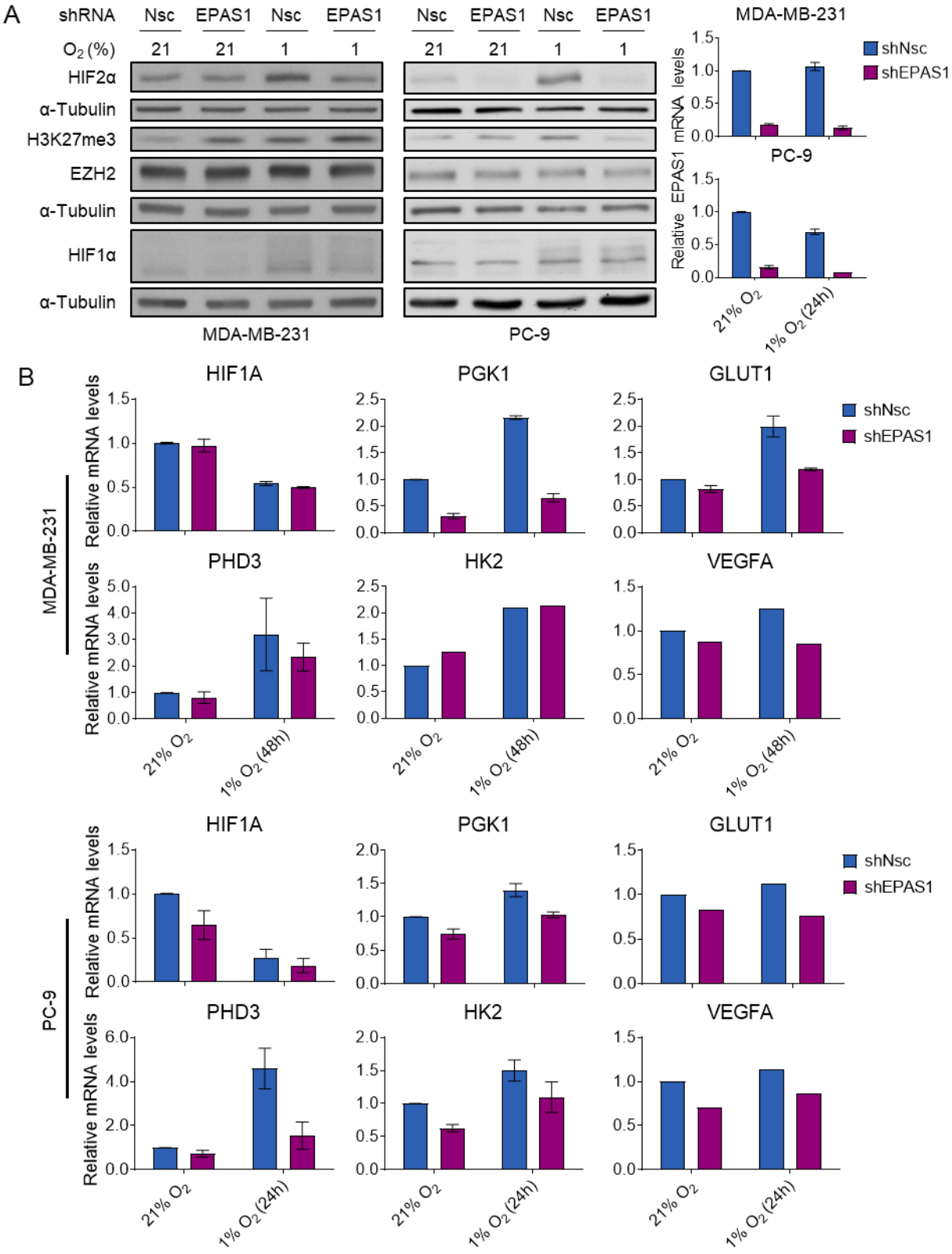

Figure 2.15: Identification of HIF2α target genes.

HIF2α was knocked down with shRNA in MDA-MB-231 (n=2) and PC-9 (n=2) cells, and were exposed to normoxic (21% O_2) or hypoxic (1% O_2) conditions for 48 or 24 hours, respectively. **A)** Western blots showing EPAS1 knockdown efficiency. RT-qPCR analyses show corresponding mRNA levels relative to HPRT1 (MDA-MB-231) or ACTB (PC-9). **B)** RT-qPCR analysis of potential HIF2α target genes. The data are presented as mean ± SD. *Nsc: non-silencing control*.

In PC-9 cells siRNA-mediated knockdown of EZH2 was utilized and PHD3 was not downregulated upon EZH2 knockdown (Fig. 2.16B). However, the results were inconsistent with two experiments showing a small decrease, and the third showing an almost two-fold increase in PHD3 levels upon EZH2 knockdown under hypoxic conditions. Further experiments in shNsc and shEZH2 PC-9 cells are therefore required to conclude about the effect of EZH2 depletion on HIF2α target genes, in which other potential target genes should also be monitored.

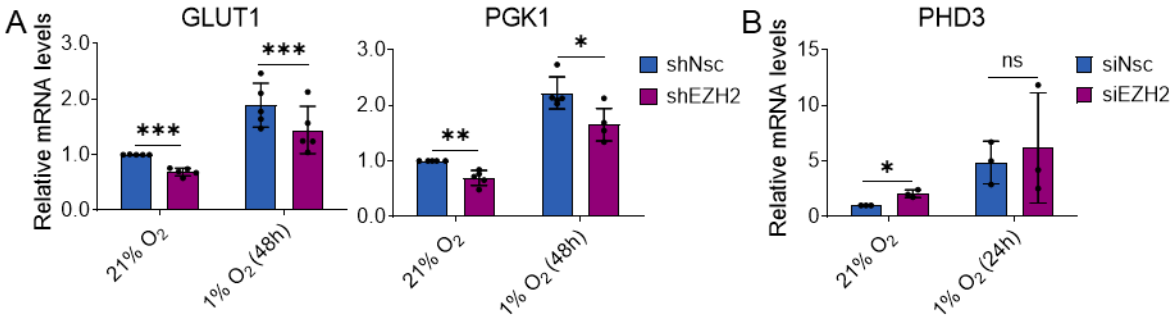

Figure 2.16: The effect of EZH2 knockdown on HIF2α target genes.

A) RT-qPCR analysis of HIF2α target gene mRNA levels relative to HPRT1 in MDA-MB-231 shNsc and shEZH2 cells under normoxic (21% O_2) or hypoxic (1% O_2) conditions for 48 hours (n=5). **B)** RT-qPCR analysis of HIF2α target mRNA levels relative to ACTB in PC-9 cells transfected with siNsc or siEZH2 for 48 hours under normoxic (21% O_2) or hypoxic (1% O_2) conditions for 24 hours (n=3). The data are presented as mean ± SD. Statistical significance was determined using a two-tailed paired t-test. ns $p > 0.05$; * $p < 0.05$; ** $p < 0.01$; *** $p < 0.001$; **** $p < 0.0001$. *Nsc: non-silencing control.*

2.3.2. EZH2 knockdown affects anchorage-dependent and -independent growth in PC-9 cells

Next the functional effect of EZH2 knockdown was investigated in PC-9 cells by monitoring cell growth under anchorage-dependent and -independent conditions.

Cells were kept under normoxic or hypoxic conditions for up to 72 hours starting on day 2 and cell counts were determined daily as described in section 4.3.1.1. PC-9 shEZH2 cells grew significantly slower compared to the shNsc cells under normoxic and hypoxic conditions on day 4 ($p = 0.0094$, $p < 0.0001$, respectively) (Fig. 2.17A). On day 5, the growth difference between shEZH2 and shNsc was no longer significant under normoxic conditions ($p = 0.0745$). Under hypoxic conditions shEZH2 cells were still growing slower compared to shNsc cells ($p = 0.0028$) (Fig. 2.17A). These results demonstrate that EZH2 affects PC-9 cell growth *in vitro*, potentially through HIF2α.

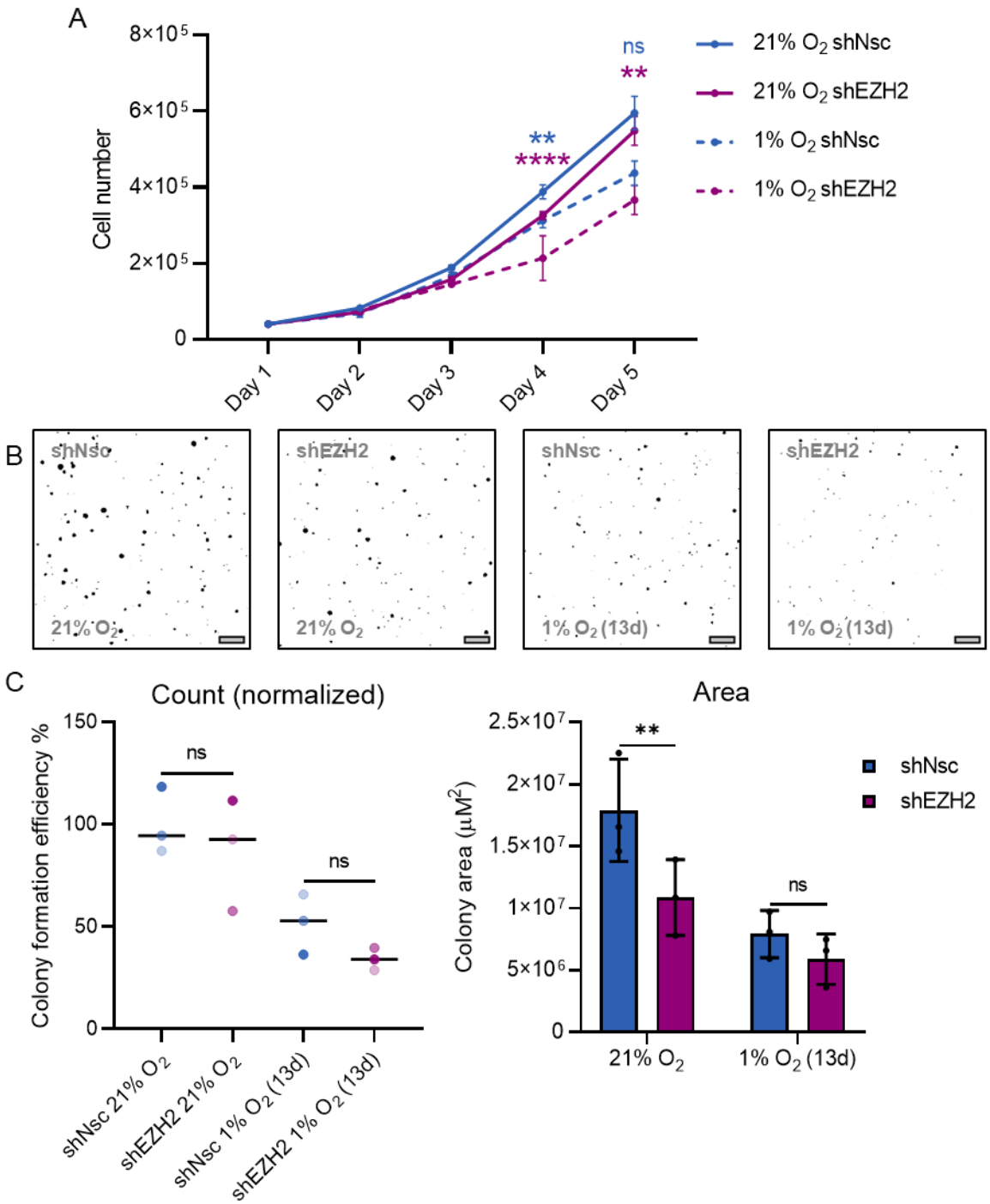

Figure 2.17: Effect of EZH2 knockdown on PC-9 anchorage-dependent and -independent growth. **A)** Cell growth curve of PC-9 shNsc and shEZH2 cells over 5 days. Cells were kept under normoxic (21% O_2) or hypoxic (1% O_2) conditions for up to 72 hours starting on day 2. Statistical analysis was performed on three technical triplicates within one representative experiment. Results were reproduced in a second independent experiment. **B)** Representative pictures of the crystal violet stained colonies. Bars represent 1 mm. **C)** Log2+1 counts normalized to shNsc 21% O_2 (left) and colony size (right) (n=3). The data are presented as mean ± SD. In **C,** the different color gradients represent the individual experiments. For **A**, two-way ANOVA with a Tukey's post-hoc test was used, and for **C**, repeated-measures two-way ANOVA with Sidak's post-hoc test was used to determine statistical significance. *Nsc: non-silencing control.*

To further study the functional consequences of EZH2 knockdown in PC-9 cells, a soft agar colony formation assay was performed to assess anchorage-independent growth capacity, an *in vitro* surrogate for tumorigenicity (241,242). Figure 2.17B shows representative images of the colonies.

I quantified both the number and size of the colonies to capture distinct aspects of tumorigenic potential. The colony count represents the proportion of cells capable of anchorage-independent growth, whereas colony size (area) reflects the proliferative capacity of the cells that underwent anchorage-independent growth. The colony count under normoxic conditions was similar between shEZH2 and shNsc cells ($p = 0.5546$) (Fig. 2.17C). In all three experiments, a lower number of colonies were formed upon EZH2 knockdown under hypoxic conditions, but together the difference was not significant ($p = 0.3639$) (Fig. 2.17C). Proliferation was significantly reduced in shEZH2 cells under normoxic conditions ($p = 0.0018$), but not significantly under hypoxic conditions ($p = 0.1246$) (Fig. 2.17D). Together, these results suggest that EZH2 depletion might interfere with the initiation and growth of anchorage-independent colonies, with HIF2α potentially contributing to colony formation.

2.3.3. HIF2α rescue strongly increases cell growth in EZH2-depleted PC-9 cells

After uncovering that EZH2 depletion affects cell growth in PC-9 cells, I aimed to determine whether this effect is HIF2α dependent under hypoxia. Thus, HIF2α was overexpressed in PC-9 shNsc and shEZH2 cells (Fig. 2.18A).

HIF2α overexpression significantly increased cell growth in both shNsc and shEZH2 cells ($p < 0.0001$; data not shown in graph). In the control cells, proliferation was significantly reduced upon EZH2 knockdown ($p = 0.0018$), supporting earlier cell growth results. The same was observed in HIF2α overexpressing cells ($p = 0.0016$) (Fig. 2.18B). However, when comparing the increase in cell growth between control and HIF2α overexpression in shNsc and shEZH2 cells, the increase was significantly greater in shEZH2 cells compared to shNsc cells ($p < 0.0001$) (Fig 2.18C). Thus, HIF2α overexpression has a clear impact on cell growth in EZH2 knockdown cells, in which HIF2α levels are lower. These data suggest that, at least in part, EZH2 affects cell growth through HIF2α regulation in PC-9 cells.

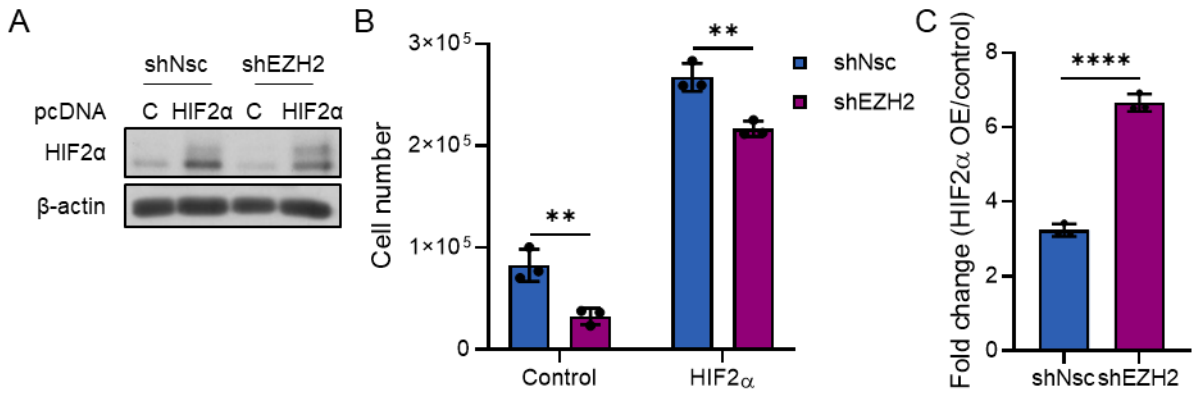

Figure 2.18: The effect of HIF2α overexpression on cell growth in control and EZH2-depleted PC-9 cells.

PC-9 shNsc and shEZH2 cells were transfected with pcDNA3 control (C) or pcDNA3.1 HIF2α WT for 24 hours and kept under hypoxic (1% O_2) conditions for 48 hours. **A)** Western blot showing the efficiency of the HIF2α overexpression (OE). **B)** Cell count 72 hours after the transfection. **C)** Cell growth fold change of HIF2α OE or rescue compared to control cells. The data are presented as mean ± SD. Repeated-measures two-way ANOVA with Sidak's post-hoc test was used on three technical triplicates within one representative experiment to determine statistical significance. Results were reproduced in a second independent experiment**.** ** $p < 0.01$; **** $p < 0.0001$.*; Nsc: non-silencing control.*

2.3.4. Cell invasion is reduced in EZH2-depleted MDA-MB-231 cells

MDA-MB-231 cells are known for their metastatic potential to the brain. Instead of relying on invasive animal experiments, an *ex vivo* organotypic brain slice culture method, as described by Uroz *et al.* (243), was used to examine the invasion of tumor cells in a brain microenvironment. A schematic overview of the procedure is shown in Figure 2.19A. The main readout of this experiment was the measurement of the invasion depth of tumor cells into the brain tissue based on green fluorescent protein (GFP) signal of the labeled tumor cells. First, the depths of the baseline (3-hour) and 48-hour time points were determined. Under normoxic conditions, there appeared to be a small, non-significant, increase in invasion by shEZH2 cells ($p = 0.9721$), whereas the trend was reversed under hypoxic conditions ($p = 0.8362$) (Fig. 2.19B).

Next, I analyzed the difference at the 48-hour time point invasion relative to baseline from the surface (first clear 4′,6-diamidino-2-phenylindole (DAPI) signal) or the first GFP signal. Under normoxic conditions, there was no significant difference between shNsc and shEZH2 cells measured from the surface or the first GFP signal ($p = 0.9001$, $p = 0.4715$, respectively). However, shEZH2 cells exhibited a significant decrease in invasion compared to shNsc cells under hypoxic conditions, as measured both from

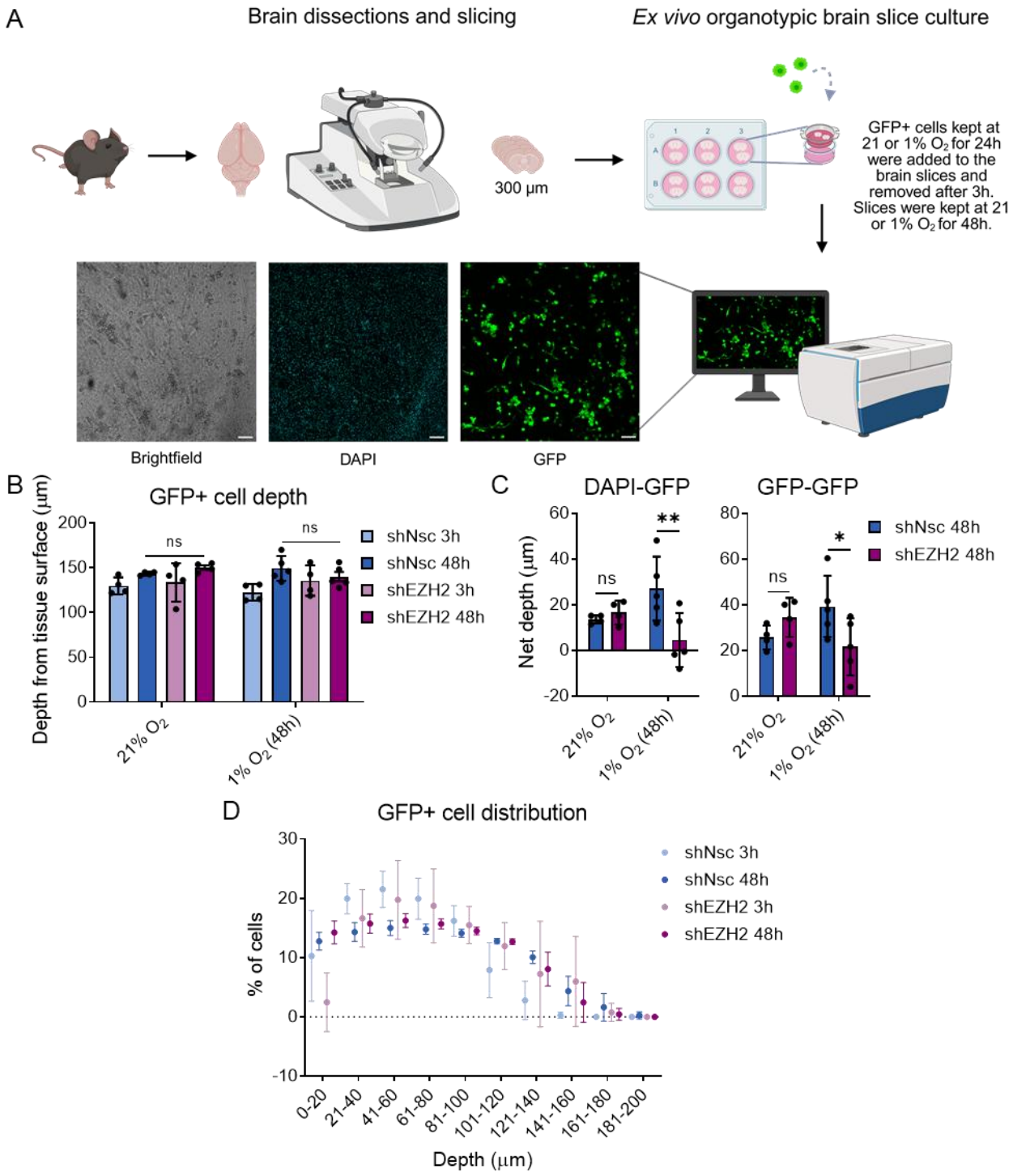

Figure 2.19: The effect of EZH2 knockdown on invasive capacity in MDA-MB-231 cells.

A) A schematic overview of the organotypic brain slice culture procedure. Created with BioRender.com. **B)** Invasion depth of MDA-MB-231 shNsc and shEZH2 cells at 3 hours (baseline) (n=4) and 48 hours (n=5) under normoxic (21% O_2) or hypoxic (1% O_2) conditions based on GFP signal from the start of the tissue surface determined by DAPI signal. **C)** Net invasion calculated by subtracting the mean 3 hours depth from the 48 hours depth starting from the tissue surface (left) or the first GFP signal (right). **D)** Cell percentage over different depths based on Log2+1 values. The data are presented as mean ± SD. Two-way ANOVA with Sidak's post-hoc test was used to determine statistical significance. ns > 0.05, ** $p < 0.01$. The experiments were performed in collaboration with Nazli Salik. *Nsc: non-silencing control.*

the surface and from the first GFP signal ($p = 0.0068$, $p = 0.0430$, respectively) (Fig. 2.19C).

To further understand this effect, I analyzed the distribution of GFP-positive cells across tissue depth under hypoxic conditions. While most cells in all conditions remained at depths between 21 and 100 µm, a small subpopulation of MDA-MB-231 shNsc cells invaded deeper into the tissue (Fig. 2.19D), although no statistical difference was found (data not shown in graph). This cell population appeared to cause the increased net invasion observed in shNsc cells. In addition, more 48-hour time point cells than baseline cells were present near the slice surface. Together these results suggest that EZH2 contributes to overall invasion capacity under hypoxic conditions, potentially through the regulation of HIF2α.

2.3.5. High EZH2 and EPAS1 expression is associated with poor prognosis in breast cancer patients

To explore the clinical relevance of my findings, publicly available RNA sequencing (RNA-seq) data from breast cancer patients were analyzed using the Kaplan-Meier Plotter (244). Kaplan-Meier survival curves revealed that high mean expression of EPAS1-EZH2 was associated with poorer overall survival in breast cancer patients receiving endocrine treatment but no chemotherapy as shown in Figure 2.20. This result was reversed in the same patient cohort for mean EPAS1-SUZ12 or EPAS1-EED expression. No EPAS1-EZH2-specific effect on survival was observed in other patient cohorts. These results support the notion that EZH2 and HIF2α may cooperate to promote aggressive tumor behavior under specific cancer settings, consistent with the previous functional findings.

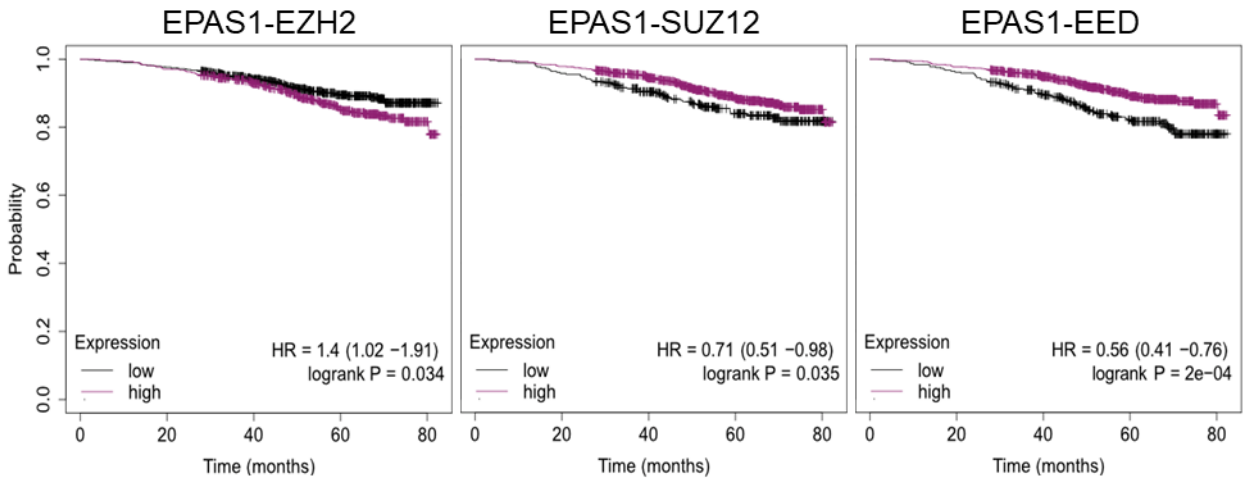

Figure 2.20: Kaplan-Meier plots showing the relationship between overall survival and the mean expression of EPAS1 plus individual PRC2 subunits in breast cancer patients.

The mean expression of EPAS1-EZH2, EPAS1-SUZ12, or EPAS1-EED was used to create the survival curves of endocrine therapy but no chemotherapy treated breast cancer patients with the Kaplan-Meier plotter. RNA-seq data from breast cancer patients were used (244). *HR: Hazard ratio.*

3. Discussion

EZH2 and HIF2α are critical regulators of cancer progression in multiple tumor types, including breast and lung cancer. The oncogenic roles of EZH2 involve both its methyltransferase activity and non-canonical functions, which contribute to increased cancer cell proliferation and metastatic potential (98,101–106,108,109). Likewise, HIF2α promotes tumor progression by modulating diverse mechanisms essential for cancer cell growth and metastasis formation (49,52,192–195,209–212). In this study, a novel regulatory link between EZH2 and HIF2α was elucidated.

3.1. HIF dynamics and the effect of EZH2 knockdown on HIFs

3.1.1. Determining the HIF dynamics in MDA-MB-231 and PC-9 cells

The reduction of HIF2α protein levels upon stable shRNA-mediated EZH2 depletion was originally identified in our laboratory by Sandra Baumgart in MDA-POR cells subjected to cycling intermittent hypoxia treatment (30 cycles of 48 hours 1% O_2 + 48 hours of 21% O_2, as established by Omelyan Trompak (245)), followed by an additional 48 hours 1% O_2 treatment. MDA-POR cells are derivatives of MDA-MB-231 cells that were generated in our laboratory and extensively characterized. POR (**p**Lenti6-CMVp-**O**DD/FLuc-SV40p-**R**Luc) is a plasmid encoding a hypoxia-responsive reporter protein consisting of a fusion of firefly luciferase and HIF2α-ODD, expressed under the control of a CMV promoter, as well as a hypoxia non-responsive Renilla luciferase control protein expressed under the control of an SV40 promoter (245,246). MDA-MB-231 cells were transduced with viruses containing this plasmid and a single-cell clone was picked. The resulting MDA-POR cells were then subjected to cycling intermittent hypoxia treatment. To rule out the possibility that EZH2-dependent changes in HIF2α levels depend on cycling intermittent hypoxia treatment, also untreated MDA-POR cells were examined by Isabel Schröter in our laboratory (247). The results of this work showed that depletion of EZH2 reproducibly leads to reduced HIF2α protein levels and EPAS1 mRNA levels in MDA-POR cells kept under hypoxic conditions for 48 hours, regardless of prior cycling intermittent hypoxia treatment, while HIF1α protein and HIF1A mRNA levels are not reproducibly affected under the same condition. The results obtained in the same study in A549 lung adenocarcinoma and G55

glioblastoma cells were less clear with regard to the HIF2α-specific effects of EZH2 depletion. In G55 cells, a reduction in HIF1α protein levels was observed, while HIF1A mRNA levels fluctuated in the individual experiments. The reduction in EPAS1 mRNA levels following EZH2 knockdown was less consistent in G55 cells than in MDA-POR cells, although a reduction in HIF2α protein levels was observed in the same experiments under hypoxia. In A549 cells, HIF1α protein levels showed fluctuations in individual experiments, HIF1A mRNA was unchanged, while HIF2α protein and EPAS1 mRNA levels were mildly reduced after a lower-efficiency EZH2 knockdown.

Taken together, the initial observations regarding specific HIF2α protein and EPAS1 mRNA regulation were made in the shEZH2 and shNsc derivatives of a single cell clone from the MDA-POR cell line, which could behave differently from the MDA-MB-231 parental cells (248). Furthermore, hypoxia treatment was limited to a setting of 1% O_2 for 48 hours in these experiments. One issue with hypoxia research is that there is no consensus on what constitutes acute versus chronic hypoxia in terms of timing. Some describe only a few hours as chronic hypoxia, whereas others consider more than 48 hours as chronic hypoxia (249,250).

It is well established that a time-dependent HIF switch occurs, where HIF1α predominates during the acute phase and HIF2α during the chronic phase of hypoxia (37). Since a hypoxia time-course experiment had not been performed in any derivative of the MDA-MB-231 cell line, the kinetic changes of HIF protein and mRNA levels were unknown. Thus, I determined the HIF dynamics in the MDA-MB-231 TNBC and PC-9 lung adenocarcinoma cell lines. The cell lines were selected based on initial tests of the effect of EZH2 depletion on HIF2α. These initial findings were considerably expanded later, as described in section 2.1.2 and discussed further in section 3.1.2. The aim was to find out which time-points were most suitable, especially since we did not know whether HIF1α, the acute hypoxia responder, could also be affected by EZH2 knockdown, and when and how long HIF2α levels peak in these cell lines.

As shown in Figure 2.1, there are marked differences in HIF dynamics between the two cell lines. Even though the particular setup shown in Figure 2.1 was only performed once, several other time-point experiments were performed in MDA-MB-231 shNsc and PC-9 shNsc cells, all showing similar results except for some small variations in HIF1α. Clearly increased HIF2α levels were detectable in parental MDA-MB-231 and

shNsc cells under hypoxic conditions for 24 and 48 hours, and in PC-9 cells for 24 hours. Generally, the changes in HIF1α levels showed a decline after 8 hours.

When comparing the cell lines, HIF2α levels were found to be less responsive to 1% O_2 treatment in MDA-MB-231 cells compared to PC-9 cells time wise. However, HIF2α levels decreased earlier in PC-9 cells than MDA-MB-231 cells. This difference in kinetics between the cell lines complicates the distinction between acute and chronic hypoxia. However, in both cell lines the HIF switch was observed.

Based on these findings, subsequent experiments involving 1% O_2 treatment were standardized as follows: MDA-MB-231 cells were generally exposed to hypoxia for 24 or 48 hours, while PC-9 cells were treated for 24 hours for regulatory experiments. Throughout this study, hypoxia treatment lasting 24 hours or longer is defined as chronic hypoxia, since HIF1α levels had decreased significantly in both key cell lines by this time point.

Another noteworthy observation across all hypoxia experiments was the induction of the repressive histone modification H3K27me3 under hypoxic conditions. Additionally, in glioblastoma tissue, our lab observed high H3K27me3 levels within hypoxic or necrotic tumor regions, whereas the active H3K4me3 mark was present on the outside of the H3K27me3-enriched and hypoxic zones (data not shown). These findings support previous reports describing global transcriptional repression under hypoxia and underscore the broader impact of oxygen deprivation on the epigenetic landscape (75,76,78).

3.1.2. Validating the effects of EZH2 knockdown on HIF2α protein and EPAS1 mRNA levels in MDA-MB-231 and other cell lines

After defining the hypoxia time-point in MDA-MB-231 and PC-9 parental cells, the next aim was to thoroughly validate the preliminary findings. For this, the results obtained using a single shRNA against EZH2 were validated by various ways of EZH2 depletion using other shRNAs, siRNAs, and single guide RNAs (sgRNAs) (CRISPR/Cas9), all well-established and widely used genetic inactivation tools in molecular cell biology research.

ShRNAs were used in lentiviral constructs for stable knockdowns, whereas siRNAs were used for transient-transfection-based knockdowns. Both small non-coding RNA

types function by forming a complex with RNA-induced silencing complex, leading to degradation of the targeted mRNA (251). In contrast, sgRNAs in combination with CRISPR/Cas9 induce double-strand breaks in DNA, activating repair pathways that often result in frameshift mutations (252,253). These mutations typically generate premature stop codons, preventing the production of functional proteins (252,253).

The efficiency of shRNA knockdown depends on the proportion of cells that express the short hairpin RNA and on the level of expression, while siRNA efficiency depends on delivery and cellular uptake (251). SgRNA-mediated knockout is generally very efficient, but often not 100% complete (254). In this study, three sgRNAs were designed to target EZH2. Two of them efficiently knocked out EZH2 and reduced global H3K27me3 levels (data not shown). However, HIF2α protein and EPAS1 mRNA levels were not affected (data not shown). This could have been caused by cellular mechanisms such as translation reinitiation or alternative splicing (e.g., exon skipping) which enable the expression of a truncated or mutated protein (255). Both effective sgRNAs target regions are close to the EZH2 RT-qPCR primer binding sites and the antibody epitope site used for detection. These sites are downstream of the TAD domain of the EZH2 protein and the TAD domain encoding region of the EZH2 mRNA. It is therefore possible that a truncated EZH2 protein containing the TAD domain is expressed in sgRNA-targeted cells, which may not be detected by RT-qPCR or western blot, but could still regulate EPAS1/HIF2α transcription if the TAD or other remaining domains are required for this regulatory axis.

Also, six shRNAs targeting EZH2 were tested by transient transfection in HEK293T cells by Sarah Goos. The two most efficient shRNAs targeting EZH2 were used in a stable knockdown setup in this study, as shown in Figure 2.2. Both shRNAs targeting EZH2 resulted in a HIF2α decrease at the protein and EPAS1 mRNA level in parental MDA-MB-231 cells, of the two shRNAs, #2 gave the most stable results. These results confirm that the previously identified EZH2-HIF2α regulatory axis is not dependent on the clonal selection of the MDA-POR cells and/or cycled intermittent hypoxia. In contrast, HIF1α protein levels were not reproducibly affected by EZH2 depletion. At the mRNA level, HIF1A expression was reduced in shEZH2 #1 cells but not in shEZH2 #2 cells.

Preliminary experiments in our laboratory also addressed the potential role of EZH2 in regulating HIF2α protein stability in addition to controlling the EPAS1 mRNA levels.

These experiments included testing the effect of EZH2 knockdown on 1) overexpressed HIF2α levels in MDA-POR cells (by Isabel Schröter; data not shown), 2) the effect of proteasomal degradation inhibition on HIF2α levels (partially by Isabel Schröter; data not shown), 3) POR luciferase activity (by Isabel Schröter; data not shown) (247), and 4) PHD1-3 protein levels in MDA-MB-231 cells (data not shown). These experiments did not support a role of EZH2 as a stabilizer of HIF2α directly or through regulating PHDs.

Furthermore, the effect of shRNA-mediated knockdown of EZH2 on HIF2α was also validated in PC-9 cells as shown in Figure 2.2. EZH2 knockdown resulted in decreased HIF2α protein levels, while the effect on EPAS1 mRNA showed a trend toward reduction but was inconsistent between biological replicates. Moreover, shEZH2 #1 gave different results compared to shEZH2 #2, and its performance differed from that in MDA-MB-231 cells, experiments with shEZH2 #1 were therefore discontinued. Besides shEZH1 #1 not working well, performing RT-qPCR in PC-9 cells was less reliable because of larger variability in the housekeeping genes hypoxanthine phosphoribosyltransferase 1 (HPRT1) and actin beta (ACTB) (gene encoding β-actin) between the different conditions within one experiment.

After establishing that shRNA-mediated EZH2 knockdown reduces HIF2α levels in both MDA-MB-231 and PC-9 cells, I next sought to confirm that the observed effect on HIF2α was not specific to the particular shRNA constructs. Thus, I have selected two siRNAs targeting EZH2, which were previously reported to efficiently deplete EZH2 (127). In my experiments only one of these two siRNAs knocked down EZH2 efficiently. Figure 2.3A,B shows that this siRNA caused a clear decrease in HIF2α protein and EPAS1 mRNA levels under both normoxic and hypoxic conditions in PC-9 cells, suggesting that regulation also occurs at the mRNA level in PC-9 cells, similar to shEZH2-manipulated MDA-MB-231 cells. When using siRNA-mediated depletion in MDA-MB-231 cells, a clear decrease in HIF2α protein level was observed. The decrease in EPAS1 mRNA levels was small but significant under normoxic conditions, whereas no clear decrease was found under hypoxic conditions (Fig. 2.3A,B). However, four days after siEZH2 washout, EZH2 levels were still low and HIF2α clearly decreased in two out of three experiments (Fig. 2.7A), suggesting that there might be a delayed response to EZH2 depletion in MDA-MB-231 cells. However, since HIF2α protein levels were already reduced, this could also suggest a negative feedback loop.

Though negative feedback loops have been described for HIF1α (256), no transcriptional feedback loops are currently known for HIF2α.

Following the initial analysis in the MDA-MB-231 and PC-9 cell lines, the effect of EZH2 knockdown on HIF2α levels was also examined in additional breast and lung cancer cell lines, as well as in glioblastoma cell lines.

To initially characterize additional cell lines I performed a comparison study of PRC2 subunits in several breast cancer and lung cancer cell lines available in the lab, similar to the approach applied by Yu *et al*. They reported, based on RNA-seq data from The Cancer Genome Atlas, that EZH2, but not EZH1, EED, or SUZ12, is highly upregulated in TNBC samples compared to non-TNBC samples (257). They also found that EZH2 protein and mRNA levels are higher in the TNBC cell lines MDA-MB-231, MDA-MB-436, and MDA-MB-453 compared to the non-TNBC cell lines SKBR3, MDA-MB-361, BT-474, and MCF-7 (257). Thus, I have tested the cell lines available in the lab, including the TNBC cell lines MDA-MB-231, MDA-MB-157, and BT-549, and the non-TNBC cell line and MCF-7. The TNBC cell lines MDA-MB-157 and BT-549 and the non-TNBC cell line MCF-7 had lower EZH2, EED, and SUZ12 levels than MDA-MB-231, but I have not detected specific differences in PRC2 subunit levels between these TNBC and non-TNBC cell lines (data not shown). EZH2 was knocked down in these cell lines, but HIF2α levels were not downregulated in BT-549 and MCF-7 cells as shown in Figure 2.4. Only in MDA-MB-157 cells did EPAS1 mRNA appear decreased in EZH2 knockdown cells, but the difference at the protein level was minor, and HIF2α levels were not responsive to hypoxia treatment. Therefore, this cell line was excluded from further experiments (Fig. 2.4). EZH2 was additionally depleted in the non-TNBC cell line MDA-MB-361, in which no effect on HIF2α levels was observed (Fig. 2.4).

The lung adenocarcinoma cell lines A549, H2030, and H441 were also included in the cell line comparison experiments. The A549 cell line initially showed a potential EZH2-HIF2α regulatory axis in experiments performed by Isabel Schöter (247), and the EZH2, EED, and SUZ12 protein levels were similar to the levels in MDA-MB-231 cells (data not shown), but validation experiments did not find a clearly and reproducibly detectable reduction of HIF2α protein and EPAS1 mRNA levels after stable shRNA-mediated EZH2 depletion. It is worth emphasizing that EZH2 knockdown was also less efficient in this cell line compared to other cell lines even after boosting the knockdown (Fig. 2.5). The H2030 cell line was included in the study because it has a matching

brain metastatic derivative, H2030-BM, and Zhang *et al.* reported higher EZH2 expression at the mRNA and protein level in BM samples compared to primary tumors of breast, lung, and melanoma in both patient cohorts and animal experiments (106). In addition, You *et al*. found that HIF2α protein and EPAS1 mRNA levels are increased in BM samples compared to primary lung cancer and melanoma patient samples (210). Moreover, RNA-seq data (GSE183862) showed increased EPAS1 levels in MDA-MB-231-BM cells compared to MDA-MB-231 cells (258). These outcomes suggest that the EZH2-HIF2α regulatory axis might be stronger in BM cells. However, I found similar levels of EZH2 in MDA-MB-231 wildtype and BM cells, while HIF2α levels were lower in MDA-MB-231-MB cells under hypoxic conditions. In H2030 cells, EZH2 levels were increased in BM cells, but HIF2α levels were also decreased in H2030-BM cells compared to H2030 wildtype cells under hypoxic conditions (data not shown). Thus, the regulation of HIF2α by EZH2 was not further investigated in matched non-BM and BM cell lines. Additionally, the expression of all analyzed PRC2 subunits in H2030 cells were lower than in MDA-MB-231 cells (data not shown), and no effect of EZH2 knockdown on HIF2α levels was observed in the parental cell line (Fig. 2.5). The H441 cell line was selected based on EZH2 and EPAS1 expression data from the DepMap Data Explorer (259), which indicated similarities to MDA-MB-231. Levels of PRC2 subunits were also closer to those in MDA-MB-231 compared with other cell lines (data not shown). However, EZH2 knockdown did not reduce HIF2α levels in H441 cells (Fig. 2.5).

The identification of the lung cancer cell line PC-9 as a model system for investigating EZH2-dependent HIF2α regulation was accidental. Cell authentication of a morphologically suspicious culture, which suggested cross-contamination, identified PC-9 cells mixed with MDA-MB-231 cells in a cell population that had been transduced with shNsc- and shEZH2-expressing lentiviruses and exhibited EZH2-dependent HIF2α regulation. Comprehensive analysis of EZH2 depletion in authenticated PC-9 cells compared to authenticated MDA-MB-231 cells confirmed that, although differences in HIF kinetics and the extent of HIF2α regulation are detectable when using the same shRNA or siRNA, the key findings regarding EZH2-dependent HIF2α regulation in these breast and lung cancer cell models are highly consistent.

The effect of EZH2 knockdown on HIF2α regulation was also studied in G55 and U87 glioblastoma cell lines as shown in Figure 2.6. Experiments performed by Isabel

Schröter were not conclusive regarding EZH2-dependent HIF2α regulation in G55 cells as summarized in section 3.1.1. My experiments in G55 cells and additional analyses in the widely used U87 glioblastoma cells showed no detectable reduction in HIF2α levels upon shRNA-mediated stable EZH2 knockdown under the conditions used.

These results suggest that the regulation of HIF2α by EZH2 is context specific and cannot be attributed to a particular cancer type or subtype in the analyzed cellular model systems of cancer. Since data on EZH2 knockdown in healthy mammary and prostate epithelial cells also show a reduction in EPAS1 mRNA levels (231) (Fig. 2.3C), EZH2-dependent HIF2α regulation could also be considered in non-cancerous biological contexts. It would be important to further investigate and precisely determine the cellular conditions under which EZH2-dependent HIF2α regulation occurs, as demonstrated here in MDA-MB-231, PC-9 cells, and detected by others in non-transformed mammary and prostate epithelial cells.

3.1.3. Restoring EZH2 and its effect on EPAS1 mRNA levels

To test whether HIF2α levels could be restored upon EZH2 rescue, transient transfections were performed using pcDNA6.2 constructs encoding shRNA-resistant wildtype EZH2, a catalytically inactive mutant (F672I), or a catalytically hyperactive mutant (Y646F) (generated in collaboration with Nadja Ritschel). While EZH2 levels were restored upon transfection, H3K27me3 and HIF2α levels were not rescued in MDA-MB-231 shEZH2 cells. Only the hyperactive mutant plasmid was able to partially restore H3K27me3 levels (data not shown). To rule out potential issues with the level and transient nature of overexpression, I generated pLenti6 plasmids containing the same EZH2 cDNA constructs and established stable cell lines in shNsc and shEZH2 MDA-POR, as well as in the parental MDA-MB-231 background. However, in these stable cell lines the rescue was also not functional (data not shown). We then questioned whether or not the exogenously expressed EZH2 was present in the nucleus. Immunofluorescence staining revealed that rescued EZH2 was indeed present in the nucleus of shEZH2 MDA-MB-231 cells, ruling out a localization defect (data not shown). Another possibility for the inactivity of the EZH2 rescue plasmid was the location of the V5 tag. In my construct, the V5 tag was present at the C-terminus, whereas most commercially available EZH2 plasmids carry a tag in the N-terminus, which could affect protein folding and potentially result in an inactive protein. To test this possibility, I removed the V5 tag, but this did not restore the function of the EZH2

rescue plasmid (data not shown). A further possible explanation for the inactivity of the plasmid is that it encodes EZH2 isoform A, which contains 751 amino acids, whereas the canonical isoform C contains 746 amino acids (84,260). The additional amino acids, along with a single change in isoform A, are located in exon 7/8 near the SANT1 and TAD domains (96). While direct evidence is lacking, these extra residues could potentially affect EZH2 function.

An attempt was also made to generate shNsc and shEZH2 cell lines with a pTRIPZ backbone, which enables inducible shRNA expression in the presence of doxycycline and restoration of EZH2 levels after doxycycline removal. However, the HEK293T cells used for virus production did not tolerate the construct, and the pTRIPZ-based approach could not be pursued further. Thus, optimization of the virus production protocol would be needed when considering this experimental setup in future investigations.

Since all previous rescue strategies were unsuccessful, a siEZH2 washout experiment was designed and performed as shown in Figure 2.7. EZH2 levels recovered slowly after transient transfection, with the first full restoration observed on day 15. This recovery was accompanied by increased HIF2α levels in both MDA-MB-231 and PC-9 cells, suggesting that restoring EZH2 levels rescues EPAS1 mRNA levels, which is consistent with the other observations pointing to the EZH2-dependent HIF2α regulation.

It is worth mentioning that this experimental setup had some technical limitations. Cell growth rate was generally very slow in both cell lines transfected with siEZH2. As a result, there were no day 8 results for PC-9 cells, since all dishes seeded on day 4 were needed for subsequent passages. Only from day 11 to day 15 did cell growth rates begin to approach those of siNsc cells. Also, given the extended timeframe and the stress and slow growth after siRNA transfection, it was not practical to keep the cells in the hypoxia chamber for comparative normoxia versus hypoxia analyses. Consequently, all experiments were conducted under normoxic conditions. Due to the limited number of samples that could be collected without significantly increasing costs, the higher sensitivity of the RT-qPCR assay compared to immunoblot analyses, and the fact that our previous results suggested regulation at the EPAS1 mRNA level, protein samples were not collected in the siEZH2 washout experiments. Future experiments using large initial cell populations could overcome these limitations.

However, efficient siRNA-mediated EZH2 knockdown may require optimization if the experiment were to be scaled up.

3.2. Mechanisms of HIF2α regulation by EZH2

3.2.1. Determining the role of the PRC2 and EZH2's methyltransferase function in the regulation of HIF2α

After demonstrating EZH2-dependent HIF2α regulation in a breast and a lung cancer cell line, and that restored EZH2 levels rescued EPAS1 mRNA expression, the next aim was to determine how EZH2 regulates HIF2α. As shown in Figure 1.4, EZH2 can act via interacting with proteins, mRNA, or DNA, and, as illustrated in Figure 1.5, HIF2α is regulated at all of these levels. This provides a wide range of possible mechanisms through which EZH2 could control HIF2α levels.

The first aim was to determine if the PRC2-dependent canonical repressor function of EZH2 is responsible for HIF2α regulation. For this purpose, two of the PRC2 subunits were knocked down: SUZ12 and EED. As shown in Figure 2.8, the knockdowns of these PRC2 subunits did not affect HIF2α protein and EPAS1 mRNA levels, while they reduced H3K27me3 levels comparable to EZH2 knockdown. Thus, EZH2 does not require an intact canonical PRC2 complex and H3K27 tri-methylation for HIF2α regulation. Nevertheless, the EZH2-HIF2α regulatory axis could still depend on EZH2's methyltransferase activity, as shown previously for EZH2-dependent STAT3 and β-catenin activation (122,123,261).

To address the possible requirement of EZH2's methyltransferase activity in HIF2α regulation, I used the widely applied EZH2 inhibitor GSK126, which blocks the SAM binding site in the SET domain of EZH2 but not EZH1 (121,147). The concentrations and timing of GSK126 were optimized in MDA-POR, G55, and A549 cells by Isabel Schröter (247) and adjusted in this study for parental MDA-MB-231 and PC-9 cells. While H3K27me3 steadily decreased with the increasing GSK126 concentrations, HIF2α protein levels remained largely stable, with only a minor decrease observed in some experiments at 1 μM GSK126. EPAS1 mRNA was also not decreased upon GSK126 treatment.

These results showed that EZH2 does not require the PRC2 or its methyltransferase activity for HIF2α regulation.

3.2.2. Elucidating the role of EZH1 on EZH2-dependent regulation of HIF2α

A facultative subunit of the PRC2 is EZH1, the paralog of EZH2 that can replace EZH2 in the PRC2. They form the mutually exclusive PRC2:EZH1 and PRC2:EZH2 complexes that share in their core the EED, SUZ12 and RBBP4/7 subunits. Even though EZH1 and EZH2 and thus PRC2:EZH1 and PRC2:EZH2 are structurally similar, their regulation and functional roles differ. Regulation wise, EZH1 is ubiquitously expressed and more abundant in quiescent cells, whereas EZH2 expression is associated with proliferative states. Functionally, EZH2 possesses stronger methyltransferase activity than EZH1 and requires PRC1 for chromatin compaction (233). In contrast, EZH1 relies less on its methyltransferase activity and can form PRC2:EZH1 homodimers that directly compact chromatin without PRC1 (233,262). Unlike EZH2, EZH1 is not commonly linked to cancer progression, although gain-of-function mutations have been identified in autonomous thyroid adenomas (263). Similar to EZH2, non-canonical functions have been reported for EZH1. For example, EZH1 was found to be involved in the upregulation of Notch signaling, like EZH2, in muscle cells (264). EZH1 knockout resulted in decreased protein levels of the Notch target gene Hes1. Moreover, ChIP-qPCR analyses showed that EZH1 binds to the promotor regions of NOTCH3, and Notch target genes HES1 and HEY1, independent of its methyltransferase activity (264). In such a scenario, the activity of the protein could be mediated by its TAD domain, which was originally described by Jiao *et al*. (96). However, these ChIP-qPCR results were presented as fold enrichment without accounting for input chromatin, and no negative control locus was included (265). The absence of such controls weakens the conclusions. Nonetheless, the findings suggest an activator function for EZH1. In addition to regulating Notch signaling, EZH1 has also been reported to be involved in transcriptional elongation (266), which will be discussed later.

Given the close relationship of EZH1 to EZH2, I aimed to determine whether EZH1 contributes to EZH2-dependent HIF2α regulation. The first step was to examine EZH1 levels upon EZH2 knockdown in MDA-MB-231 cells. Figure 2.10A shows a clear increase in EZH1 levels upon EZH2 knockdown, raising the possibility that EZH1 might

replace EZH2 in the PRC2 and PRC2:EZH1 could act as a repressor of HIF2α. This repressor activity would also require the EED and SUZ12 subunits. However, as shown previously, EED and SUZ12 were not required for regulation of HIF2α protein or EPAS1 mRNA levels.

Nonetheless, to rule out the function of EZH1 as repressor of HIF2α in EZH2-depleted cells, MDA-MB-231 shNsc and shEZH2 cells were transfected with siNsc or siEZH1. The results showed that HIF2α protein levels were not increased in shEZH2 + siEZH1 cells (Fig. 2.10B), suggesting that EZH1 is not responsible for the EZH2-dependent decrease of HIF2α protein levels. Unexpectedly, EPAS1 mRNA levels decreased upon EZH1 knockdown, whereas EZH2 mRNA levels were unaffected, and a less pronounced reduction in HIF1A mRNA was also detected as shown in Figure 2.10C.

These results contradict the idea that EZH1 mediates HIF2α repression. If this were the case, EZH1 knockdown would be expected to increase HIF2α protein and EPAS1 mRNA levels. Instead, EPAS1 mRNA levels decreased, indicating that EZH2 does not regulate HIF2α through EZH1.

3.2.3. Determining the role of Notch1 in the EZH2-dependent regulation of HIF2α

Both EZH2 and HIF2α are linked to Notch signaling, either by regulating it or being regulated by it. EZH2 has been shown to regulate Notch signaling in different ways:

- It regulates microRNAs that affect Notch signaling (267,268),
- It binds to the promotor of NOTCH1 and induces its transcription (130,131),
- It activates Notch signaling indirectly by activating STAT3 (269).

Hu *et al.* described HIF2α as a Notch signaling repressor by binding to the NICD (270). Conversely, Mutvei *et al.,* reported that HIF2α is regulated by Notch at transcriptional level, however they could not detect direct binding of the canonical Notch signaling mediator RBPJ to the EPAS1 promoter using ChIP-seq in MDA-MB-231 cells (236). They also found that HIF2α was required for the transcription of several Notch target genes (236), contradicting the findings from Hu *et al.* (270). Moreover, a research group at JLU did observe direct binding of RBPJ at the EPAS1 promoter, leading to the hypothesis that EZH2 could regulate EPAS1 through or with Notch.

Gonzalez *et al.* identified NOTCH1 as a target gene of EZH2's methyltransferase-independent function in MDA-MB-231 cells, as previously mentioned (130). They also reported a reduction in Notch pathway genes in the breast cancer cell line SUM149 upon EZH2 knockdown and an induction in NICD upon EZH2 overexpression in MCF10 and MDA-MB-231 cells. To test if I could reproduce the NOTCH1 dependency on EZH2, mRNA levels were measured in MDA-MB-231 cells. Figure 2.11A shows that NOTCH1 mRNA levels do not depend on EZH2, therefore EZH2 does not regulate HIF2α through NOTCH1 gene regulation.

The next aim was to investigate the dependency of HIF2α on Notch signaling as a possible co-regulator for EZH2. To test this, MDA-MB-231 shNsc and shEZH2 cells were treated with the Notch signaling inhibitor DAPT, but no clear reduction was observed in HIF2α at the protein and EPAS1 mRNA levels (Fig. 2.11B). Thus, HIF2α regulation is not dependent on Notch signaling. NICD overexpression was performed to further test whether Notch functions as a co-regulator for EZH2, but it did not alter HIF2α protein levels, supporting the previous findings (Fig. 2.11C). However, this experiment was performed only once, and excessive NICD expression may have had adverse effects on cellular signaling pathways (271). Overall, these experiments suggest that EZH2-dependent regulation of HIF2α does not occur through or together with Notch as a co-regulator.

In addition to Notch, previously identified co-regulators of EPAS1, including RelA, RelB, and NFκB, were considered. However, ChIP-seq data from Dardis *et al*. did not detect binding of any of these factors to the EPAS1 promoter in MDA-MB-231 cells (GSE223959) (128). Other potential co-regulators include c-Myc and N-Myc (60, 94, 95), which have been shown to be stabilized by EZH2 in neuroblastoma and small cell carcinoma (72). Additionally, links between c-Myc and HIF2α have been reported, with evidence suggesting that HIF2α can influence c-Myc regulation (272–275). Moreover, Das *et al.* found direct binding of c-Myc to the EPAS1 promoter in a T-cell lymphoma model expressing stem cell antigen 1 (219). Based on this, EZH2 could potentially regulate EPAS1 through or together with c-Myc. However, c-Myc levels were not reduced upon EZH2 knockdown in MDA-MB-231 cells (data not shown), ruling out that EZH2 regulates EPAS1 through c-Myc, though a co-regulatory function remains possible. Unfortunately, multiple attempts by myself and colleagues to perform c-Myc ChIP experiments yielded very low % input levels, which were considered background

noise even at positive control loci. Consequently, further optimization of the c-Myc ChIP protocol would be necessary to investigate this hypothesis more thoroughly in the future. Another possible co-regulator future research could focus on is E2F1, which is a target gene of EZH2's transcriptional activator function and has been shown to cooperate with EZH2 to induce the transcription of its target genes (136,137). Furthermore, Monitz *et al.* found direct binding of E2F1 to the EPAS1 promoter at two sites (-1218 bp and −2447 bp) in Hela cells (217), making it a plausible co-regulator.

3.2.4. Elucidating if EZH2 affects EPAS1 elongation

EZH1 has been shown to be involved in the regulation of transcriptional elongation. Mousavi *et al.* showed that EZH1 can co-occupy many genes with SUZ12 and interact with RNA Pol II (266). Upon EZH1 depletion, binding of elongating RNA Pol II (pS2) and the elongation marker H3K36me3 were reduced in C2C12 myocytes (266), indicating a direct effect of EZH1 on transcriptional elongation. EZH2 has also been implicated in transcriptional elongation, through indirectly affecting RNA Pol II transcription under heat shock responses (239).

We thus hypothesized that EZH2 could affect transcriptional elongation at the EPAS1 gene. To test this, four loci ranging from the EPAS1 TSS to approximately 28 kb downstream were assessed for RNA Pol II binding in MDA-MB-231 shNsc and shEZH2 cells using ChIP-qPCR. The signal at all loci was above the background (IgG) in both shNsc and shEZH2 cells, suggesting there was actual binding as shown in Figure 2.12B. The binding ratio relative to the TSS was similar between shNsc and shEZH2 cells (Fig. 2.12C). If EZH2 promoted elongation, this ratio would have been reduced in shEZH2 cells. Therefore, these results indicate that EZH2 likely does not affect transcriptional elongation of EPAS1.

Interestingly, RNA Pol II binding at the TSS was lower in shEZH2 cells compared to shNsc cells, suggesting that EZH2 may play a role in the initiation or early stages of EPAS1 transcription. One important limitation is that a pS2-specific RNA Pol II antibody that recognizes the serine 2-phosphorylated form of the carboxy-terminal domain of the largest subunit of RNA Pol II was not used. This modification marks transcriptional elongation (276). A ChIP experiment investigating this mark could have improved the RNA Pol II transcriptional elongation analyses.

3.2.5. Determining direct regulation of EPAS1 by EZH2

After determining that HIF2α is regulated by EZH2 at the mRNA level independent of its methyltransferase activity, not through EZH1 and Notch signaling, and most likely not by affecting elongation, the question remained open as to whether the regulation takes place at the transcriptional or post-transcriptional level. Thus, I next investigated the direct binding of EZH2 to the EPAS1 gene. Studies investigating the regulation of HIF2α have largely focused on protein stability, while post-transcriptional mechanisms involving the iron-responsive element in the 5'UTR of EPAS1 mRNA have also been uncovered in mechanistic detail as discussed in section 1.1.2 and 1.4, respectively. However, transcriptional regulation of the EPAS1 gene remains less well understood.

For studying the direct binding of EZH2 to EPAS1, I designed primers based on EPAS1 promoter sequence information from Kristan *et al.* (218) and ENCODE ChIP-seq and ReMap data of EZH2-EPAS1 binding in the UCSC Genome Browser (277). Most of the 65 designed primer pairs were based on these data. The Kim *et al.* paper focusing on AR transcriptional regulation, reported EZH2 binding 1.4 kb-1.7 kb downstream of the TSS of the AR gene. They also transfected HEK293 cells with different regions of the AR promoter and found that EZH2 bound 1.2 kb-1.6 kb downstream of the TSS. ChIP-seq and ChIP-qPCR was used for the analysis of the endogenous AR locus, while the analysis of the transfected AR promoter fragments was performed by ChIP-qPCR and a luciferase reporter assay. In the reporter assays, they found that overexpression of EZH2 activated the reporter with the 1.7–2.5 kb AR region, but not the one with the 1.1–1.7 kb AR region (132). Together, these data showed that EZH2 acts far downstream of the promoter in AR gene regulation. Based on these findings, primers hybridizing in a similar distance to the TSS of the EPAS1 gene were also designed. The four final primer pairs were selected based on distance/distribution parameters and primer efficiency measurements (data not shown).

To comprehensively control the ChIP-qPCR assay, a negative locus was included to ensure binding specificity, and positive control loci were included to confirm assay efficiency. The following controls for EZH2 and H3K27me3 were chosen:

- **RPL30** was selected as a negative control for EZH2 and H3K27me3 because this housekeeping gene is stably and constitutively expressed and efficiently working primer pairs were reported in the literature (278,279),

- **MYT1** is an EZH2 target gene and commonly used as a positive control for H3K27me3 and EZH2 (101,280–282),
- **NOTCH1** was chosen as an EZH2 positive control and H3K27me3 negative control based on the results and locus region provided by Gonzalez *et al*. (130).

Additional potential controls and EZH2 antibodies were tested, but the selected ones produced the most consistent results.

As an additional control for EZH2-specific regulation of EPAS1, an EED antibody was tested. However, EED unexpectedly bound to NOTCH1 (a negative control locus), and its binding was not consistently reduced in MDA-MB-231 shEED cells, indicating that the ChIP results obtained with this antibody are unreliable. EZH2 binding to EPAS1 was also assessed in shEED cells, and overall, EED knockdown had no clear effect on EZH2 occupancy at EPAS1 locus #4, suggesting that EZH2 binding to EPAS1 is largely independent of EED, as expected (data not shown). Extensive optimization of ChIP procedures by myself and colleagues ultimately produced a robust method for EZH2, RNA Pol II, H3K27me3, and H3K4me3 ChIP.

Figure 2.13B shows that EZH2 binding at locus #4 was clearly detectable, whereas H3K27me3 binding was absent in shNsc MDA-MB-231 cells. This indicates that EZH2 regulates EPAS1 by directly binding to this region. The presence of the active chromatin mark H3K4me3 at locus #4, with levels comparable to the active gene controls RPL30 and NOTCH1, further supports this conclusion. Additional evidence comes from ChIP-seq data from Dardis *et al.* (GSE223959), showing EZH2 occupancy at EPAS1 spanning locus #4 (128) (Fig. 2.13C). Together, these data suggest that EZH2 binds approximately 1.7 kb downstream of the TSS and directly regulates EPAS1 transcription. However, EZH2 has many different roles and can regulate the same gene or protein in different ways, it is therefore well possible that this direct binding is not the only way EPAS1 is regulated by EZH2.

3.2.6. The effect of Src inhibition on HIF2α regulation

Posttranslational modifications, particularly phosphorylation, have been reported to induce functional switches in EZH2 (283). The most well-known example is Akt-mediated phosphorylation of S21, which alters EZH2's substrate preference from histones to other targets while still requiring its methyltransferase activity (118,119,133). In breast cancer, the only study demonstrating an EZH2 switch from a

methyltransferase to a transcriptional activator independent of its methyltransferase function was reported by Zhang *et al.* (106). They found that Src-mediated phosphorylation of Y696 was responsible for the transcriptional activator function of EZH2 for c-JUN in MDA-MB-231 cells (106). This observation led to the hypothesis that phosphorylation at Y696 could also induce the EZH2-HIF2α regulatory axis. Thus, to test the hypothesis, Src was inhibited using Saracatinib as shown in Figure 2.14. In PC-9 cells, HIF2α protein and EPAS1 mRNA levels were decreased upon Src inhibition, which would be consistent with EZH2-dependent regulation of HIF2α. Unfortunately, Src inhibition strongly reduced EZH2 protein and mRNA levels, suggesting that the observed HIF2α changes are more likely explained by reduced EZH2 expression rather than by a phosphorylation-dependent switch in EZH2 activity. In MDA-MB-231 cells, EZH2 levels were also reduced upon Src inhibition, but the level of reduction was inconsistent between the experiments. HIF2α protein levels were unchanged in MDA-MB-231 cells upon Src inhibition and EPAS1 mRNA levels increased. These observations clearly illustrate the limitations of pharmacological Src inhibition as an experimental approach to study EZH2-dependent HIF2α regulation and raise the question of how Src regulates EZH2 levels. Src is not known to directly downregulate or degrade EZH2. While Smith *et al.* reported that hyperactivated Src can enhance mTORC1 activity, thereby increasing EZH2 translation (284), this does not explain the observed decrease in EZH2 mRNA levels in PC-9 cells.

Taken together, the question whether phosphorylation at Y696 mediates EPAS1 regulation could not be answered, as Src inhibition caused an overall reduction in EZH2 levels, and no commercially available antibody exists for pY696. To exclude that off target effects of Saracatinib affected EZH2/HIF2α levels, experiments with genetic depletion of Src should be considered. This could include transient depletion by siRNA transfection, inducible or constitutive shRNA expression from stably transduced lentiviral vectors, or Cas9-sgRNA-mediated CRISPR knockout.

3.3. Biological consequences of EZH2 knockdown under chronic hypoxia and clinical significance

3.3.1. Identifying HIF2α target genes in MDA-MB-231 and PC-9 cells and assessing the impact of EZH2 depletion

Upon elucidating the EZH2-HIF2α regulatory link, I investigated whether this regulation has downstream effects in cancer cells. The first aim was to determine whether HIF2α target genes are downregulated upon EZH2 depletion. Due to limited consensus on HIF1α and HIF2α target genes, I first aimed to identify HIF2α-specific targets in my experimental model systems.

For this, I knocked down EPAS1 and monitored the expression of the following HIF target genes by RT-qPCR: PGK1, GLUT1, PHD3, HK2, and VEGFA, with HIF1A included as a control. These target genes were selected based on experiments previously performed in our laboratory and several publications as shown below:

- Lombardi *et al.* identified PGK1 and HK2, among other genes, as HIF target genes (40),
- Hu *et al.* found HIF2α binding to the PGK1 and GLUT1 promoter in HEK293 cells. However HIF2α depletion or rescue did not affect PGK1 mRNA levels in HEK293 cells, while GLUT1 levels were increased upon HIF2α rescue, but also not reduced upon HIF2α depletion (285),
- Wallace *et al.* used the HIF2α specific inhibitor PT2385 (286), which blocks HIF2α and HIF1β dimerization, in renal cell carcinoma cells. At the mRNA level they found a reduction of GLUT1 and VEGFA, but not PGK1 (287),
- Arnaiz *et al*. found decreased VEGFA and PHD3 expression in RNA-seq analyses following PT2385 treatment in renal cell carcinoma cells (288),
- Octamer-binding transcription factor 4 (OCT4) has also been reported as a HIF2α target gene (289). However, no change of its expression was observed upon HIF2α depletion in my initial experiments in MDA-MB-231 cells (data not shown), and thus this gene was excluded from further comprehensive analyses.

Based on the results shown in Figure 2.15, GLUT1 and PGK1 were considered HIF2α target genes in MDA-MB-231 cells and PHD3 in PC-9 cells. In MDA-MB-231 cells, EZH2 knockdown reduced both selected HIF2α target genes, suggesting that there is

a downstream effect of EZH2 knockdown on hypoxia signaling. In contrast, PHD3 levels were not reduced upon EZH2 knockdown in PC-9 cells. However, ACTB has been used as the housekeeping gene for the EPAS1 knockdown experiments, which may not have been optimal. Repeating the RT-qPCRs with HPRT1 is recommended to further analyze these and other target genes in future experiments.

3.3.2. The functional consequences of EZH2 depletion on cancer progression *in vitro*

After demonstrating the effect of EZH2 depletion on HIF2α target genes in MDA-MB-231 cells, I next investigated the functional consequences of EZH2 depletion.

Initially, mammosphere formation was tested with MDA-MB-231 cells to study the effect of EZH2 knockdown on stemness, since HIF2α has been shown to be an important regulator of this phenotypic trait of cancer cells (196–199). Even though MDA-MB-231 cells were capable of forming spheres, they were loose, irregular, and small. It was therefore difficult to distinguish them from cell clumps. PC-9 cells did not form spheres at all under the tested experimental conditions. In addition, the expression of the stem cell markers OCT4, SRY-box transcription factor (SOX2), and SRY-box transcription factor (SOX9) was also assessed in MDA-MB-231 shNsc and shHIF2α cells, but no reduction was observed. Since OCT4 and SOX9 have been reported as potential HIF2α target genes (289,290), the role of the EZH2-HIF2α axis in the regulation of stemness could be further explored using different experimental setups.

Next, the effect of EZH2 depletion on cell survival and proliferative capacity was studied using a colony formation assay. MDA-MB-231 cells formed large colonies, but PC-9 cells did not, and therefore the assay was only applied to MDA-MB-231 cells. Because very low cell numbers were required to avoid overgrowth, results were sensitive to seeding errors, which likely contributed to the variability between experiments. Overall, only a small and non-significant decrease in colony formation was observed upon EZH2 depletion under hypoxic conditions (data not shown). To test whether nutrient stress might enhance the effect, cells were cultured in glutamine-rich or glutamine-deprived medium without pyruvate throughout the experiment. These conditions caused a slightly greater reduction in colony formation under hypoxic conditions in shEZH2 compared to shNsc cells than with regular medium, but the effect

remained moderate and non-significant. A similar reduction was also observed under normoxic conditions, suggesting that the potential decrease in colony formation is independent of HIF2α (data not shown). Thus, additional repeats and testing of different conditions are necessary to clarify whether EZH2 has a robust effect on colony formation in this model.

To further study proliferation, I also assessed cell growth by cell counting. A significantly decreased growth rate was observed in PC-9 under normoxia and hypoxia on day 4, but on day 5 the difference was only significant under hypoxic conditions as shown in Figure 2.17A. This supports a role for the EZH2-HIF2α regulatory axis in PC-9 cell growth. In line with this, Gonzalez *et al.*, observed a significant decrease in MDA-MB-231 cell proliferation after four days based on the Wst-1 assay under normoxic conditions (291). Since no significant difference between EZH2 knockdown and control MDA-MB-231 cells was observed in my experiments under different EZH2 depletion conditions (data not shown), additional assay settings should be tested.

Furthermore, anchorage-independent growth was assessed using a soft agar colony formation assay. In Figure 2.17B,C, PC-9 shEZH2 cells displayed reduced colony formation efficiency across three independent experiments compared to shNsc cells under hypoxic conditions, although the effect did not reach significance due to variability. Additional experiments will be needed to accurately assess if there is a diminished colony formation capacity under hypoxic conditions. While colony formation was not affected under normoxic conditions in EZH2 depleted cells in the soft agar assay, the colony size was decreased. This suggests that although tumorigenicity and transformative capacity under normoxia are not affected by EZH2 knockdown, its depletion under this condition could play a role in the proliferation of tumorigenic cells. MDA-MB-231 cells did not form colonies in soft agar and were therefore not suitable for this assay.

To test if the observed effects of EZH2 depletion on proliferation and tumorigenicity was through HIF2α downregulation, I created stable HIF2α rescue and control MDA-MB-231 and PC-9 shNsc and shEZH2 cell lines. Since the control cell lines were growing much faster than the HIF2α rescue cell lines, this approach was unfortunately not feasible. As an alternative, I used an experimental approach with transient overexpression of HIF2α. However, in this configuration, I was only able to conduct short-term experiments due to the decrease in HIF2α expression levels after a few

days. Consequently, only the growth experiment was performed with HIF2α transient overexpression in PC-9 shNsc and shEZH2 cells under hypoxic conditions. The HIF2α expressing cells had a regular growth rate, but the cells did not tolerate the control plasmid well, which could have been caused by the high DNA:FuGENE ratio. Despite this problem, the experiments did give the expected result. In cells transfected with the control or HIF2α rescue plasmid, the EZH2 depleted cells grew slower compared to the control cells (Fig. 2.18B). However, when comparing the growth difference between the cells transfected with the control or HIF2α plasmids, the growth increase was greater in shEZH2 cells than in shNsc cells as shown in Figure 2.18C. This suggests that the reduction in PC-9 proliferation upon EZH2 depletion is mediated under hypoxic conditions, at least in part, through downregulation of HIF2α.

3.3.3. The functional consequences of EZH2 depletion on cancer progression in an *ex vivo* organotypic brain slice culture

In vitro assays do not always reflect *ex vivo* or *in vivo* experimental outcomes. For this reason, I wanted to use a non-invasive and relatively robust experimental setup to investigate the effect of EZH2 depletion on invasion in the brain, as both lung and breast cancer are well known to cause BM (173,174). For this purpose, I performed an *ex vivo* organotypic brain slice invasion assays in collaboration with Nazli Salik.

Our laboratory has previously used spheres for these invasion assays. However, as described earlier, MDA-MB-231 spheres did not grow large enough, and PC-9 cells did not form spheres at all. Another option would be to inject single cells into the brain slice, but this method is technically challenging and prone to damaging the tissue. Instead, I adopted a method described recently by Uroz *et al*. (243), in which the brain slice is incubated with a 1 ml suspension of cancer cells for two to four hours, followed by removal of excess cells and time-lapse imaging. This approach minimizes tissue damage and is relatively simple.

Due to the limited availability of mice, only one cell line could be used in these experiments. MDA-MB-231 cells were selected because they had not shown any consistent functional effects on growth or proliferation *in vitro*, and I wanted to determine whether a functional effect related to EZH2-dependent HIF2α regulation, namely invasive capacity, could be demonstrated in an *ex vivo* model that more closely approximates a biologically relevant context. Remarkably, EZH2 depletion significantly

reduced the net invasion depth under hypoxic conditions (Fig. 2.19C). This indicates that EZH2 contributes to the invasion capacity of MDA-MB-231 cells under chronic hypoxia, plausibly through HIF2α. However, several limitations of the method became apparent.

First, at baseline, cells appeared up to approximately 156 µm deep within the tissue under hypoxic conditions. It is unlikely that cells migrated this distance within three hours purely by invasion. Alterations in the structure of brain slices, due to the high amount of medium, may have led to small openings in the tissue, providing a potential explanation for the observed effects (292). We could see that the shape changed when the cell suspension was removed and approximately 250 µl fresh medium was added to keep the brain slice from drying out. When assessing the invasion depth reported by Uroz *et al.* it seems like they may have had the same issue. They only found an approximate 7 µm invasion depth at their 24-hour time point, while I found approximately 17 µm net invasion depth at my 48-hour time point under normoxic conditions measured from the brain surface (243). It is very likely that Uroz *et al*. also displayed the net invasion depth, although they have not stated this. I expect this because Spennati *et al.* found approximately 100 µm invasion depth of MDA-MB-231 cells at their 24-hour time point without baseline measurements (293), which comes closer to the highest average depth of MDA-MB-231 shEZH2 cell invasion under normoxic conditions of approximately 150 µm at the 48-hour time point in my experiments. Admittedly, their setup was different (25 µl cell suspension incubated for five hours). Taken together, the actual depth is likely much higher than the reported approximately 7 µm depth by Uroz *et al.* This highlights the need for optimization of the assay, which could prevent this “invasion” during the first three hours. It is unfortunate that the study by Spennati *et al*. did not have baseline measurements, this would have confirmed if the amount of medium added to the slice contributes to the observed effect.

A related issue is that the peak GFP signal intensity at baseline (3 hours) was at approximately the same depth as at 48 hours, but the starting point of the GFP signal was deeper at baseline than at 48 hours (Fig. 2.19D). This further supports the idea that the initial measurements do not represent active invasion. It is likely that for some other reason the cells passively infiltrate the tissue in these three hours and then actively migrate deeper into the tissue, but also back to the surface. For this reason, I

reported invasion both as net depth from the tissue surface and from the first detectable GFP signal in Figure 2.19C. Importantly, in both analyses, EZH2 depletion reduced invasion under hypoxia.

Another limitation was that time-lapse imaging could not be performed, meaning baseline and 48-hour time point measurements were taken from several different brain slices, which increased variability. Furthermore, DAPI staining did not penetrate the entire slice, making it difficult to determine the top and bottom of the brain slices in fluorescence microscopy imaging.

Morphological differences between normoxic and hypoxic cells were also observed. Under normoxia, cells were more elongated, consistent with previous reports describing vessel-associated migration (243). Under hypoxia, cells remained rounder, but invaded to similar depths as under normoxic conditions. This observation could be explained by hypoxia inducing amoeboid migration (294,295), which is a form of migration characterized by cells adopting a round shape, and undergoing cycles of expansion and contraction, which allow them to squeeze through gaps in the extracellular matrix (296). The cell shape could therefore be further investigated in future experiments to test this possibility.

Unfortunately, these results cannot directly demonstrate that HIF2α mediates the reduced invasion capacity under hypoxia in EZH2-depleted cells. Ideally, the experiment would have been repeated using shNsc and shEZH2 MDA-MB-231 cells with HIF2α overexpression and control constructs, but the marked growth differences between the overexpression and control lines prevented this. Possible alternatives for future studies would be transient overexpression of HIF2α or the use of a HIF2α-specific inhibitor, such as PT2385. If EZH2 regulates invasion via HIF2α, PT2385 treatment should reduce invasion more strongly in shNsc cells than in shEZH2 cells. However, we currently do not have a reliable readout to assess PT2385 treatment efficiency on HIF2α-dependent cellular processes in MDA-MB-231 cells.

3.3.4. Relevance of the EZH2-HIF2α axis in patients

Since no previous studies have investigated the relationship between EZH2 and HIF2α, judging clinical validity is challenging. The Kaplan-Meier Plotter database, which includes RNA-seq data from breast cancer patients (244), provides some insights. Among patients who received endocrine therapy but no chemotherapy, high

expression of EZH2 and EPAS1 was associated with poorer overall survival, whereas high levels of EED and SUZ12 showed the opposite trend as shown in Figure 2.20. This survival disadvantage was not observed in untreated patients, in those who received chemotherapy alone, or in those treated with both endocrine therapy and chemotherapy. However, these results do not align with my observation in MDA-MB-231 cells, which is a TNBC cell line. Since TNBC patients generally lack hormonal receptors, they typically do not receive endocrine therapy (297). Although there are cases in which endocrine therapy could be beneficial in TNBC (297), none of the patients receiving only endocrine therapy were TNBC patients in the Kaplan-Meier database. However, since the EZH2-dependent regulation of HIF2α is cell line-dependent but not TNBC-specific, it could very well be that this regulation also plays a role in other breast cancer subtypes. A critical limitation of these analyses is that survival curves are based on mRNA expression levels. High mRNA levels do not necessary translate to high protein levels, which is the effector level. Data based on protein expression would be necessary to make more precise claims about the effect of high EZH2 and HIF2α expression on clinical outcome.

3.4. Conclusive summary and perspectives

In this study, I investigated the regulatory relationship between EZH2 and HIF2α (encoded by the EPAS1 gene) and assessed its potential functional and clinical relevance in breast and lung cancer. My results provide evidence that EZH2 regulates HIF2α at the transcriptional level in a manner independent of its methyltransferase activity. This regulation was not mediated by EZH1 and Notch signaling. Instead, I demonstrated that EZH2 binds directly to the EPAS1 locus, particularly at a region approximately 1.7 kb downstream of the TSS, where it likely contributes to transcriptional activation. This binding occurred in the absence of H3K27me3 enrichment, supporting a non-canonical activator role for EZH2. Although hypoxic conditions are generally associated with a globally repressive chromatin landscape, EZH2 appears to maintain transcriptional activity by promoting HIF2α expression, thereby contributing to the sustained hypoxic response.

Mechanistically, I could not conclusively determine whether phosphorylation at Y696 by Src kinase underlies the observed switch in EZH2 function, as Src inhibition reduced EZH2 levels overall rather than inducing a clear functional change. Instead of using

pharmacological inhibition, genetic depletion of Src could be used to further explore its possible role in turning EZH2 from a chromatin modifier and transcriptional repressor into a transcriptional activator in the model systems used in this study. Future work should also focus on developing reliable tools, such as phospho-specific antibodies for pY696 EZH2, or better, mass spectrometry-based approaches, which will be crucial to determine whether this or other modifications underlie the non-canonical activator function observed.

Functionally, EZH2 depletion impaired the expression of selected HIF2α target genes, including GLUT1 and PGK1 in MDA-MB-231 cells, indicating that the EZH2-HIF2α regulatory axis has a downstream impact on hypoxia signaling. These transcriptional changes translated into measurable effects on cancer progression. In PC-9 cells, EZH2 knockdown reduced proliferation under hypoxia, which could be rescued with transient HIF2α restoration, and showed a decreased anchorage-independent growth trend in soft agar that correlates with decreased tumorigenicity. In MDA-MB-231 cells, EZH2 depletion reduced invasion capacity in an *ex vivo* organotypic brain slice culture under chronic hypoxia, plausibly mediated through HIF2α. Together, these findings highlight the potential importance of the EZH2-HIF2α regulatory axis in driving malignant phenotypes such as growth and invasion. Despite these advances, several limitations remain.

Technical challenges prevented the use of stable HIF2α and EZH2 overexpression or rescue lines, restricting mechanistic confirmation of whether HIF2α fully mediates the observed functional effects of EZH2 depletion, and which EZH2 domains are required for EPAS1 regulation. Future studies could overcome these issues by testing other viral promoters and controls for HIF2α overexpression, optimizing virus production protocols for inducible shRNA systems such as pTRIPZ, and removing the additional amino acids in the pLenti6 EZH2 plasmid to create isoform C, which might induce its function. If this is the case, it could be used to create inducible overexpression cells using the pSLIK system (298), which could also be applied for HIF2α overexpression. In addition, ChIP assays were not functional for c-Myc, a potential co-regulator of EPAS1, suggesting that further optimization of antibody selection and experimental conditions will be required to explore this potential interaction. To further follow up on potential co-regulators, E2F1 could be the next target. E2F1 is a suggested

transcription factor for EPAS1 (217) and has been shown to work together with EZH2 to induce gene transcription (137).

Future research should also expand the analysis of HIF2α target genes beyond the set tested in this study. RNA-seq following EZH2 or HIF2α depletion, under both normoxic and hypoxic conditions, would provide a broad overview of the transcriptional programs regulated by the EZH2-HIF2α regulatory axis. RNA-seq would also be beneficial in other cell lines, where no EZH2-dependent regulation of HIF2α was observed to identify cancer type-specific differences, potentially informing us what causes the EZH2-HIF2α regulatory axis.

Also the use of a HIF2α inhibitor such as PT2385, could serve as a pharmacological tool to test whether EZH2-driven invasion and growth phenotypes indeed depend on HIF2α activity. Combining these inhibitors with EZH2 depletion could clarify the extent to which HIF2α mediates EZH2's oncogenic role.

Additionally, extending these studies to *in vivo* models would be beneficial for validating the EZH2-HIF2α regulatory axis in a physiologically relevant microenvironment.

Moreover, while my study relied on mRNA-based clinical datasets, protein-level analyses would be beneficial to validate the functional and prognostic relevance of the EZH2-HIF2α regulatory axis in patient samples.

Taken together, this study provides new insights into a previously unexplored regulatory link between EZH2 and HIF2α. It establishes EZH2 as a non-canonical transcriptional activator of EPAS1, and suggests that this regulation contributes to cancer cell growth and invasion under hypoxic conditions, potentially through HIF2α signaling, where EZH2 sustains HIF2α expression and transcriptional activity despite an overall repressive chromatin state. This mechanism is summarized in Figure 3.1, which illustrates how EZH2 supports HIF2α-driven transcription under hypoxia. These findings broaden our understanding of the function of EZH2 beyond its canonical role as a repressive methyltransferase and opens possibilities for future research into the therapeutic targeting of the EZH2-HIF2α regulatory axis in cancer.

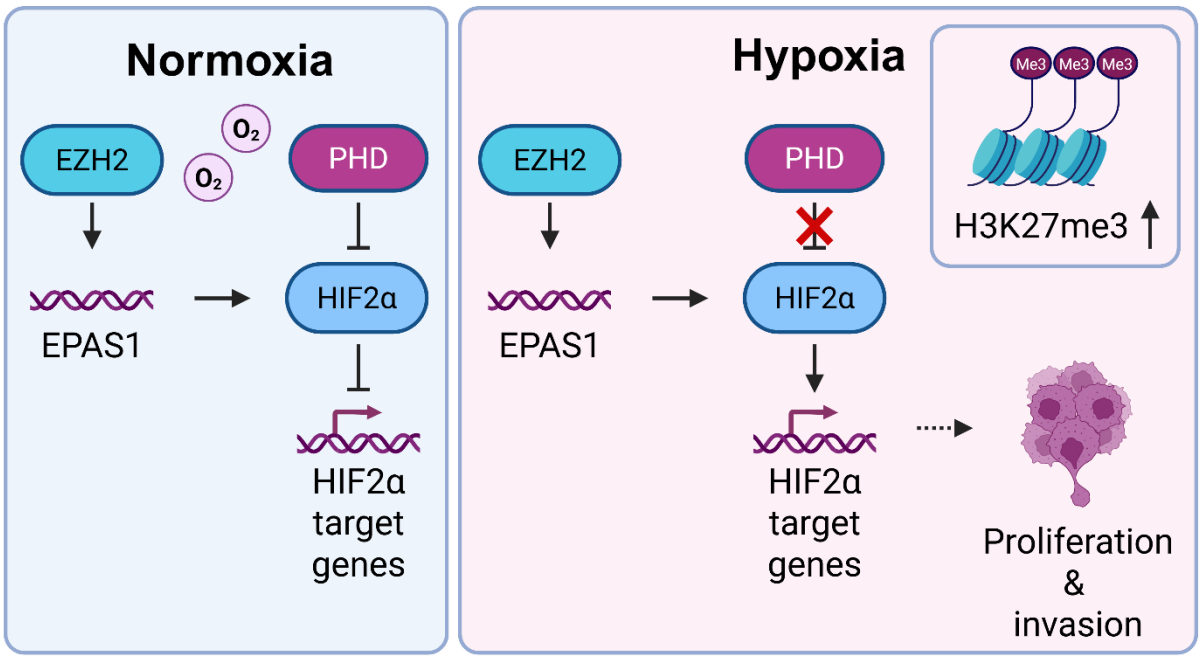

Figure 3.1: Graphical abstract of this study.

EZH2 regulates HIF2α signaling under normoxic and hypoxic conditions as a transcriptional activator of EPAS1 in a PRC2-independent manner. Under normoxia, HIF2α is degraded through PHD-mediated hydroxylation, limiting target gene expression. Under hypoxia, repressive H3K27me3 levels accumulate, while EZH2-dependent EPAS1 transcription persists and HIF2α is stabilized, leading to activation of HIF2α target genes which may promote tumor cell proliferation and invasion.

4. Materials and methods

4.1. Materials

Plasticware, including petri dishes, multiwell plates, and serological pipettes, was purchased from Greiner Bio-One (Kremsmünster, Austria) and SARSTEDT AG & Co. KG (Nürnbrecht, Germany), unless otherwise stated.

4.2. Chemicals, Media, and other reagents

Standard laboratory chemicals were purchased from Carl Roth (Karlsruhe, Germany) and Sigma Aldrich/Merck (Darmstadt, Germany) unless otherwise indicated.

4.2.1. Cell culture

0.05 % Trypsin-EDTA #25300-054, Thermo Fisher Scientific (Waltham, MA, USA)
5x siRNA Buffer #B-002000-UB-100, Horizon Discovery/Revvity (Waltham, MA, USA)
Agar-Agar, Noble Quality # 3558, Carl Roth (Karlsruhe, Germany)
Amphotericin B #A2942, Sigma-Aldrich/Merck (Darmstadt, Germany), stock concentration 150 µg/mL in sterile deionized H_2O
Basal Medium Eagle (BME) (1x) with Earle's Salts, without L-Glutamine #41010,Gibco/Thermo Fisher Scientific (Waltham, MA, USA)
CASY ton solution #5651808, OMNI Life Sciences (Bremen, Germany)
Crystal violet #61135, Fluka/Honeywell (Charlotte, NC, USA)
D-(+)-Glucose solution #50-99-7, Sigma-Aldrich/Merck (Darmstadt, Germany)
Dimethyl Sulfoxide (DMSO) #A994.1, Carl Roth (Karlsruhe, Germany)
Dulbecco's Modified Eagle Medium (DMEM) (1x) with 4.5 g/L D-Glucose, Phenol Red, without L-glutamine, Pyruvate #11960, Gibco/Thermo Fisher Scientific (Waltham, MA, USA)
Dulbecco's Modified Eagle Medium (DMEM) (1x) with 4.5 g/L D-Glucose, L-glutamine, Pyruvate, Phenol Red #41966, Gibco/Thermo Fisher Scientific (Waltham, MA, USA)
Dulbecco's PBS (1x) #PBS-1A, Capricorn Scientific (Ebsdorfergrund, Germany)
Fetal Bovine Serum (FBS) #F7524, Sigma-Aldrich/Merck (Darmstadt, Germany)
GlutaMAX (100x) #35050, Gibco/Thermo Fisher Scientific (Waltham, MA, USA)
HEPES Buffer Solution (1M) #15630, Gibco/Thermo Fisher Scientific (Waltham, MA,

USA)

Horse Serum heat inactivated #1138, Sigma-Aldrich/Merck (Darmstadt, Germany)

Hydrochloric acid solution #H9892, Sigma-Aldrich/Merck (Darmstadt, Germany)

Minimum Essential Medium (MEM) (1x) with Earle's Salts, L-Glutamine #31095, Gibco/Thermo Fisher Scientific (Waltham, MA, USA)

Opti-MEM Reduced Serum Medium #11058021, Thermo Fisher Scientific (Waltham, MA, USA)

Penicillin Streptomycin (Pen-Strep) #15140, Gibco/Thermo Fisher Scientific (Waltham, MA, USA)

Plasmocin treatment #MPT-40-01, InvivoGen (San Diego, CA, USA)

Polybrene (Hexadimethrine bromide) #9268, Sigma-Aldrich/Merck (Darmstadt, Germany)

Puromycin #ant-pr, InvivoGen, stock concentration 10mg/mL in HEPES, final concentration was cell line dependent

RPMI Medium 1640 (1x) with 4.5 g/L D-Glucose, 2.383 g/L HEPES buffer, L-glutamine,1.5 g/L Sodium Bicarbonate, 110 mg/L Sodium Pyruvate, Phenol Red #A10491-01, Gibco/Thermo Fisher Scientific (Waltham, MA, USA)

Sodium Bicarbonate (7,5%) #25080, Gibco/Thermo Fisher Scientific (Waltham, MA, USA)

Sodium hydroxide solution (NaOH) #S2770, Sigma-Aldrich/Merck (Darmstadt, Germany)

4.2.2. Transfection reagents

FuGENE HD Transfection Reagent #2312, Promega (Fitchburg, WI, USA)

Lipofectamine RNAiMAX reagent #13778150, Invitrogen/Thermo Fisher Scientific (Waltham, MA, USA)

PEI 25K (Polyethylenimine) #23966, Polysciences (Warrington, PA, USA)

4.2.3. Inhibitors

Chloroquine #C6628, Sigma-Aldrich, stock concentration 10 mM in sterile deionized H_2O

DAPT #565770, Merck (Darmstadt, Germany), stock concentration 10mM in DMSO

GSK126 #HY-13470, MedChemExpress (Monmouth Junction, NJ, USA), stock concentration 20 mM in DMSO

Saracatinib #HY-10234, MedChemExpress (Monmouth Junction, NJ, USA), stock concentration 10 mM in DMSO

4.2.4. Chromatin immunoprecipitation (ChIP)

16% Formaldehyde Solution (w/v), methanol-free #28908, Thermo Fisher Scientific (Waltham, MA, USA)

Agarose NEEO Ultra-Quality, #2267.4, Carl Roth (Karlsruhe, Germany)

Buffer NTB #740595.150, Macherey-Nagel (Düren, Germany)

cOmplete Mini, EDTA-free #11 836 170 001, Roche Diagnostics (Mannheim, Germany)

EDTA Disodium Salt 2-hydrate BioChemica #A1104,0250, PanReac AppliChem (Darmstadt, Germany)

GeneRuler 1 kb Plus DNA Ladder #SM1333, Thermo Fisher Scientific (Waltham, MA,USA)

Lithium Chloride (LiCl) #L960, Sigma-Aldrich/Merck (Darmstadt, Germany)

NP-40 (10% in H_2O) #2011-100, BioVision (Milpitas, CA, USA)

NucleoSpin Gel and PCR Clean-up #740609.250, Macherey-Nagel (Düren, Germany)

Orange G #HY-135712, MedChemExpress (Monmouth Junction, NJ, USA), 6x in 50% glycerol

p-APMSF, Hydrochloride #178281, EMD Millipore (Billerica, MA, USA), stock concentration 50mM in deionized H_2O

Proteinase K #BIO-37037, Bioline/Meridian Bioscience (London, UK), stock concentration 20 mg/mL

RNase A, DNase and protease-free #EN0531, Thermo Fisher Scientific (Waltham, MA, USA)

SDS ultra pure #2326.1, Carl Roth (Karlsruhe, Germany)

SYBR Safe DNA gel stain #S33102, Thermo Fisher Scientific (Waltham, MA, USA)

Triton X-100 #T8787, Sigma-Aldrich/Merck (Darmstadt, Germany)

4.2.5. RNA isolation, reverse transcription and quantitative real time polymerase chain reaction (qPCR)

Maxima H Minus First Strand cDNA Synthesis Kit #K1652, Thermo Fisher Scientific (Waltham, MA, USA)

PowerUp SYBR Green Master Mix #A2574, Thermo Fisher Scientific (Waltham, MA, USA)

RNase-Free Dnase Set #79256, Qiagen (Hilden, Germany)

RNeasy Mini Kit #74106, Qiagan (Hilden, Germany)

4.2.6. Western blotting

Albumin bovine Fraction V #11946.02, SERVA Electrophoresis (Heidelberg, Germany)

Ammonium persulfate (APS) #A1142, AppliChem (Darmstadt, Germany), stock 10% in deionized H_2O

DC Protein Assay Reagents Package #500-0116, Bio-Rad Laboratories (Hercules, CA, USA)

PageRuler protein ladder (10 -180 kDa) #26617, Thermo Fisher Scientific (Waltham, MA, USA)

Pierce ECL Western Blotting Substrate #32106, Thermo Fisher Scientific (Waltham, MA, USA)

Spectra High Range protein ladder (40-300 kDa) #26625, Thermo Fisher Scientific (Waltham, MA, USA)

Western Lightning Plus ECL #0RT2655, Revvity (Waltham, MA, USA)

4.2.7. Fixation and staining

DAPI/Antifade-Solution (ultra) #MT-0002-0,8, Zytovision (Bremerhaven, Germany), stock concentration 1000 ng/mL

Fluorescence Mounting Medium #S3023, Dako (Hamburg, Germany)

Paraformaldehyde (PFA) #0335.3, Carl Roth (Karlsruhe, Germany)

4.2.8. Antibodies

Primary antibodies were purchased from Abcam (Cambridge, UK), Cayman Chemical (Ann Arbor, MI, USA), Cell Signaling Technology (Danvers, MS, USA), Dianova (Hamburg, Germany), Novus Biologicals (Centennial, CO, USA), Proteintech (Rosemont, IL, USA), Santa Cruz (Dallas, TX, USA), and Sigma-Aldrich/Merck (Darmstadt, Germany). Secondary antibodies goat anti-mouse/rabbit IgG (#115-035-146, #111-035-144, respectively) were purchased from Jackson ImmunoResearch

(Ely, UK). All used primary antibodies and their experimental usage are shown in table 4.1.

Table 4.1 Antibodies used in this study.

Antigen	Species	Product number	Manufacturer	Dilution/ amount	Usage
α-Tubulin	Mouse	#DLN09992 #sc-32293	Dianova Santa Cruz	1:10000 1:5000	WB (ECL)
β-Actin	Mouse	#A5316	Sigma-Aldrich/Merck	1:10000	WB (ECL)
Cleaved Notch1 (Val1744)	Rabbit	#2421	Cell Signaling Technology (CST)	1:1000	WB (ECL PLUS)
EED	Rabbit	#ab240650	Abcam	1:1000	WB (ECL)
EZH1	Rabbit	#20852-1-AP	Proteintech	1:500	WB (ECL PLUS)
EZH2	Rabbit	#5246	CST	1:5000 5 µg	WB (ECL) ChIP
H3K27me3	Rabbit	#9733	CST	1:2000 5 µg	WB (ECL) ChIP
H3K4me3	Rabbit	#9751	CST	5 µg	ChIP
HIF1α	Rabbit	#10006421	Cayman Chemical	1:1000	WB (ECL PLUS)
HIF2α	Rabbit	#NB100-122	Novus Biologicals	1:500	WB (ECL PLUS)
Normal Rabbit IgG	Rabbit	#2729	CST	5 µg	ChIP
pSrc (Tyr416)	Rabbit	#6943	CST	1:1000	WB (ECL PLUS)
RNA Pol II	Mouse	#NB200-598	Novus Biologicals	5 µg	ChIP
Src	Rabbit	#2109	CST	1:1000	WB (ECL PLUS)
SUZ12	Rabbit	#3737	CST	1:1000	WB (ECL)

4.2.9. Primers

All oligonucleotides were ordered from Sigma-Aldrich/Merck (Darmstadt, Germany). Primers were designed using PrimerBlast (299), Primer3 (300–302), or Geneious Prime (2019.2.3, Dotmatics (Boston, MS, USA)). RT-qPCR primers were designed to be intron spanning to prevent the amplification of genomic DNA sequences. All primers were tested for efficiency. Table 4.2 contains the information for all used RT-qPCR primers and Table 4.3 contains the information for the ChIP-qPCR primers.

4.2.10. Short interfering RNAs (siRNA)

siRNA control: ON-TARGETplus Non-targeting pool siRNA #D-001810-10, Horizon Discovery/Revvity (Waltham, MA, USA):
GACUCUGAAUGCAGUUGCU
UGGUUUACAUGUUGUGUGA
UGGUUUACAUGUUUUCUGA
UGGUUUACAUGUUUUCCUA
siRNA targeting human EZH1: ON-TARGETplus Human EZH1 siRNA SMARTpool #L-004217-00, Horizon Discovery/Revvity (Waltham, MA, USA):
GGAAAGGUCUAUGACAAAU
GAAAGCGACAUGCUAUUGA
GAUCCGUUCUGAUUAGUGA
GCAGUCAAAGAAUCACUUA
siRNA targeting human EZH2: Custom siRNA, Standard, Horizon Discovery/Revvity (Waltham, MA, USA):
GACUCUGAAUGCAGUUGCU

4.2.11. Plasmids

4.2.11.1. General plasmids

pCI-VSVG: Lentiviral envelope plasmid encoding vesicular stomatitis virus G #1733, Addgene (Watertown, MA, USA)
psPAX2: Lentiviral packaging plasmid encoding the Gag and Pol genes #12260, Addgene (Watertown, MA, USA)
pcDNA3: Mammalian expression vector, Invitrogen/Thermo Fisher Scientific (Waltham, MA, USA)

Table 4.2: RT-qPCR primers used in this study.

Primer	Sequence (5'-3')
ACTB For	*AGAAAATCTGGCACCACACC*
ACTB Rev	*AGAGGCGTACAGGGATAGCA*
EED For	*GAAATTCCATCCAAGAGATCCA*
EED Rev	*TGGATATTCCATAATCGTAAAGCA*
EPAS1 For	*CGAACACACAAGCTCCTCTC*
EPAS1 Rev	*GTCACCACGGCAATGAAAC*
EZH1 For	*ACTGCTTCCTTCACCCTTTTCA*
EZH1 Rev	*GGGTTGTGGAGCATGGCATA*
EZH2 For	*GTACACGGGGATAGAGAATGTGG*
EZH2 Rev	*GGTGGGCGGCTTTCTTTATCA*
GLUT1 For	*GATTGGCTCCTTCTCTGTGG*
GLUT1 Rev	*CAGGATCAGCATCTCAAAGG*
HES1 For	*GGCTAAGGTGTTTGGAGGCT*
HES1 Rev	*TGGTGTAGACGGGGATGACA*
HIF1A For	*CCATTAGAAAGCAGTTCCGC*
HIF1A Rev	*TGGGTAGGAGATGGAGATGC*
HK2 For	*GGAACCCAGCTGTTTGACCA*
HK2 Rev	*CAGGGGAACGAGAAGGTGAAA*
HPRT For	*CCGGCTCCGTTATGGC*
HPRT Rev	*GGTCATAACCTGGTTCATCATCA*
NOTCH1 For	*ACTGCGAGGTCAACACAGAC*
NOTCH1 Rev	*CACTCGTCCACATCGTACTGG*
PGK1 For	*ATGGATGAGGTGGTGAAAGC*
PGK1 Rev	*CAGTGCTCACATGGCTGACT*
PHD3 For	*CTATGTCAAGGAGCGGTCCAA*
PHD3 Rev	*GTCCACATGGCGAACATAACC*
SUZ12 For	*GGGAGACTATTCTTGATGGGAAG*
SUZ12 Rev	*ACTGCAACGTAGGTCCCTGA*
VEGFA For	*TCACCAAGGCCAGCACATAG*
VEGFA Rev	*CCGGGATTTCTTGCGCTTTC*

Table 4.3: ChIP-qPCR primers used in this study.

Primer	Sequence (5'-3')
EPAS1 #1 elongation/#3 For	*ACAATCCTCGGCAGTGTCCT*
EPAS1 #1 elongation/#3 Rev	*GGCTCGAATGCTGGGAGTC*
EPAS1 #1 For	*AATACGTCTACTTCCCGGCC*
EPAS1 #1 Rev	*ACCTCAAGTGATCTGCCCAA*
EPAS1 #2 elongation For	*CCCTGCACTGTGAACCTAGA*
EPAS1 #2 elongation Rev	*CACGGCTTGCTTCTCTCTTG*
EPAS1 #2 For	*CATCCCCGCCAAAACCAAA*
EPAS1 #2 Rev	*AAATTGATCTAGGGCTGCGC*
EPAS1 #3 elongation For	*ACCAGCCCCACATGTCATAA*
EPAS1 #3 elongation Rev	*ATGGTCCCTGCCTTCATGAA*
EPAS1 #4 elongation For	*CTGGCTTTTGTGCTGGTGAT*
EPAS1 #4 elongation Rev	*AGTGAGCGTGTATGTCCCAA*
EPAS1 #4 For	*GCCGAGGTTGATTTGCTCTT*
EPAS1 #4 Rev	*CAAATCCTTATCGGTGCCCC*
MYT1 For	*ACAAAGGCAGATACCCAACG*
MYT1 Rev	*GCAGTTTCAAAAAGCCATCC*
NOTCH1 For	*CTGGAGTAGGAGGGCTAAGC*
NOTCH1 Rev	*TCTGGGGTTTCTGCAGCC*
RPL30 For	*CAAGGCAAAGCGAAATTGGT*
RPL30 Rev	*GCCCGTTCAGTCTCTTCGATT*

hHIF2α_pcDNA3.1 HIS-TOPO: Mammalian expression vector containing the full human HIF2α sequence, generated by Yuanbin Xie

V5-Notch1 ICD expression vector: Mammalian expression vector containing the intracellular domain of murine NOTCH1 (bp 5,230 to bp 7,593 (303)), gifted by Prof. Dr. Michael Potente

4.2.11.2. Lentiviral shRNA knockdown plasmids

pGIPZ-shNsc: The pGIPZ non-silencing shRNA lentiviral vector is a negative control for any knockdown experiments performed using pGIPZ shRNA constructs. It contains no homology to known mammalian genes #RHS4346, Horizon Discovery/Revvity (Waltham, MA, USA)

pGIPZ-shEPAS1 (V2LHS_113750): Short hairpin RNA against human EPAS1 # Horizon Discovery/Revvity (Waltham, MA, USA):

TGAACAGGGATTCAGTCTG

pGIPZ-shEZH2 #1 (V2LHS_63066): Short hairpin RNA against human EZH2 #RHS4430-200182803, Horizon Discovery/Revvity (Waltham, MA, USA):
TTACTGTCCCAATGGTCAG

pGIPZ-shEZH2 #2 (V2LHS_17510): Short hairpin RNA against human EZH2 **#**RHS4430-200159841 Horizon Discovery/Revvity (Waltham, MA, USA):
TTATCATACACTTTCCCTC

pGIPZ EED shRNA (V3LHS_385764): Short hairpin RNA against human EED #RHS4430-200299484, Horizon Discovery/Revvity (Waltham, MA, USA):
AATCGTAAAGCATGATCTT

pGIPZ SUZ12 shRNA (V2LHS_74301): Short hairpin RNA against human SUZ12 #RHS4430-200175206, Horizon Discovery/Revvity (Waltham, MA, USA):
AAGATTAAAGTCATGCATG

4.3. Methods

4.3.1. Cell culture

Cells were split at 60-80% confluency. Cultures were washed with 1× PBS, trypsinized with 0.05% Trypsin-EDTA for up to 5 minutes at 37°C, neutralized with fresh culture medium, and centrifuged for 3 minutes at 1,000 rpm (Rotina 420 R, Andreas Hettich GmbH & Co. KG, Tüttlingen, Germany). Cell pellets were resuspended in fresh culture medium, and an appropriate fraction was plated on plastic culture dishes or well-plates based on cell growth rate and confluency. Cultures were maintained in a CO_2 incubator (5% CO_2, 95% humidity; Heracell, Thermo Fisher Scientific, Waltham, MA, USA) for a maximum of four months. The cell lines and corresponding culture media used are summarized in Table 4.4.

4.3.1.1. Cell counting

Cell number, size distribution, and viability were measured using the CASY Cell Counter and Analyzer Model TT (Roche Innovatis AG (Reutlingen, Germany)). 100 µL cell suspension was diluted in 10 mL CASY ton solution and measured according to the manufacturer's protocol. Specific programs were stored for each cell line.

Table 4.4: Cell lines used in this study.

Breast cancer cell line	Source	Culture medium
BT-549	ATCC (#HTB-122)	RPMI, 10% FBS
MDA-MB-157	ATCC (#HTB-24)	DMEM, 10% FBS
MDA-MB-231	DSMZ (#ACC-732)	DMEM, 10% FBS
MDA-MB-361	Original source unknown (from collaboration), authenticated by Eurofins	DMEM, 20% FBS
MCF-7	Unknown	DMEM, 10% FBS
Lung cancer cell lines		
A549	ATCC (#CCL-185)	DMEM, 10% FBS
H2030	ATCC (#CRL-5914)	RPMI, 10% FBS
H441	Original source unknown (from collaboration)	RPMI, 10% FBS
PC-9	Original source unknown (from collaboration), authenticated by Eurofins	RPMI, 10% FBS, 2mM GlutaMAX
Glioblastoma cell lines		
G55	Manfred Westphal (Hamburg, Germany)	DMEM, 10% FBS
U87-MG	ATCC (#HTB-14)	DMEM, 10% FBS
Human embryonic kidney cells, for virus production		
HEK293T	Invitrogen/Thermo Fisher Scientific	DMEM, 10% FBS

4.3.1.2. Cryopreservation of cells

Cells at 60-80% confluency were trypsinized, centrifuged, and resuspended in freezing medium (5-10% DMSO in culture medium). Cell pellets from one 10 cm dish were resuspended in 2 mL freezing medium and transferred to cryovials (#123277, Greiner Bio-One (Kremsmünster, Austria)). Cryovials were placed in a -80°C freezer for ≥ 24 hours in an isopropanol-containing or Styrofoam container, then transferred to liquid nitrogen for long-term storage.

4.3.1.3. Thawing of cells

Cryopreserved vials were rapidly thawed in a 37°C water bath, resuspended in 10 mL culture medium, and plated. Medium was refreshed the next day to remove residual freezing medium. Antibiotics were added if required for transgene expression and maintenance of selection.

4.3.1.4. Treatments

Hypoxia: For hypoxia experiments, plates containing cells or brain slices were incubated in a 37°C hypoxic glove chamber (Toepffer Lab Systems (Göppingen, Germany)) at 5% CO_2 and 1% O_2, calibrated monthly. All treatments and harvesting of cells or brain slices were performed inside the hypoxia chamber. Media and reagents used in hypoxia experiments were pre-equilibrated inside the chamber overnight, with lids loosely placed to allow oxygen to escape.

Transient Transfections: Cells were seeded in 6-well plates to achieve ~50% confluency the following day. Before transfection, the medium was replaced with 1 mL fresh culture medium.

- **Notch1 NICD overexpression:** 3 µg of the V5-Notch1 ICD expression vector or pcDNA3 plasmid DNA mixed with 9 µL FuGENE (3:1 DNA:FuGENE ratio) and 500 µL Opti-MEM; incubated 5 minutes at RT.
- **HIF2α overexpression:** 2 µg of the hHIF2α_pcDNA3.1 HIS-TOPO or pcDNA3 plasmid DNA mixed with 9 µL FuGENE (4.5:1) and 500 µL Opti-MEM; incubated 5 minutes at RT.

The transfection mixture was added dropwise. Medium was replaced the next day, followed by subsequent treatments.

SiRNA transfections: siRNAs were resuspended in 1× siRNA buffer (nuclease-free H_2O) to 20 pmol/µL and quantified using a NanoDrop 2000 Spectrophotometer (Thermo Fisher Scientific (Waltham, MA, USA)). Aliquots were stored at -80°C. Cells at ~50% confluency in 6-well plates were transfected using Lipofectamine RNAiMAX:

- Mixture 1: 9 µL Lipofectamine RNAiMAX + 150 µL Opti-MEM
- Mixture 2: 3 µL siRNA (20 pmol/µL) + 150 µL Opti-MEM

Mixtures were combined and incubated for 20 minutes at RT. In the meantime, the medium of the 6-well plates was refreshed. Upon incubation, the transfection mix was

added dropwise to the cells. Medium was replaced the next day, and further treatments were applied.

Inhibitors: GSK126, DAPT, and Saracatinib were prepared in DMSO and diluted in culture medium. Final DMSO concentration was equal across all treatment and control groups. Cells were incubated for indicated durations.

Glutamine Deprivation: For glutamine deprivation, DMEM lacking L-glutamine and pyruvate was supplemented with GlutaMAX to final glutamine concentrations of 4 mM or 0.25 mM. After trypsinization, cells were seeded in DMEM containing the appropriate glutamine concentration.

4.3.2. Working with lentiviruses

All lentiviral work was performed in a Biosafety Level 2 (BSL-2) laboratory with proper approvals.

4.3.2.1. Lentivirus production

T75 flasks were seeded with 4.5 × 10^6 HEK293T cells in 10 mL DMEM + 10% FBS. Two hours prior to transfection, medium was replaced with 6 mL fresh culture medium.

Transfection mix per flask:

- 500 µL Opti-MEM
- 7.5 µg plasmid encoding gene of interest
- 2.63 µg pCI-VSVG envelope plasmid
- 4.88 µg psPAX2 packaging plasmid
- 45 µL PEI 25K (equilibrated to RT)

The mixture was vortexed gently, incubated 20 minutes at RT, and added dropwise to cells pre-treated with 10 µM chloroquine. Cells were incubated 24 hours at 37°C, then medium was replaced with 10 mL fresh culture medium.

Virus-containing supernatant was collected 48 hours post-transfection, centrifuged at 250 × g for 5 minutes, filtered through 0.45 µm PVDF filters (#P667.1, Carl Roth (Karlsruhe, Germany)), and stored at 4°C. A second collection was performed on day 5.

4.3.2.2. *Lentivirus concentration*

Up to 30 mL viral supernatant per ultracentrifuge tube (#253060, Herolab (Wiesloch, Germany)) was balanced to 0.1 g accuracy. Tubes were centrifuged at 20,000 rpm for 4 hours at 4°C (Sorvall WX ULTRA ultracentrifuge, AH-629 rotor, Thermo Fisher Scientific (Waltham, MA, USA)).

Following centrifugation, the supernatant was carefully discarded, and tubes were placed upside-down on UV-treated tissue paper for 10 minutes to remove residual liquid. The viral pellet was then resuspended in 70-100 µL of plain DMEM and transferred to a 50 mL tube and kept at 4°C for 20 minutes. Samples derived from the same plasmid were resuspended again and pooled in a 1.5 mL tube, briefly centrifuged at 13,000 rpm for 3 minutes at 4°C, and the clarified supernatant was divided into aliquots and stored at -80°C.

4.3.2.3. Lentivirus titration

G55 cells were seeded in 6-well plates (5×10^4 cells/well). Lentiviral stocks were thawed on ice and diluted in DMEM + 10% FBS + 8 µg/mL polybrene, serially from 10^{-2} to 10^{-9}. Virus dilutions were applied to cells; one well received medium only as mock control. After 24 hours, medium was replaced, and selective medium (2 µg/mL puromycin) was applied 48 hours post-infection. The selective medium was refreshed every 2–3 days.

Colonies were visualized 16-17 days post-infection, or once all cells in the mock control had died. The cells were washed twice with PBS, and 100 µL of filtered 0.5% crystal violet (in 20% Methanol/H_2O) in 1 mL culture medium was added to each well. After a 15-minute incubation at RT, excess stain was removed with three additional PBS washes, or until the colonies were clearly visible. Subsequently, the plates were scanned with the EPSON Perfection V700 Photo Scanner (Suwa (Nagano, Japan)). The colonies were quantified using the cell counter plugin in Fiji (304).

To determine the titer in transducing units per mL (TU/mL), the following formula was used.

$$\text{Titer calculation (TU/mL)} = \frac{\text{Count}_1 \times \text{dilution}_1 + \text{count}_2 \times \text{dilution}_2}{2}$$

4.3.2.4. Lentivirus transduction

For stable lentiviral transduction, 1 × 10^4 or 1.5 × 10^4 cells were seeded in 48-well tissue culture plates, 2 × 10^4, 2.5 × 10^4, or 3 × 10^4 cells in 24-well plates, or 5.4 × 10^4 cells in 12-well plates, including one mock control.

On the next day, the transduction mix was prepared containing culture medium, 8 µg/mL polybrene, and concentrated virus. The amount of virus was adjusted according to the MOI, which was specific for each cell line (Table 4.5). The culture medium was removed, the transduction mix was added, and cells were incubated for 24 hours at 37°C.

The following day, the medium was replaced with regular culture medium. One day later, the medium was changed to selective culture medium containing puromycin (Table 4.5). Cells were refreshed 2-3 times per week and cultured under standard conditions.

After at least five washes and one split, cells were frozen once the mock control had died. In some cases, cells were re-transduced after the first split to increase knockdown efficiency. An overview of the generated cell lines is provided in Table 4.5.

All newly generated cell lines were tested for mycoplasma using PCR with HotStarTaq DNA Polymerase (Pisal *et al.* (305)) and primers/internal control plasmid (Uphoff and Drexler (306)).

4.3.3. Working with bacteria

Plasmids were isolated from bacteria stored as glycerol stocks. Bacteria were inoculated in 200-300 mL autoclaved LB medium + 100 µg/mL ampicillin and cultured overnight at 37°C, 225 rpm (Multitron Incubator Shaker, Infors AG (Bottmingen, Switzerland)). Plasmids were isolated using the PureLink HiPure Plasmid Maxiprep Kit (#K210007, Thermo Fisher Scientific (Waltham, MA, USA)), the concentration was measured with the NanoDrop 2000 Spectrophotometer and stored at -20°C.

4.3.4. Western blotting

All buffer and solution recipes used for western blotting are shown in Table 4.6.

Table 4.5: Generated cell lines.

Cell line name	MOI	Puromycin concentration µg/ml
A549 shNsc	100+100	1
A549 shEZH2 #2	100+100	1
BT-549 shEZH2 #2	30	1
BT-549 shNsc	30	1
G55 shEZH2 #2	20	2
G55 shNsc	20	2
H2030 shEZH2 #2	50	1
H2030 shNsc	50	1
H441 shEZH2 #2	25	1
H441 shNsc	25	1
MCF-7 shEZH1 #1	50	1
MCF-7 shEZH2 #2	50	1
MCF-7 shNsc	50	1
MDA-MB-157 shEZH2 #2	30+30	1
MDA-MB-157 shNsc	30+30	1
MDA-MB-231 shEED	50	2
MDA-MB-231 shEPAS1	50	2
MDA-MB-231 shEZH2 #1	50	2
MDA-MB-231 shEZH2 #2	50	2
MDA-MB-231 shNsc	50	2
MDA-MB-231 shSUZ12	50	2
MDA-MB-361 shEZH2 #2	50	4
MDA-MB-361 shNsc	50	4
PC-9 shEPAS1	50	2
PC-9 shEZH2 #2	50	2
PC-9 shNsc	50	2
U87-MG shEZH2 #1	30	1
U87-MG shEZH2 #2	30	1
U87-MG shNsc	30	1

4.3.4.1. Cell lysis

Cells were seeded as described in section 4.3.1. For protein lysate harvesting, cells were washed once with PBS. Subsequently, 50-100 µL Laemmli buffer was added depending on dish size and confluency (e.g. 50 µL per well for a 70-80% confluent 6 cm dish). Cells were scraped with a cell scraper (TPP Techno Plastic Products AG

(Trasadingen, Switzerland)) and collected in a 1.5 mL Eppendorf tube. The protein lysate was incubated for 5 minutes at 95°C, followed by sonication at 90% amplitude with 0.5 seconds pulse periods for 30 seconds using the Sonoplus (BANDELIN electronic GmbH & Co. KG (Berlin, Germany)). Protein lysates were stored at −20°C until further use.

4.3.4.2. Determination of protein concentration and sample preparation

Protein concentrations were quantified using the Lowry method which relies on a two-step chemical reaction producing a color change (307), measured at 750 nm using a multimode microplate reader (Berthold Technologies GmbH & Co. KG (Bad Wildbad, Germany)). Colorimetric measurements were performed with the DC Protein Assay Reagents Package, following the manufacturer's protocol. Pure Laemmli buffer served as the blank control. Protein amounts were calculated from a standard curve generated with serial dilutions of bovine serum albumin (BSA). For SDS-PAGE, 30-55 µg of total protein was mixed with Laemmli buffer and 4× sample buffer.

4.3.4.3. SDS-PAGE and immunoblotting

Protein samples were denatured by heating at 95°C for 5 minutes prior to electrophoresis. Denatured proteins were separated by SDS-PAGE. SDS ensures proteins acquire a uniform negative charge proportional to their mass, allowing size-dependent separation (308,309).

Standard discontinuous SDS-PAGE was performed using the Mini-PROTEAN 3 system (Bio-Rad Laboratories (Hercules, CA, USA)) with 15-well or 10-well combs. For each lane, 20 µL or 30 µL of denatured protein sample was loaded onto either 8%/15% double-percentage gels or 8% single-percentage gels with a 4% stacking gel. Electrophoresis was initiated at 80 Volt until proteins migrated into the resolving gel, then voltage was increased to 130 Volt for the remainder of the run.

Following electrophoresis, proteins were transferred onto 0.45 µm PVDF membranes (#88518, Thermo Fisher Scientific (Waltham, MA, USA)) using the Mini-PROTEAN 3 system at a constant current of 125–250 mA per blot for 2 to 2.5 hours.

PVDF membranes were cut according to protein sizes and blocked in 5% milk blocking buffer or 5% BSA blocking buffer for pSrc (Tyr416) for 1 hour at RT. After blocking,

primary antibodies (in corresponding blocking buffer; see Table 4.1 for all antibodies) were added and incubated overnight at 4°C.

The next day, membranes were washed with washing buffer three times for 10 minutes each, followed by incubation with HRP-coupled secondary antibody (in corresponding blocking buffer) for at least 1 hour at RT. Membranes were then washed twice with washing buffer and once with PBS for 10 minutes each. All washing and incubation steps were carried out while shaking.

Protein bands were visualized by incubating the membranes with either Pierce ECL Western Blotting Substrate or Western Lightning Plus ECL for up to 5 minutes to generate a chemiluminescent signal (Table 4.1). After substrate removal, membranes were placed in a developing cassette, and luminescent signals were recorded on CL-XPosure™ Film (#34089, Thermo Fisher Scientific (Waltham, MA, USA)) with exposure times ranging from 2 seconds to 20 minutes depending on signal intensity. Developed films were scanned using an EPSON Perfection V700 Photo Scanner, and figures were prepared with Microsoft PowerPoint 2016.

4.3.4.4. Membrane stripping

When the same membrane region needed to be probed with a different primary antibody, bound antibodies were removed by washing membranes three times with washing buffer for 10 minutes each, followed by incubating blots twice with stripping buffer for 20 minutes each at RT. Membranes were then washed three times for 10 minutes in PBS-T to eliminate residual stripping buffer and re-blocked for at least 1 hour before incubation with the next primary antibody.

4.3.5. Working with RNA

4.3.5.1. RNA isolation

Cells were seeded as described in section 4.3.1. For RNA harvesting, cells were washed once with PBS. Subsequently, 350-600 µL RLT buffer (from the RNeasy Qiagen Kit, according to its protocol) was added depending on dish size and confluency. Cells were scraped with a cell scraper and collected in a 1.5 mL Eppendorf tube and kept on ice. Cells were stored at -80°C until RNA isolation. RNA isolation was performed using the RNeasy Mini Kit according to the manufacturer's protocol. Optional on-column DNase digestion was performed using the RNase-Free DNase Set

Table 4.6: Western blot Buffer/solution recipes.

Buffer/solution	Recipe
SDS PAGE running buffer	25 mM TRIS, 190 mM Glycine, 0.1% SDS, pH 8.3
Upper buffer (for stacking gel)	0.5 M TRIS (pH 6.8), 0.4% SDS
Lower buffer (for separating gel)	1.5 M TRIS (pH 8.8), 0.4% SDS
Laemmli lysis buffer	10 mM TRIS-HCl (pH 7.5), 2 % SDS, 2 mM EGTA, 20 mM NaF
Stripping buffer	200 mM Glycine, 0.05% Tween-20, pH 2.5
Sample buffer (4x)	20 mL 20% SDS solution, 16 mL 1 M TRIS (pH 6.8), 23.26 mL 86% glycerol, 35.74 mL deionized H_2O. Per 800 µL of this buffer, 200 µL 1% bromphenolblue solution and 50 µL β-mercaptoethanol was added.
Washing buffer (PBS-T)	0.1% Tween-20 (#A4974,0100, AppliChem) in 1x PBS
Wet transfer buffer	20 mM TRIS, 150 mM Glycine, 20% methanol
8% separating gel Per single-percentage gel	4.65 mL deionized H_2O, 2.6 mL lower buffer, 2.7 mL 30% acrylamide, 100 µL 10% APS, 5 µL TEMED
15% separating gel Per single-percentage gel	2.4 mL deionized H_2O, 2.6 mL lower buffer, 5.025 mL 30% acrylamide, 100 µL 10% APS, 5 µL TEMED
4% stacking gel Per two gels	3.05 mL deionized H_2O, 1.3 mL upper buffer, 0.65 mL, 30% acrylamide, 50 µL 10% APS, 5 µL TEMED
5% milk blocking buffer	1x PBS, 0.1% Tween-20, 5% milk powder
5% BSA blocking buffer	1x PBS, 0.1% Tween-20, 5% BSA

to eliminate residual genomic DNA. RNA was eluted in 30 µL nuclease-free H_2O. RNA concentration was subsequently determined using the NanoDrop 2000 Spectrophotometer. RNA was stored at −80°C until reverse transcription.

4.3.5.2. Reverse transcription and qPCR

Reverse transcription was performed to generate cDNA for RT-qPCR from 1 µg of isolated RNA using the Maxima H Minus First Strand cDNA Synthesis Kit according to

the manufacturer's protocol. Reaction cycles were carried out on a ProFlex PCR System (Thermo Fisher Scientific (Waltham, MA, USA)). After synthesis, the cDNA was diluted with nuclease-free H_2O to a final concentration of 100 ng/µL, which was subsequently used for qPCR analyses.

Gene expression at the mRNA level was assessed by quantitative PCR using the QuantStudio 3 Real-Time PCR System (Applied Biosystems/Thermo Fisher Scientific (Waltham, MA, USA)). All samples were measured in triplicate, with each reaction containing 4 µL of 100 ng/µL cDNA, 4 µL of forward and reverse primer mix at 1 µM each (Table 4.2), 2 µL nuclease-free H_2O, and 10 µL1× PowerUp SYBR Green Master Mix, which includes Taq polymerase, dNTPs, PCR buffer, and SYBR Green dye. The standard amplification program used for all reactions is detailed in Table 4.7.

Table 4.7: RT-qPCR cycling program for the SYBR Green method.

Step	Time	Temperature °C	Number of cycles
Enzyme activation part 1	2 min	50	1
Enzyme activation part 2	2 min	95	1
Denaturation	30 sec	95	45
Primer annealing	30 sec	60	
Extension	35 sec	72	
Melt curve step 1	1 min	95	1
Melt curve step 2	1 min	60	1
Melt curve step 3/ Dissociation	15 sec	95	Ramp rate 0.1°C/s

Relative gene expression levels were calculated using the 2^−ΔΔCt method. Target gene expression was first normalized to the HPRT or ACTB housekeeping gene and then compared to the corresponding control group. Data in figures represent the mean of biological replicates (each averaged from three technical replicates), with standard deviation calculated from the biological replicates.

4.3.6. Chromatin Immunoprecipitation (ChIP)

4.3.6.1. Crosslinking

MDA-MB-231 shNsc and shEZH2 cells were seeded in 15 cm dishes with 1.25 × 10^6 cells to have approximately 1.0 × 10^7 cells at harvesting (day 4). To ensure the correct amount of lysis buffer later on, the final cell concentration on day 4 was counted three

times prior to starting the ChIP experiments and used for calculating the amount of lysis buffer needed later on.

On day 4, the medium was removed and the cells were washed with PBS. The cells were then crosslinked using 1% formaldehyde solution in 10 mL DMEM containing 10% FBS for 10 minutes at RT with gentle shaking by hand. Crosslinking was stopped by adding 2 M glycine solution to a final concentration of 0.125 µM, followed by gentle shaking and incubation for 5 minutes at RT. Cells from each dish were scraped and transferred into a 15 mL tube, followed by centrifugation for 5 minutes at 1600 × g at 4°C. The pellet was resuspended in 1 mL cold PBS-Plus (1 mL PBS + 5 µL p-APMSF) per 15 mL tube to wash out the formaldehyde and centrifuged again. The washing step was repeated once. After the second wash, the pellet was resuspended in PBS-Plus, transferred to PET Plug Seal Cap 15 mL tubes (#430053, Corning Incorporated (Corning, NY, USA)), and centrifuged. The supernatant was aspirated, and the cell pellet was transferred to liquid nitrogen for shock freezing. The crosslinked material was stored at -80°C.

4.3.6.2. Chromatin preparation

Crosslinked cell pellets were lysed with 300 µL lysis buffer (all buffer recipes can be found in Table 4.9) per 9.0 × 10^5 cells and incubated for 5 minutes on ice. Then, 300 µL sample was transferred to ice cold 1.5 mL Bioruptor Microtubes (#C30010016, Diagenode/Hologic (Marlborough, MA, USA)). The samples were subsequently sonicated using the Bioruptor Pico (Diagenode/Hologic (Marlborough, MA, USA)) at 4°C using the following program: Power high 3 cycles, 20 seconds on, 30 seconds off. This setting was aimed to fragment the sample to 300-500 bp. The sonicated samples were then centrifuged for 15 minutes at 13200 rpm at RT. The supernatant was collected in a 15 mL tube and aliquoted into 1.5 mL Eppendorf tubes and transferred to liquid nitrogen for shock freezing. The aliquots were frozen at -80°C. In addition, two times 20 µL was collected for test input. To the 20 µL, 100 µL TE buffer and 1µL RNase was added and incubated for 30 minutes at 37°C while gently shaking in a thermomixer (Eppendorf (Hamburg, Germany)). Then 7.5 µL 10% SDS (in Milli-Q (MQ) H_2O) and 3.8 µL proteinase K was added and incubated for 2 hours at 37°C while gently shaking. The crosslinking was reversed overnight at 65°C while gently shaking. The following day, the test input was cleaned up using NTB buffer and the NucleoSpin Gel and PCR Clean-up kit, partially according to the manufactures protocol for DNA clean-up with

SDS. The test input was mixed with 240 µL NTB buffer, added to the column, and spun down. The column membrane was washed twice with 600 µL NT3 buffer. The column membrane was dried and the sample was eluted in 50 µL elution buffer and the DNA concentration was measured with the NanoDrop 2000 Spectrophotometer.

4.3.6.3. Agarose gel electrophoresis

To validate fragmentation, 2% agarose gels were prepared using NEEO agarose dissolved by boiling (microwave) in 1× TAE buffer (40 mM Tris, 20 mM glacial acetic acid, 1 mM EDTA). The volume was dependent on the gel tray size (70, 90, or 140 mL). After cooling to approximately 50°C, 4 µL/100 mL SYBR Safe DNA gel stain was added and mixed until dissolved. The solution was poured into the gel tray, and a comb was added. Gels were left to solidify for 25 minutes in a chemical hood.

To 17.5 µL of test input, 3.5 µL 6× Orange G loading dye was added, and samples were loaded on the gel in a chamber filled with 1× TAE buffer. GeneRuler 1kb Plus DNA ladder was used to assess fragment length. Electrophoresis ran for 30-45 minutes at 100 Volt. DNA was visualized using a blue/green light-equipped gel documentation system (FastGene FAS-V Imaging System, NIPPON Genetics EUROPE (Düren, Germany)).

4.3.6.4. Immunoprecipitation

For each IP, 850 µL dilution buffer was added to 10 µg or 25 µg chromatin in 150 µL lysis buffer (for chromatin or transcription factors, respectively). For the input sample, 10% (100 µL) of the chromatin mix was collected and stored at -20°C. To the diluted chromatin, 2 µg of primary histone antibodies or 5 µg for other primary antibodies and IgG controls were added and incubated overnight in an end-over-end rotator (#7-0045, neoLabLine (Heidelberg, Germany)) at 4°C. The next day, 20 µL magnetic beads were added to the IP samples and rotated for 2 hours at 4°C. Beads were washed using a magnetic rack (FastGene 1.5 mL MagnaStand, #FG-SSMAG1,5, NIPPON Genetics EUROPE (Düren, Germany)) as follows: samples were placed in the rack for 2 minutes, supernatant was removed, 900 µL washing buffer was added, beads were resuspended, and samples rotated for 5 minutes at 4°C. IP samples were washed sequentially with each 900 µL low salt buffer, high salt buffer, LiCl buffer, and twice with TE buffer containing 4.5 µL 10% SDS. After the last wash, 100 µL TE buffer and 1 µL RNase A were added to IP and input samples (per 100 µL), and incubated for 30

minutes at 37°C. Then, 7.5 µL 10% SDS and 3.8 µL proteinase K (per 100 µL) were added and incubated for 2 hours at 37°C The crosslinking was reversed overnight at 65°C. The following day, DNA was cleaned up as described in section 4.3.6.2. Samples were eluted in 65 µL elution buffer and stored at −20°C.

4.3.6.5. ChIP-qPCR and analysis

ChIP samples were analyzed by quantitative PCR using the QuantStudio 3 Real-Time PCR System. All samples were measured in triplicate, with each reaction containing 2 µL of IP sample or 10% input sample (corresponding to 1% of total chromatin), 4 µL of forward and reverse primer mix at 1 µM each (Table 4.3), 4 µL nuclease-free H_2O, and 10 µL 1× PowerUp SYBR Green Master Mix. Standard amplification program is detailed in Table 4.8.

Table 4.8: ChIP-qPCR cycling program for the SYBR Green method.

Step	Time	Temperature °C	Number of cycles
Enzyme activation part 1	2 min	50	1
Enzyme activation part 2	2 min	95	1
Denaturation	1 sec	95	50
Primer annealing/Extension	30 sec	60	
Melt curve step 1	15 sec	95	1
Melt curve step 2	1 min	60	1
Melt curve step 3/ Dissociation	15 sec	95	Ramp rate 0.1°C/s

Input Ct values were adjusted to represent 100% of chromatin by accounting for the 1% input used. ΔCt was calculated as the difference between ChIP Ct and adjusted input. The percentage of input for each ChIP sample was determined using the formula:

$$\% \text{ of Input} = 100 \times 2^{\Delta Ct}$$

Relative occupancy (O_a) was calculated as:

$$O_a = \% \text{ of Input } X_a - \% \text{ of Input } X_{IgG}$$

This approach normalizes ChIP signals to total chromatin and accounts for the fraction of input in the qPCR reaction.

Table 4.9: ChIP buffer recipes.

Buffers	Recipe
Dilution buffer	200 µL 10% SDS, 22 mL 10% Triton-X-100, 480 µL 0.5M EDTA (pH8.0), 33.4 mL 1M NaCL, 4 mL 1M TRIS-HCl (pH 8.1), 140.58 mL MQ H_2O
High salt buffer	2 mL 10% SDS, 20 ml 10% Triton-X-100, 800 µL 0.5M EDTA (pH8.0), 100 mL 1M NaCL, 4 mL 1M TRIS-HCl (pH 8.1), 73.2 mL MQ H_2O
LiCl buffer	10 mL 1.25M LiCL, 5 mL 10% NP-40, 5 mL 10% Deoxycholate, 100 µL 0.5M EDTA (pH8.0), 500 µL 1M TRIS-HCl (pH 8.1), 29.4 mL MQ H_2O
Low salt buffer	2 mL 10% SDS, 20 ml 10% Triton-X-100, 800 µL 0.5M EDTA (pH8.0), 30 mL 1M NaCL, 4 mL 1M TRIS-HCl (pH 8.1), 143,2 mL MQ H_2O
Lysis buffer	20 mL 10% SDS, 4 mL 0.5M EDTA (pH8.0), 10 mL 1M TRIS-HCl (pH 8.1), 166 mL MQ H_2O
TE buffer	2 mL 1M TRIS-HCl (pH 8.1), 0.5M EDTA (pH8.0), 197.6 ml MQ H_2O

4.3.7. Cell growth curve

For the cell growth curve experiment, 4 × 10^4 cells were seeded in a 6-well plate in triplicate. One plate was counted on day 2 as described in section 4.3.1.1, with each well counted twice. The remaining plates were transferred to the hypoxia chamber or kept under normoxic conditions. This procedure was continued until day 5.

For the rescue experiment, 5.5 × 10^4 cells were seeded in a 6-well plate in triplicate. Cells were transfected on day 2 as described in section 4.3.1.4. On day 3, the medium was refreshed, and cells were transferred to the hypoxia chamber. Counting was performed on day 5 in the same manner as the standard cell growth curve experiment.

4.3.8. Soft agar colony formation assay

The bottom agar layer was prepared on the day of the experiment or one day prior to adding the second cell layer. To create the bottom layer of 0.6%, autoclaved 3% agar (in MQ H_2O) was melted in the microwave, kept in a 60°C water bath, and mixed with RPMI culture medium supplemented with 10% FBS and 2 mM GlutaMAX to make a final 0.6% agar concentration. Then, 1 mL was quickly added to pre-heated 6-well plates using pre-heated pipets. Plates were left with the lid partially open in the cell culture hood until solidified, and then transferred to a 5% CO2 and 37°C incubator for immediate use or wrapped in Parafilm and stored at 4°C for future use.

For the second layer, 7.5 × 10^3 cells were resuspended in culture medium and mixed with 3% agar (~40°C) to create a final 0.45% agar layer. This layer was solidified for 15 minutes at RT, followed by 15 minutes at 4°C, another 15 minutes at RT, and then moved to a 5% CO2 and 37°C incubator. On day 2, plates were moved to the hypoxia chamber or kept under normoxic conditions. Twice a week, 500 µL culture medium was added to the wells.

On day 15, 0.5% crystal violet was diluted to 0.02% in 10% ethanol (in MQ H_2O). The medium was carefully removed from the wells, and 1 mL of 0.02% crystal violet solution was added to each well and incubated for 30 minutes at RT. The crystal violet solution was then carefully removed, and wells were washed three times with MQ H_2O every 20-30 minutes. The final wash was kept for at least 3 hours and then removed. Plates were wrapped in Parafilm and stored at 4°C.

Brightfield images were taken using the Confocal Quantitative Image Cytometer (CQ1) (Yokogawa, Tokyo, Japan) with an excitation power of 20% and an exposure time of 50 ms. The CQ1 did not have a template for our 6-well plates, therefore it was not possible to image the full wells. Colonies were quantified using the Analyze Particles function in Fiji after the images were cropped to ensure that the same frame size was used for all wells. Brightness was set at 150-180, and threshold was set at 0-150. Log2 counts were normalized to the PC-9 shNsc normoxia sample log2 count.

4.3.9. Organotypic brain slice *ex vivo* invasion assay

4.3.9.1. Brain dissection and slicing

Before starting the experiment, the microtome (VT1200 S, Leica Biosystems (Nußloch, Germany)) was prepared and configured as follows: Speed 0.20 mm/s, amplitude 0.90 mm, thickness 300 µm. Healthy 3-6 months old C57BL/6 mouse heads were provided by the groups of Professor Wolfgang Kummer and Professor Norbert Weissmann, JLU.

The brain was washed with PBS, followed by 70% and 100% ethanol to remove blood and hair. The brain was dissected and glued onto the microtome plate against a 5% agarose block for stabilization. Subsequently, the brain was sliced into 300 µm sections in cold dissection medium (medium recipes are listed in Table 4.10). Slices containing the striatum were collected and kept in cold dissection medium.

Next, 1 mL of brain culture medium was added to the wells of a 6-well plate below the ThinCert cell culture inserts (#657641, Greiner Bio-One (Kremsmünster, Austria)) and 1 mL on top of the insert. A maximum of two brain slices were transferred to each insert. Slices were washed twice by carefully removing the medium and adding fresh medium. After the last wash, 1 mL of brain culture medium was added below the insert and 500 µL to the insert. Slices were incubated for 3 hours at 37°C.

4.3.9.2. Co-culture

Two days prior to brain dissection, 5.0 × 10^5 MDA-MB-231 shNsc and shEZH2 cells were seeded in 6 cm dishes and transferred to the hypoxia chamber the following day or kept under normoxic conditions for 24 hours before co-culture.

Cells were washed, trypsinized, and resuspended by pipetting up and down, as described in section 4.3.1. Brain culture medium was added to stop trypsinization, and cells were counted, as described in section 4.3.1.1. Next, 1 mL of brain culture medium was added below the insert, and 1 mL containing 3.0 × 10^5 cells was added to the insert. Cells and brain slices were incubated together for 3 hours. After incubation, the medium and cells were carefully removed, and the brain slice was gently washed with 250 µL PBS. Subsequently 1 mL brain culture medium was added below the insert and 250 µL was added to the insert to avoid the brain slice from drying out. Slices were incubated at 21% or 1% O_2 for an additional 45 hours**.** Baseline slices (3 hours) were fixed by adding 1 mL of 4% PFA (in PBS) below the insert and 1 mL to the insert for 40 minutes. Slices were washed twice with PBS and stored in PBS wrapped in Parafilm at 4°C. The same procedure was used for slices at 48 hours.

Fixed slices were later stained with 1:2000 DAPI in PBS for 1.5 hours to determine the brain surface. Slices were washed twice with PBS and once with deionized H_2O, and mounted on microscope slides using DAKO mounting medium. The slides were kept at RT for several hours, then stored to a 4°C fridge.

4.3.9.3. Imaging and analysis

Slides were scanned using the CQ1. Two to four areas with few or no cell clumps in or near the striatum were scanned with 5 µm steps across the 300 µm slices.

- **Brightfield:** excitation power 20%, exposure time 50 ms
- **DAPI and GFP:** excitation power 40%, exposure time 500 ms

- **Contrast enhancement:** 100-500 for DAPI, 100-4000 for GFP

The surface of the brain slice was determined visually by the first clear DAPI signal on the same day for all slices. Further analysis was performed in Fiji.

- GFP brightness was set at 100-10000
- Thresholds were determined per picture
- Adjustable watershed was used with a tolerance of 0.1
- GFP-positive cells were counted per stack using Analyze Particles (size 78-17663 pixels)
- GFP intensity was determined using histogram measurements
- The last stack was used as a negative control; only stacks with intensity ≥ 20 and at least one visible cell were considered GFP-positive

Data from different areas of the same slice were considered technical replicates; different mouse brains were considered biological replicates. For distribution analysis, only areas without clumps with at least 20 cells were analyzed. Log2 data were used for distribution analysis.

Net invasion was calculated using the formula:

Net invasion depth per mouse (µm) = Total depth at 48h - Average total depth at 3h

Table 4.10: Organotypic brain slice *ex vivo* invasion assay media recipes.

Media	Recipe
Dissection medium	94.1 mL MEM, 1 mL GlutaMAX, 1 mL -(+)-Glucose, 2.5 mL HEPES, 2 mL Pen-Strep, 400 µL NaOH. pH was adjusted to 7.3-7.4 by using hydrochloric acid solution and NaOH.
Brain culture medium	42 mL MEM, 25 mL BME, 25 mL horse serum, 1 mL GlutaMAX, 1.5 mL -(+)-Glucose, 2.5 mL HEPES, 1 mL Pen-Strep, 2 mL sodium bicarbonate, 1 ml Amphotericin B. pH was adjusted to 7.3 by using hydrochloric acid solution and NaOH.

4.3.10. Statistical analysis

All data are presented as mean ± SD. Statistical analyses were performed using GraphPad Prism version 8.4.3. The specific statistical tests used are indicated in the

corresponding figure legends. Statistical significance was defined as follows: ns, $p > 0.05$; * $p < 0.05$; ** $p < 0.01$; *** $p < 0.001$; **** $p < 0.0001$.

Bibliography

1. Thompson CB. Into Thin Air: How We Sense and Respond to Hypoxia. Cell. 2016;167(1):9–11.
2. Semenza GL. Oxygen sensing, hypoxia-inducible factors, and disease pathophysiology. Annu Rev Pathol Mech Dis. 2014;9:47–71.
3. Rankin EB, Giaccia AJ. Hypoxic control of metastasis. Science. 2016;352(6282):175–80.
4. Hanahan D, Weinberg RA. Hallmarks of cancer: The next generation. Cell. 2011;144(5):646–74.
5. Hanahan D. Hallmarks of Cancer: New Dimensions. Cancer Discov. 2022;12(1):31–46.
6. Rankin EB, Nam J-M, Giaccia AJ. Hypoxia: Signaling in the Metastatic Cascade. Trends Cancer. 2016;2(6):295–304.
7. Eales KL, Hollinshead KER, Tennant DA. Hypoxia and metabolic adaptation of cancer cells. Oncogenesis. 2016;5(1):e190–e190.
8. Lee P, Chandel NS, Simon MC. Cellular adaptation to hypoxia through hypoxia inducible factors and beyond. Nat Rev Mol Cell Biol. 2020;21(5):268–83.
9. Batie M, del Peso L, Rocha S. Hypoxia and chromatin: A focus on transcriptional repression mechanisms. Biomedicines. 2018;6(2):47.
10. Cavadas MAS, Cheong A, Cormac T. The regulation of transcriptional repression in hypoxia. Exp Cell Res. 2017;356(2):173–81.
11. Liu L, Cash TP, Jones RG, Keith B, Thompson CB, Simon MC. Hypoxia-Induced Energy Stress Regulates mRNA Translation and Cell Growth. Mol Cell. 2006;21:521–31.
12. Liao D, Johnson RS. Hypoxia : A key regulator of angiogenesis in cancer. Cancer Metastasis Rev. 2007;26:281–90.
13. Kaelin WG, Ratcliffe PJ. Oxygen Sensing by Metazoans: The Central Role of the HIF Hydroxylase Pathway. Mol Cell. 2008;30(4):393–402.
14. Wang GL, Jiang BH, Rue EA, Semenza GL. Hypoxia-inducible factor 1 is a basic-helix-loop-helix-PAS heterodimer regulated by cellular O2 tension. Proc Natl Acad Sci U S A. 1995;92(12):5510–4.
15. Tian H, McKnight SL, Russell DW. Endothelial PAS domain protein 1 (EPAS1), a transcription factor selectively expressed in endothelial cells. Genes Dev.

1997;11(1):72–82.
16. Flamme I, Fröhlich T, Reutern M Von, Kappel A, Damert A, Risau W. HRF, a putative basic helix-loop-helix-PAS-domain transcription factor is closely related to hypoxia-inducible factor-1a and developmentally expressed in blood vessels. Mech Dev. 1997;63:51–60.
17. Ema M, Taya S, Yokotani N, Sogawa K, Matsuda Y, Fujii-Kuriyama Y. A novel bHLH-PAS factor with close sequence similarity to hypoxia-inducible factor 1α regulates the VEGF expression and is potentially involved in lung and vascular development. Proc Natl Acad Sci U S A. 1997;94(9):4273–8.
18. Keith B, Johnson RS, Simon MC. HIF-1a and HIF-2a sibling rivalry in hypoxic tumor growth and progression. Nat Rev cancer. 2012;12(1):9–22.
19. Schofield CJ, Ratcliffe PJ. Oxygen sensing by HIF hydroxylases. Nat Rev Mol Cell Biol. 2004;5(5):343–54.
20. Bruick RK, McKnight SL. A conserved family of prolyl-4-hydroxylases that modify HIF. Science. 2001;294(5545):1337–40.
21. Jaakkola P, Mole DR, Tian YM, Wilson MI, Gielbert J, Gaskell SJ, et al. Targeting of HIF-α to the von Hippel-Lindau ubiquitylation complex by O2-regulated prolyl hydroxylation. Science. 2001;292:468–72.
22. Ivan M, Kondo K, Yang H, Kim W, Valiando J, Ohh M, et al. HIFα Targeted for VHL-Mediated Destruction by Proline Hydroxylation: Implications for O2 Sensing. Science. 2001;292:464–8.
23. Maxwell, Patrick H. Wiesener MS, Chang G-W, Clifford SC, Vaux EC, Cockman, Matthew E. Wykoff CC, Pugh, Christopher W. Maher ER, et al. The tumour suppressor protein VHL targets hypoxia-inducible factors for oxygen-dependent proteolysis. Nature. 1999;399:271–5.
24. Lando D, Peet DJ, Gorman JJ, Whelan DA, Whitelaw ML, Bruick RK. FIH-1 is an asparaginyl hydroxylase enzyme that regulates the transcriptional activity of hypoxia-inducible factor. Genes Dev. 2002;16(12):1466–71.
25. Masson N, Singleton RS, Sekirnik R, Trudgian DC, Ambrose LJ, Miranda MX, et al. The FIH hydroxylase is a cellular peroxide sensor that modulates HIF transcriptional activity. EMBO Rep. 2012;13(3):251–7.
26. Lando D, Peet DJ, Whelan DA, Gorman JJ, Whitelaw ML. Asparagine hydroxylation of the HIF transactivation domain: A hypoxic switch. Science. 2002;295:858–61.

27. Bracken CP, Fedele AO, Linke S, Balrak W, Lisy K, Whitelaw ML, et al. Cell-specific regulation of hypoxia-inducible factor (HIF)-1α and HIF-2α stabilization and transactivation in a graded oxygen environment. J Biol Chem. 2006;281(32):22575–85.
28. Yan Q, Bartz S, Mao M, Li L, Kaelin WG. The Hypoxia-Inducible Factor 2 α N-Terminal and C-Terminal Transactivation Domains Cooperate To Promote Renal Tumorigenesis In Vivo . Mol Cell Biol. 2007;27(6):2092–102.
29. Bakleh MZ, Al Haj Zen A. The Distinct Role of HIF-1α and HIF-2α in Hypoxia and Angiogenesis. Cells. 2025;14(9):1–22.
30. Li Z, Bao S, Wu Q, Wang H, Eyler C, Sathornsumetee S, et al. Hypoxia-Inducible Factors Regulate Tumorigenic Capacity of Glioma Stem Cells cancer stem cell specific molecules involved in neoangiogenesis, including HIF2α and its regulated factors. Cancer Cell. 2009;15(6):501–13.
31. Holmquist-Mengelbier L, Fredlund E, Löfstedt T, Noguera R, Navarro S, Nilsson H, et al. Recruitment of HIF-1α and HIF-2α to common target genes is differentially regulated in neuroblastoma: HIF-2α promotes an aggressive phenotype. Cancer Cell. 2006;10(5):413–23.
32. Nilsson H, Jögi A, Beckman S, Harris AL, Poellinger L, Påhlman S. HIF-2α expression in human fetal paraganglia and neuroblastoma: Relation to sympathetic differentiation, glucose deficiency, and hypoxia. Exp Cell Res. 2005;303(2):447–56.
33. Uchida T, Rossignol F, Matthay MA, Mounier R, Couette S, Clottes E, et al. Prolonged hypoxia differentially regulates hypoxia-inducible factor (HIF)-1α and HIF-2α expression in lung epithelial cells: Implication of natural antisense HIF-1α. J Biol Chem. 2004;279(15):14871–8.
34. Bartoszewski R, Moszyńska A, Serocki M. Primary endothelial cell – specific regulation of hypoxia- inducible factor (HIF) -1 and HIF-2 and their target gene expression profiles during hypoxia. (1).
35. Koh MY, Jr RL, Liu X, Powis G. The Hypoxia-Associated Factor Switches Cells from HIF-1α– to HIF-2α–Dependent Signaling Promoting Stem Cell Characteristics, Aggressive Tumor Growth and Invasion. Cancer Res. 2011;11(71):4015–4027.
36. Luo W, Zhong J, Chang R, Hu H, Pandey A, Semenza GL. Hsp70 and CHIP selectively mediate ubiquitination and degradation of hypoxia-inducible factor

(HIF)-1α but not HIF-2α. J Biol Chem. 2010;285(6):3651–63.
37. Koh MY, Powis G. Passing the baton: The HIF switch. Trends Biochem Sci. 2012;37(9):364–372.
38. Henze A, Riedel J, Diem T, Wenner J, Flamme I, Pouyseggur J, et al. Prolyl Hydroxylases 2 and 3 Act in Gliomas as Protective Negative Feedback Regulators of Hypoxia-Inducible Factors. Cancer Res. 2010;70(1):357–66.
39. Appelhoffl RJ, Tian YM, Raval RR, Turley H, Harris AL, Pugh CW, et al. Differential function of the prolyl hydroxylases PHD1, PHD2, and PHD3 in the regulation of hypoxia-inducible factor. J Biol Chem. 2004;279(37):38458–65.
40. Lombardi O, Li R, Halim S, Choudhry H, Ratcliffe PJ, Mole DR. Pan-cancer analysis of tissue and single-cell HIF-pathway activation using a conserved gene signature. Cell Rep. 2022;41(7):111652.
41. Smythies JA, Sun M, Masson N, Salama R, Simpson PD, Murray E, et al. Inherent DNA -binding specificities of the HIF -1α and HIF -2α transcription factors in chromatin. EMBO Rep. 2019;20(1):e46401.
42. Zhong H, De Marzo AM, Laughner E, Lim M, Hilton DA, Zagzag D, et al. Overexpression of hypoxia-inducible factor 1α in common human cancers and their metastases. Cancer Res. 1999;59(22):5830–5.
43. Talks KL, Turley H, Gatter KC, Maxwell PH, Pugh CW, Ratcliffe PJ, et al. The expression and distribution of the hypoxia-inducible factors HIF-1α and HIF-2α in normal human tissues, cancers, and tumor-associated macrophages. Am J Pathol. 2000;157(2):411–21.
44. Bos R, Van der Groep P, Greijer AE, Shvarts A, Meijer S, Pinedo HM, et al. Levels of hypoxia-inducible factor-1α independently predict prognosis in patients with lymph node negative breast carcinoma. Cancer. 2003;97(6):1573–81.
45. Schindl M, Schoppmann SF, Samonigg H, Hausmaninger H, Kwasny W, Gnant M, et al. Overexpression of hypoxia-inducible factor 1α is associated with an unfavorable prognosis in lymph node-positive breast cancer. Clin Cancer Res. 2002;8(6):1831–7.
46. Charpin C, Tavassoli F, Secq V, Giusiano S, Villeret J, Garcia S, et al. Validation of an immunohistochemical signature predictive of 8-year outcome for patients with breast carcinoma. Int J Cancer. 2012;131(3):E236-43.
47. Wang HX, Qin C, Han FY, Wang XH, Li N. HIF-2α as a prognostic marker for

breast cancer progression and patient survival. Genet Mol Res. 2014;13(2):2817–26.

48. Roig EM, Yaromina A, Houben R, Groot AJ, Dubois L, Vooijs M. Prognostic role of hypoxia-inducible factor-2α tumor cell expression in cancer patients: A meta-analysis. Front Oncol. 2018;8:224.
49. Helczynska K, Larsson AM, Mengelbier LH, Bridges E, Fredlund E, Borgquist S, et al. Hypoxia-inducible factor-2α correlates to distant recurrence and poor outcome in invasive breast cancer. Cancer Res. 2008;68(22):9212–20.
50. Hung JJ, Yang MH, Hsu HS, Hsu WH, Liu JS, Wu KJ. Prognostic significance of hypoxia-inducible factor-1α, TWIST1 and Snail expression in resectable non-small cell lung cancer. Thorax. 2009;64(12):1082–9.
51. Han S, Huang T, Hou F, Yao L, Wang X, Wu X. The prognostic value of hypoxia-inducible factor-1α in advanced cancer survivors: a meta-analysis with trial sequential analysis. Ther Adv Med Oncol. 2019;11:1758835919875851.
52. Gao ZJ, Wang Y, Yuan WD, Yuan JQ, Yuan K. HIF-2α not HIF-1α overexpression confers poor prognosis in non-small cell lung cancer. Tumor Biol. 2017;39(6):1010428317709637.
53. Wu XH, Qian C, Yuan K. Correlations of hypoxia-inducible factor-1α/hypoxia-inducible factor -2α expression with angiogenesis factors expression and prognosis in non-small cell lung cancer. Chin Med J (Engl). 2011;124(1):11–8.
54. FDA approves belzutifan for cancers associated with von Hippel-Lindau disease [Internet]. U.S. Food & Drug Administration. 2021. Available from: https://www.fda.gov/drugs/resources-information-approved-drugs/fda-approves-belzutifan-cancers-associated-von-hippel-lindau-disease
55. Jesduvroq (daprodustat) approved by US FDA for anaemia of chronic kidney disease in adults on dialysis [Internet]. GSK. 2023. Available from: https://www.gsk.com/en-gb/media/press-releases/jesduvroq-daprodustat-approved-by-us-fda-for-anaemia-of-chronic-kidney-disease-in-adults-on-dialysis/
56. Akebia Receives FDA Approval of Vafseo® (vadadustat) Tablets for the Treatment of Anemia due to Chronic Kidney Disease in Adult Patients on Dialysis [Internet]. Akebia. 2024. Available from: https://ir.akebia.com/news-releases/news-release-details/akebia-receives-fda-approval-vafseor-vadadustat-tablets#:~:text=PDF Version-,Akebia Receives FDA Approval of

Vafseo® (vadadustat) Tablets for,now approved in 37 countries.
57. Acker T, Diez-Juan A, Aragones J, Tjwa M, Brusselmans K, Moons L, et al. Genetic evidence for a tumor suppressor role of HIF-2α. Cancer Cell. 2005;8(2):131–41.
58. Hayflick L, Moorhead P. The serial cultivation of human diploid cell strains. Exp Cell Res. 1961;25:585–621.
59. Yatabe N, Kyo S, Maida Y, Nishi H, Nakamura M, Kanaya T, et al. HIF-1-mediated activation of telomerase in cervical cancer cells. Oncogene. 2004;23(20):3708–15.
60. Kim JW, Tchernyshyov I, Semenza GL, Dang C V. HIF-1-mediated expression of pyruvate dehydrogenase kinase: A metabolic switch required for cellular adaptation to hypoxia. Cell Metab. 2006;3(3):177–85.
61. Qiu B, Ackerman D, Sanchez D.J, Li B, Ochocki J.D, Grazioli A, Bobrovnikova-Marjon E, Diehl J.A, Keith B, Simon M.C. HIF-2α dependent lipid storage promotes endoplasmic reticulum homeostasis in clear cell renal cell carcinoma. Cancer Discov. 2015;5(6):652–67.
62. Li W, Chen C, Zhao X, Ye H, Zhao Y, Fu Z, et al. HIF-2α regulates non-canonical glutamine metabolism via activation of PI3K/mTORC2 pathway in human pancreatic ductal adenocarcinoma. J Cell Mol Med. 2017;21(11):2896–908.
63. Zou Y, Palte MJ, Deik AA, Li H, Eaton JK, Wang W, et al. A GPX4-dependent cancer cell state underlies the clear-cell morphology and confers sensitivity to ferroptosis. Nat Commun. 2019;10(1):1617.
64. Qing G, Simon MC. Hypoxia inducible factor-2α: a critical mediator of aggressive tumor phenotypes. Curr Opin Genet Dev. 2009;19(1):60–6.
65. Ruan K, Song G, Ouyang G. Role of hypoxia in the hallmarks of human cancer. J Cell Biochem. 2009;107(6):1053–62.
66. Joshi S, Singh AR, Zulcic M, Durden DL. A macrophage-dominant PI3K isoform controls hypoxia-induced HIF1α and HIF2α stability and tumor growth, angiogenesis, and metastasis. Mol Cancer Res. 2014;12(10):1520–31.
67. Wicks EE, Semenza GL. Hypoxia-inducible factors: cancer progression and clinical translation. J Clin Invest. 2022;132(11):e159839.
68. Camuzi D, de Amorim Í, Ribeiro Pinto L, Oliveira Trivilin L, Mencalha A, Soares Lima S. Regulation Is in the Air: The Relationship between Hypoxia and

Epigenetics in Cancer. Cells. 2019;8(4):300.
69. Wise DR, Ward PS, Shay JES, Cross JR, Gruber JJ, Sachdeva UM, et al. Hypoxia promotes isocitrate dehydrogenasedependent carboxylation of α-ketoglutarate to citrate to support cell growth and viability. Proc Natl Acad Sci U S A. 2011;108(49):19611–6.
70. Metallo CM, Gameiro PA, Bell EL, Mattaini KR, Yang J, Hiller K, et al. Reductive glutamine metabolism by IDH1 mediates lipogenesis under hypoxia. Nature. 2012;481(7381):380–4.
71. Schmitt AM, Schmid S, Rudolph T, Anlauf M, Prinz C, Klöppel G, et al. VHL inactivation is an important pathway for the development of malignant sporadic pancreatic endocrine tumors. Endocr Relat Cancer. 2009;16(4):1219–27.
72. Yang S, Park YS, Cho JH, Moon B, An H, Lee JY, et al. Regulation of hypoxia responses by flavin adenine dinucleotide-dependent modulation of HIF -1α protein stability . EMBO J. 2017;36(8):1011–28.
73. Li T, Mao C, Wang X, Shi Y, Tao Y. Epigenetic crosstalk between hypoxia and tumor driven by HIF regulation. J Exp Clin Cancer Res. 2020;39(1):1–25.
74. Lachance G, Uniacke J, Audas TE, Holterman CE, Franovic A, Payette J, et al. DNMT3a epigenetic program regulates the HIF-2α oxygen-sensing pathway and the cellular response to hypoxia. Proc Natl Acad Sci U S A. 2014;111(21):7783–8.
75. Chakraborty AA, Laukka T, Myllykoski M, Ringel AE, Booker MA, Tolstorukov MY, et al. Histone demethylase KDM6A directly senses oxygen to control chromatin and cell fate. Science. 2019;363(6432):1217–22.
76. Batie M, Frost J, Frost M, Wilson JW, Schofield P, Rocha S. Hypoxia induces rapid changes to histone methylation and reprograms chromatin. Science. 2019;363:1222–6.
77. Bernstein BE, Mikkelsen TS, Xie X, Kamal M, Huebert DJ, Cuff J, et al. A Bivalent Chromatin Structure Marks Key Developmental Genes in Embryonic Stem Cells. Cell. 2006;125:315–26.
78. Prickaerts P, Adriaens ME, Beucken T Van Den, Koch E, Dubois L, Dahlmans VEH, et al. Hypoxia increases genome - wide bivalent epigenetic marking by specific gain of H3K27me3. Epigenetics Chromatin. 2016;9:46.
79. Shi X, Hong T, Walter KL, Ewalt M, Michishita E, Hung T, et al. ING2 PHD domain links histone H3 lysine 4 methylation to active gene repression. Nature.

2006;442:96–9.
80. Metallo CM, Vander Heiden MG. Understanding Metabolic Regulation and Its Influence on Cell Physiology. Mol Cell. 2013;49(3):388–98.
81. Kohli RM, Zhang Y. TET enzymes, TDG and the dynamics of DNA demethylation. Nature. 2013;502(7472):472–479.
82. Schwartz YB, Pirrotta V. A new world of Polycombs: Unexpected partnerships and emerging functions. Nat Rev Genet. 2013;14(12):853–64.
83. Tan JZ, Yan Y, Wang XX, Jiang Y, Xu HE. EZH2: Biology, disease, and structure-based drug discovery. Acta Pharmacol Sin. 2014;35(2):161–74.
84. Margueron R, Margueron R. The Polycomb Complex PRC2 and its Mark in Life. Nature. 2011;469(7330):343–9.
85. Wang J, Wang GG. No easy way out for ezh2: Its pleiotropic, noncanonical effects on gene regulation and cellular function. Int J Mol Sci. 2020;21(24):9501.
86. Czermin B, Melfi R, McCabe D, Seitz V, Imhof A, Pirrotta V. Drosophila enhancer of Zeste/ESC complexes have a histone H3 methyltransferase activity that marks chromosomal Polycomb sites. Cell. 2002;111(2):185–96.
87. Müller J, Hart CM, Francis NJ, Vargas ML, Sengupta A, Wild B, et al. Histone methyltransferase activity of a Drosophila Polycomb group repressor complex. Cell. 2002;111(2):197–208.
88. Cao R, Wang L, Wang H, Xia L, Erdjument-Bromage H, Tempst P, et al. Role of histone H3 lysine 27 methylation in X-inactivation. Science. 2002;298(5595):1039–43.
89. Kuzmichev A, Nishioka K, Erdjument-Bromage H, Tempst P, Reinberg D. Histone methyltransferase activity associated with a human multiprotein complex containing the enhancer of zeste protein. Genes Dev. 2002;16(22):2893–905.
90. Højfeldt JW, Laugesen A, Willumsen BM, Damhofer H, Hedehus L, Tvardovskiy A, et al. Accurate H3K27 methylation can be established de novo by SUZ12-directed PRC2. Nat Struct Mol Biol. 2018;25(3):225–32.
91. Grau DJ, Chapman BA, Garlick JD, Borowsky M, Francis NJ, Kingston RE. Compaction of chromatin by diverse polycomb group proteins requires localized regions of high charge. Genes Dev. 2011;25(20):2210–21.
92. Di Croce L, Helin K. Transcriptional regulation by Polycomb group proteins. Nat

Struct Mol Biol. 2013;20(10):1147–55.
93. Justin N, Zhang Y, Tarricone C, Martin SR, Chen S, Underwood E, et al. Structural basis of oncogenic histone H3K27M inhibition of human polycomb repressive complex 2. Nat Commun. 2016;7:11316.
94. Jiao L, Liu X. Structural basis of histone H3K27 trimethylation by an active polycomb repressive complex 2. Science. 2015;350(6258):aac4383.
95. Wang B, Liu Y, Liao Z, Wu H, Zhang B, Zhang L. EZH2 in hepatocellular carcinoma: progression, immunity, and potential targeting therapies. Exp Hematol Oncol. 2023;12(1):52.
96. Jiao L, Shubbar M, Yang X, Zhang Q, Chen S, Wu Q, et al. A partially disordered region connects gene repression and activation functions of EZH2. Proc Natl Acad Sci U S A. 2020;117(29):16992–7002.
97. Wang J, Park KS, Yu X, Gong W, Earp HS, Wang GG, et al. A cryptic transactivation domain of EZH2 binds AR and AR's splice variant, promoting oncogene activation and tumorous transformation. Nucleic Acids Res. 2022;50(19):10929–46.
98. Wang J, Yu X, Gong W, Liu X, Park KS, Ma A, et al. EZH2 noncanonically binds cMyc and p300 through a cryptic transactivation domain to mediate gene activation and promote oncogenesis. Nat Cell Biol. 2022;24(3):384–99.
99. Becht DC, Biswas S, Xu C, Xuan H, Khalil M, Cai L, et al. Multiple transactivation domains of EZH2 bind to the TAZ2 domain of p300 and stimulate the acetyltransferase function of p300. 2025;482(13):955–68.
100. Varambally S, Dhanasekaran SM, Zhou M, Barrette TR, Kumar-Sinha C, Sanda MG, et al. The polycomb group protein EZH2 is involved in progression of prostate cancer. Nature. 2002;419(6907):624–9.
101. Ren G, Baritaki S, Marathe H, Feng J, Park S, Beach S, et al. Polycomb protein EZH2 regulates tumor invasion via the transcriptional repression of the metastasis suppressor RKIP in breast and prostate cancer. Cancer Res. 2012;72(12):3091–104.
102. Kleer CG, Cao Q, Varambally S, Shen R, Ota I, Tomlins SA, et al. EZH2 is a marker of aggressive breast cancer and promotes neoplastic transformation of breast epithelial cells. Proc Natl Acad Sci U S A. 2003;100(20):11606–11.
103. Zhang L, Qu J, Qi Y, Duan Y, Huang YW, Zhou Z, et al. EZH2 engages TGFβ signaling to promote breast cancer bone metastasis via integrin β1-FAK

activation. Nat Commun. 2022;13(1):2543.
104. Moore HM, Gonzalez ME, Toy KA, Cimino-Mathews A, Argani P, Kleer CG. EZH2 inhibition decreases p38 signaling and suppresses breast cancer motility and metastasis. Breast Cancer Res Treat. 2013;138(3):741–752.
105. Hirukawa A, Smith HW, Zuo D, Dufour CR, Savage P, Bertos N, et al. Targeting EZH2 reactivates a breast cancer subtype-specific anti-metastatic transcriptional program. Nat Commun. 2018;9(1):2547.
106. Zhang L, Yao J, Wei Y, Zhou Z, Li P, Qu J, et al. Blocking immunosuppressive neutrophils deters pY696-EZH2–driven brain metastases. Sci Transl Med. 2020;12(545):eaaz5387.
107. Wang L, Chen C, Song Z, Wang H, Ye M, Wang D, et al. EZH2 depletion potentiates MYC degradation inhibiting neuroblastoma and small cell carcinoma tumor formation. Nat Commun. 2022;13(1):12.
108. Zhang H, Q J, Reyes JM, Li L, Rao PK, Li F, et al. Oncogenic deregulation of EZH2 as an opportunity for targeted therapy in lung cancer. Cancer Discov. 2016;6(9):1006–1021.
109. Fan K, Zhang B hui, Han D, Sun Y chuan. EZH2 as a prognostic-related biomarker in lung adenocarcinoma correlating with cell cycle and immune infiltrates. BMC Bioinformatics. 2023;24(1):149.
110. Li X, Xing J, Wang H, Yu E. The SLC34A2-ROS-HIF-1-induced up-regulation of EZH2 expression promotes proliferation and chemo-resistance to apoptosis in colorectal cancer. Biosci Rep. 2019;39(5):BSR20180268.
111. Pang B, Zheng XR, Tian J xia, Gao T hong, Gu G yan, Zhang R, et al. EZH2 promotes metabolic reprogramming in glioblastomas through epigenetic repression of EAF2-HIF1α signaling. Oncotarget. 2016;7(29):45134–43.
112. Zingg D, Debbache J, Schaefer SM, Tuncer E, Frommel SC, Cheng P, et al. The epigenetic modifier EZH2 controls melanoma growth and metastasis through silencing of distinct tumour suppressors. Nat Commun. 2015;6:6051.
113. Souroullas GP, Jeck WR, Parker JS, Simon JM, Liu JY, Paulk J, et al. An oncogenic Ezh2 mutation induces tumors through global redistribution of histone 3 lysine 27 trimethylation. Nat Med. 2016;22(6):632–40.
114. Wang Y, Hou N, Cheng X, Zhang J, Tan X, Zhang C, et al. Ezh2 acts as a tumor suppressor in kras-driven lung adenocarcinoma. Int J Biol Sci. 2017;13(5):652–9.

115. Ntziachristos P, Tsirigos A, Vlierberghe P Van, Trimarchi T, Flaherty MS, Ferres-marco D, et al. Genetic Inactivation of the PRC2 Complex in T-Cell Acute Lymphoblastic Leukemia. Nat Med. 2012;18(2):298–301.
116. Zimmerman SM, Lin PN, Souroullas GP. Non-canonical functions of EZH2 in cancer. Front Oncol. 2023;13:1233953.
117. Eich M-L, Athar M, III JEF, Varambally S. EZH2-targeted therapies in cancer: hype or a reality. Cancer Res. 2020;80(24):5449–5458.
118. Cha TL, Zhou BP, Xia W, Wu Y, Yang CC, Chen C Te, et al. Akt-mediated phosphorylation of EZH2 suppresses methylation of lysine 27 in histone H3. Science. 2005;310(5746):306–10.
119. Kim E, Kim M, Woo DH, Shin Y, Shin J, Chang N, et al. Phosphorylation of EZH2 Activates STAT3 Signaling via STAT3 Methylation and Promotes Tumorigenicity of Glioblastoma Stem-like Cells. Cancer Cell. 2013;23(6):839–52.
120. Zhao Y, Hu Z, Li J, Hu T. EZH2 Exacerbates Breast Cancer by Methylating and Activating STAT3 Directly. J Cancer. 2021;12(17):5220–30.
121. Wozniak M, Czyz M. Exploring oncogenic roles and clinical significance of EZH2: focus on non-canonical activities. Ther Adv Med Oncol. 2025;17:1 –23.
122. Hoffmeyer K, Junghans D, Kanzler B, Kemler R. Trimethylation and Acetylation of β-Catenin at Lysine 49 Represent Key Elements in ESC Pluripotency. Cell Rep. 2017;18(12):2815–24.
123. Ghobashi AH, Vuong TT, Kimani JW, Ladaika CA, Hollenhorst PC, O'Hagan HM. Activation of AKT induces EZH2-mediated β-catenin trimethylation in colorectal cancer. iScience. 2023;26(9):107630.
124. Shi B, Liang J, Yang X, Wang Y, Zhao Y, Wu H, et al. Integration of Estrogen and Wnt Signaling Circuits by the Polycomb Group Protein EZH2 in Breast Cancer Cells. Mol Cell Biol. 2007;27(14):5105–19.
125. Jung H-Y, Jun S, Lee M, Kim H-C, Wang X, Ji H, et al. PAF and EZH2 Induce Wnt/β-Catenin Signaling Hyperactivation. Mol Cell 2013. 2013;52(2):193–205.
126. Zhao Y, Ding L, Wang D, Ye Z, He Y, Ma L, et al. EZH 2 cooperates with gain-of-function p53 mutants to promote cancer growth and metastasis. EMBO J. 2019;38(5):e99599.
127. Lee ST, Li Z, Wu Z, Aau M, Guan P, Karuturi RKM, et al. Context-Specific Regulation of NF-κB Target Gene Expression by EZH2 in Breast Cancers. Mol

Cell. 2011;43(5):798–810.
128. Dardis GJ, Wang J, Simon JM, Wang GG, Baldwin AS. An EZH2-NF-κB regulatory axis drives expression of pro-oncogenic gene signatures in triple negative breast cancer. iScience. 2023;26(7):107115.
129. Lawrence CL, Baldwin AS. Non-canonical EZH2 transcriptionally activates RelB in triple negative breast cancer. PLoS One. 2016;11(10):e0165005.
130. Gonzalez ME, Moore HM, Li X, Toy KA, Huang W, Sabel MS, et al. EZH2 expands breast stem cells through activation of NOTCH1 signaling. Proc Natl Acad Sci U S A. 2014;111(8):3098–103.
131. Zheng X, Pang B, Gu G, Gao T, Zhang R, Pang Q, et al. Melatonin inhibits glioblastoma stem-like cells through suppression of EZH2-NOTCH1 signaling axis. Int J Biol Sci. 2017;13(2):245–53.
132. Kim J, Lee Y, Lu X, Song B, Fong KW, Cao Q, et al. Polycomb- and Methylation-Independent Roles of EZH2 as a Transcription Activator. Cell Rep. 2018;25(10):2808-2820.e4.
133. Xu K, Wu ZJ, Groner AC, He HH, Cai C, Lis RT, et al. EZH2 Oncogenic Activity in Castration Resistant Prostate Cancer Cells is Polycomb-Independent. Science. 2012;338(6113):1465–1469.
134. Liu Q, Wang G, Li Q, Jiang W, Kim JS, Wang R, et al. Polycomb group proteins EZH2 and EED directly regulate androgen receptor in advanced prostate cancer. Int J Cancer. 2019;145(2):415–26.
135. Kim J, Lee Y, Lu X, Song B, Fong K-W, Cao Q, et al. Polycomb- and Methylation-Independent Roles of EZH2 as a Transcription Activator. cell r. 2018;25(10):2808–2820.
136. Yi Y, Li Y, Li C, Wu L, Zhao D, Li F, et al. Methylation-dependent and -independent roles of EZH2 synergize in CDCA8 activation in prostate cancer. Oncogene. 2022;41(11):1610–21.
137. Tabbal H, Septier A, Mathieu M, Drelon C, Rodriguez S, Djari C, et al. EZH2 cooperates with E2F1 to stimulate expression of genes involved in adrenocortical carcinoma aggressiveness. Br J Cancer. 2019;121(5):384–94.
138. Bracken AP, Pasini D, Capra M, Prosperini E, Colli E, Helin K. EZH2 is downstream of the pRB-E2F pathway, essential for proliferation and amplified in cancer. EMBO J. 2003;22(20):5323–35.
139. Mahara S, Lee PL, Feng M, Tergaonkar V, Chng WJ, Yu Q. HIFI-α activation

underlies a functional switch in the paradoxical role of Ezh2/PRC2 in breast cancer. Proc Natl Acad Sci U S A. 2016;113(26):E3735–44.
140. Chang C-J, Yang J-Y, Xia W, Chen C-T, Xie X, Chao C-H, et al. EZH2 promotes expansion of breast tumor initiating cells through activation of RAF1-β-catenin signaling. Int J Obes. 2011;19(1):86–100.
141. Yan J, Li B, Lin B, Lee PT, Chung TH, Tan J, et al. EZH2 phosphorylation by JAK3 mediates a switch to noncanonical function in natural killer/T-cell lymphoma. Blood. 2016;128(7):948–58.
142. Yu X, Wang J, Gong W, Ma A, Shen Y, Zhang C, et al. Dissecting and targeting noncanonical functions of EZH2 in multiple myeloma via an EZH2 degrader. Oncogene. 2023;42(13):994–1009.
143. Vanden Bempt M, Debackere K, Demeyer S, Van Thillo Q, Meeuws N, Prieto C, et al. Aberrant MYCN expression drives oncogenic hijacking of EZH2 as a transcriptional activator in peripheral T-cell lymphoma. Blood. 2022;140(23):2463–76.
144. Chatterjee SS, JuanF.Linares, Cid-Diaz T, Duran A, Khan MIK, Osrodek M, et al. Increased translation driven by non- canonical EZH2 creates a synthetic vulnerability in enzalutamide-resistant prostate cancer. Nat Commun. 2024;15(1):9755.
145. Tan J, Yang X, Zhuang L, Jiang X, Chen W, Puay LL, et al. Pharmacologic disruption of polycomb-repressive complex 2-mediated gene repression selectively induces apoptosis in cancer cells. Genes Dev. 2007;21(9):1050–63.
146. Kim KH, Roberts CWM. Targeting EZH2 in cancer. Nat Med. 2016;22(2):128–34.
147. McCabe MT, Ott HM, Ganji G, Korenchuk S, Thompson C, Van Aller GS, et al. EZH2 inhibition as a therapeutic strategy for lymphoma with EZH2-activating mutations. Nature. 2012;492(7427):108–12.
148. Knutson SK, Warholic NM, Wigle TJ, Klaus CR, Allain CJ, Raimondi A, et al. Durable tumor regression in genetically altered malignant rhabdoid tumors by inhibition of methyltransferase EZH2. PNAS. 2013;110(19):7922–7.
149. FDA approves tazemetostat for advanced epithelioid sarcoma [Internet]. U.S. Food & Drug Administration. 2020. Available from: https://www.fda.gov/drugs/resources-information-approved-drugs/fda-approves-tazemetostat-advanced-epithelioid-sarcoma

150. FDA granted accelerated approval to tazemetostat for follicular lymphoma [Internet]. U.S. Food & Drug Administration. 2020. Available from: https://www.fda.gov/drugs/fda-granted-accelerated-approval-tazemetostat-follicular-lymphoma#:~:text=On June 18%2C 2020%2C the,disease progression or unacceptable toxicity.
151. Keller P, Adams E, Wu R, Côté A, Arora S, Cantone N, et al. Comprehensive Target Engagement by the EZH2 Inhibitor Tulmimetostat Allows for Targeting of ARID1A Mutant ˆ t e. Cancer Res. 2024;84(15):2501–17.
152. Fan Z, Wang J, Liu D, Shen L, Fang M, Johnson P, et al. Safety and efficacy of HH2853, a novel EZH1/2 dual inhibitor, in patients with refractory solid tumours or non-Hodgkin lymphomas: a phase I study. eClinicalMedicine. 2025;86:103398.
153. Wang C, Qu L, Li S, Yin F, Ji L, Peng W, et al. Discovery of First-in-Class Dual PARP and EZH2 Inhibitors for Triple-Negative Breast Cancer with Wild-Type BRCA. J Med Chem. 2021;64(17):12630–50.
154. Chen MK. Efficacy of PARP inhibition combined with EZH2 inhibition depends on BRCA mutation status and microenvironment in breast cancer. FEBS J. 2021;288(9):2884–7.
155. Sharma S, Wang SA, Yang W Bin, Lin HY, Lai MJ, Chen HC, et al. First-in-Class Dual EZH2-HSP90 Inhibitor Eliciting Striking Antiglioblastoma Activity In Vitro and In Vivo. J Med Chem. 2024;67(4):2963–85.
156. Bao Q, Kumar A, Wu D, Zhou J. Targeting EED as a key PRC2 complex mediator toward novel epigenetic therapeutics. Drug Discov Today. 2024;29(6):103986.
157. Kong X, Chen L, Jiao L, Jiang X, Lian F, Lu J, et al. Astemizole arrests the proliferation of cancer cells by disrupting the EZH2-EED interaction of polycomb repressive complex 2. J Med Chem. 2014;57(22):9512–21.
158. Békés M, Langley DR, Crews CM. PROTAC targeted protein degraders: the past is prologue. Nat Rev Drug Discov. 2022;21(3):181–200.
159. Wang X, Cao W, Zhang J, Yan M, Xu Q, Wu X, et al. A covalently bound inhibitor triggers EZH 2 degradation through CHIP -mediated ubiquitination . EMBO J. 2017;36(9):1243–60.
160. Mei H, Wu H, Yang J, Zhou B, Wang A, Hu C, et al. Discovery of IHMT-337 as a potent irreversible EZH2 inhibitor targeting CDK4 transcription for

malignancies. Signal Transduct Target Ther. 2023;8(1):18.
161. Ma A, Stratikopoulos E, Park KS, Wei J, Martin TC, Yang X, et al. Discovery of a first-in-class EZH2 selective degrader. Nat Chem Biol. 2020;16(2):214–22.
162. Tu Y, Sun Y, Qiao S, Luo Y, Liu P, Jiang ZX, et al. Design, Synthesis, and Evaluation of VHL-Based EZH2 Degraders to Enhance Therapeutic Activity against Lymphoma. J Med Chem. 2021;64(14):10167–84.
163. Dale B, Anderson C, Park KS, Kaniskan HÜ, Ma A, Shen Y, et al. Targeting Triple-Negative Breast Cancer by a Novel Proteolysis Targeting Chimera Degrader of Enhancer of Zeste Homolog 2. ACS Pharmacol Transl Sci. 2022;5(7):491–507.
164. Velez J, Dale B, Park K-S, Kaniskan HÜ, Yu X, Jin J. Discovery of a novel, highly potent EZH2 PROTAC degrader for targeting non-canonical oncogenic functions of EZH2. Eur J Med Chem. 2024;267:116154.
165. Liu Z, Hu X, Wang Q, Wu X, Zhang Q, Wei W, et al. Design and Synthesis of EZH2-Based PROTACs to Degrade the PRC2 Complex for Targeting the Noncatalytic Activity of EZH2. J Med Chem. 2021;64(5):2829–48.
166. Wang C, Chen X, Liu X, Lu D, Li S, Qu L, et al. Discovery of precision targeting EZH2 degraders for triple-negative breast cancer. Eur J Med Chem. 2022;238:114462.
167. Cancer Stat Facts: Common Cancer Sites [Internet]. National Cancer Institute. 2025. Available from: https://seer.cancer.gov/statfacts/html/common.html
168. Siegel RL, Kratzer TB, Giaquinto AN, Sung H, Jemal A. Cancer statistics, 2025. CA Cancer J Clin. 2025;75(1):10–45.
169. Riggio AI, Varley KE, Welm AL. The lingering mysteries of metastatic recurrence in breast cancer. Br J Cancer. 2021;124(1):13–26.
170. Uramoto H, Tanaka F. Recurrence after surgery in patients with NSCLC. 2014;3(16):242–9.
171. Carvalho E, Canberk S, Schmitt F, Vale N. Molecular Subtypes and Mechanisms of Breast Cancer: Precision Medicine Approaches for Targeted Therapies. Cancers (Basel). 2025;17(7):1102.
172. Ashrafi A, Akter Z, Modareszadeh P, Modareszadeh P, Berisha E, Alemi PS, et al. Current Landscape of Therapeutic Resistance in Lung Cancer and Promising Strategies to Overcome Resistance. Cancers (Basel). 2022;14(19):4562.

173. Souza VGP, de Araújo RP, Santesso MR, Seneda AL, Minutentag IW, Felix TF, et al. Advances in the Molecular Landscape of Lung Cancer Brain Metastasis. Cancers (Basel). 2023;15(3):722.
174. Darlix A, Louvel G, Fraisse J, Jacot W, Brain E, Debled M, et al. Impact of breast cancer molecular subtypes on the incidence, kinetics and prognosis of central nervous system metastases in a large multicentre real-life cohort. Br J Cancer. 2019;121(12):991–1000.
175. Sperduto PW, Mesko S, Li J, Cagney D, Aizer A, Lin NU, et al. Survival in Patients with Brain Metastases: Summary Report on the Updated Diagnosis-Specific Graded Prognostic Assessment and Definition of the Eligibility Quotient. J Clin Oncol. 2020;38(32):3773–84.
176. Semenza GL. Molecular mechanisms mediating metastasis of hypoxic breast cancer cells. Trends Mol Med. 2012;18(9):534–43.
177. Xie J, Xiao Y, Zhu X yan, Ning Z yu, Xu H fan, Wu H min. Hypoxia regulates stemness of breast cancer MDA-MB-231 cells. Med Oncol. 2016;33(5):42.
178. Chen A, Sceneay J, Gödde N, Kinwel T, Ham S, Thompson EW, et al. Intermittent hypoxia induces a metastatic phenotype in breast cancer. Oncogene. 2018;37(31):4214–25.
179. Salem A, Asselin MC, Reymen B, Jackson A, Lambin P, West CML, et al. Targeting hypoxia to improve non–small cell lung cancer outcome. J Natl Cancer Inst. 2018;110(1):14–30.
180. Lin YJ, Shyu WC, Chang CW, Wang CC, Wu CP, Lee HT, et al. Tumor hypoxia regulates forkhead box C1 to promote lung cancer progression. Theranostics. 2017;7(5):1177–91.
181. Levallet J, Biojout T, Bazille C, Douyère M, Dubois F, Ferreira DL, et al. Hypoxia-induced activation of NDR2 underlies brain metastases from Non-Small Cell Lung Cancer. Cell Death Dis. 2023;14(12):823.
182. Cheng X. A Comprehensive Review of HER2 in Cancer Biology and Therapeutics. Genes (Basel). 2024;15(7):903.
183. Gutierrez C, Schiff R. HER2: Biology, detection, and clinical implications. Arch Pathol Lab Med. 2011;135(1):55–62.
184. Kast K, Link T, Friedrich K, Petzold A, Niedostatek A, Schoffer O, et al. Impact of breast cancer subtypes and patterns of metastasis on outcome. Breast Cancer Res Treat. 2015;150(3):621–9.

185. Gerratana L, Fanotto V, Bonotto M, Bolzonello S, Minisini AM, Fasola G, et al. Pattern of metastasis and outcome in patients with breast cancer. Clin Exp Metastasis. 2015;32(2):125–33.
186. Jin J, Gao Y, Zhang J, Wang L, Wang B, Cao J, et al. Incidence, pattern and prognosis of brain metastases in patients with metastatic triple negative breast cancer. BMC Cancer. 2018;18(1):446.
187. Vaupel P, Höckel M, Mayer A. Detection and characterization of tumor hypoxia using pO2 histography. Antioxidants Redox Signal. 2007;9(8):1221–35.
188. Semenza GL. The Hypoxic Tumor Microenvironment: A Driving Force for Breast Cancer Progression. Biochim Biophys Acta. 2016;1863(3):382–391.
189. Hu L, Zeng Y, Xin L, Yang J. SND1, a novel co-activator of HIF1α, promotes tumor initiation in PyMT-induced breast tumor. FEBS J. 2023;290(24):5759–72.
190. Shan L, Zhou X, Liu X, Wang Y, Su D, Hou Y, et al. FOXK2 Elicits Massive Transcription Repression and Suppresses the Hypoxic Response and Breast Cancer Carcinogenesis. Cancer Cell. 2016;30(5):708–22.
191. Huang Z, Tang Y, Zhang J, Huang J, Cheng R, Guo Y, et al. Hypoxia makes EZH2 inhibitor not easy—advances of crosstalk between HIF and EZH2. Life Metab. 2024;3(4):loae017.
192. Niu Y, Bao L, Chen Y, Wang C, Luo M, Zhang B, et al. HIF2-induced long noncoding RNA RAB11B-AS1 promotes hypoxia-mediated angiogenesis and breast cancer metastasis. Cancer Res. 2020;80(5):964–75.
193. Yao C, Weng J, Feng L, Zhang W, Xu Y, Zhang P, et al. SIPA1 Enhances Aerobic Glycolysis Through HIF-2α Pathway to Promote Breast Cancer Metastasis. Front Cell Dev Biol. 2022;9:779169.
194. Jarman EJ, Ward C, Turnbull AK, Martinez-Perez C, Meehan J, Xintaropoulou C, et al. HER2 regulates HIF-2α and drives an increased hypoxic response in breast cancer. Breast Cancer Res. 2019;21(1):10.
195. Wang R, Godet I, Yang Y, Salman S, Lu H, Lyu Y, et al. Hypoxia-inducible factor-dependent ADAM12 expression mediates breast cancer invasion and metastasis. Proc Natl Acad Sci U S A. 2021;118(19):e2020490118.
196. Yan Y, Liu F, Han L, Zhao L, Chen J, Olopade OI, et al. HIF-2α promotes conversion to a stem cell phenotype and induces chemoresistance in breast cancer cells by activating Wnt and Notch pathways. J Exp Clin Cancer Res. 2018;1(D):107–12.

197. Bai J, Chen W Bin, Zhang XY, Kang XN, Jin LJ, Zhang H, et al. HIF-2α regulates CD44 to promote cancer stem cell activation in triple-negative breast cancer via PI3K/AKT/mTOR signaling. World J Stem Cells. 2020;12(1):87–99.
198. Yan Y, He M, Zhao L, Wu H, Zhao Y, Han L, et al. A novel HIF-2α targeted inhibitor suppresses hypoxia-induced breast cancer stemness via SOD2-mtROS-PDI/GPR78-UPRER axis. Cell Death Differ. 2022;29(9):1769–89.
199. Ebeid SA, Abd El Moneim NA, El-Benhawy SA, Ramadan R, Ismail SE. Znhit1 and HIF-2α are correlated with cancer stem cell markers in breast cancer patients. Sci Rep. 2022;12(1):13918.
200. Smolarz B, Samulak D, Piekarska E, Romanowicz H. Lung Cancer — Epidemiology , Pathogenesis , Treatment and Molecular Aspect (Review of Literature). Int J Mol Sci. 2025;26(5):2049.
201. Leon C, Manley E, Neely AM, Castillo J, Ramos Correa M, Velarde DA, et al. Lack of racial and ethnic diversity in lung cancer cell lines contributes to lung cancer health disparities. Front Oncol. 2023;13:1187585.
202. Barzaman K, Karami J, Zarei Z, Hosseinzadeh, A, Kazemi M, Moradi-Kalbolandi, S, Safari E, Farahmand L. Breast cancer: Biology, biomarkers, and treatments. Int Immunopharmacol. 2020;84:106535.
203. Le QT, Chen E, Salim A, Cao H, Kong CS, Whyte R, et al. An evaluation of tumor oxygenation and gene expression in patients with early stage non-small cell lung cancers. Clin Cancer Res. 2006;12(5):1507–14.
204. Swinson DEB, O'Byrne KJ. Interactions between hypoxia and epidermal growth factor receptor in non-small-cell-lung cancer. Clin Lung Cancer. 2006;7(4):250–6.
205. Shi Y, Lin X, Wang J, Zhou Z, Chen S, Chen G. Advances of HIF-1α/glycolysis axis in non-small cell lung cancer (Review). Oncol Rep. 2024;51(4):55.
206. Wang J, Yang C, Xu H, Fan X, Jia L, Du Y, et al. The Interplay Between HIF-1α and EZH2 in Lung Cancer and Dual-Targeted Drug Therapy. Adv Sci. 2024;11(7):e2303904.
207. Zhao Y, Wang X xin, Wu W, Long H, Huang J, Wang Z, et al. EZH2 regulates PD-L1 expression via HIF-1α in non-small cell lung cancer cells. Biochem Biophys Res Commun. 2019;517(2):201–9.
208. Saggese P, Pandey A, Alcaraz M, Fung E, Hall A, Yanagawa J, et al. Glucose Deprivation Promotes Pseudohypoxia and Dedifferentiation in Lung

Adenocarcinoma. Cancer Res. 2024;84(2):305–27.
209. Wang WJ, Ouyang C, Yu B, Chen C, Xu XF, Ye XQ. Role of hypoxia-inducible factor-2α in lung cancer (Review). Oncol Rep. 2021;45(5):57.
210. You M, Fu M, Shen Z, Feng Y, Zhang L, Zhu X, et al. HIF2A mediates lineage transition to aggressive phenotype of cancer-associated fibroblasts in lung cancer brain metastasis. Oncoimmunology. 2024;13(1):2356942.
211. Kim WY, Perera S, Zhou B, Carretero J, Jen JY, Heathcote SA, et al. HIF2α cooperates with RAS to promote lung tumorigenesis in mice. J Clin Invest. 2009;119(8):2160–70.
212. Qi H, Wang S, Wu J, Yang S, Gray S, Ng CSH, et al. EGFR-AS1/HIF2A regulates the expression of FOXP3 to impact the cancer stemness of smoking-related non-small cell lung cancer. Ther Adv Med Oncol. 2019;11:1758835919855228.
213. Hong CF, Chen WY, Wu CW. Upregulation of Wnt signaling under hypoxia promotes lung cancer progression. Oncol Rep. 2017;38(3):1706–14.
214. Dong M, Fan XJ, Chen ZH, Wang TT, Li X, Chen J, et al. Aberrant expression of enhancer of zeste homologue 2, correlated with HIF-1α, refines relapse risk and predicts poor outcome for breast cancer. Oncol Rep. 2014;32(3):1101–7.
215. Zhou J, Lin Y, Kang X, Liu Z, Zou J, Xu F. Hypoxia-mediated promotion of glucose metabolism in non-small cell lung cancer correlates with activation of the EZH2/FBXL7/PFKFB4 axis. Cell Death Dis. 2023;14(5):326.
216. Su C, Zhang C, Tecle A, Fu X, He J, Song J, et al. Tudor staphylococcal nuclease (Tudor-SN), a novel regulator facilitating G1/S phase transition, acting as a co-activator of E2F-1 in cell cycle regulation. J Biol Chem. 2015;290(11):7208–20.
217. Moniz S, Bandarra D, Biddlestone J, Campbell KJ, Komander D, Bremm A, et al. Cezanne regulates E2F1-dependent HIF2α expression. J Cell Sci. 2015;128(15):3082–93.
218. Kristan A, Debeljak N, Kunej T. Integration and visualization of regulatory elements and variations of the epas1 gene in human. Genes (Basel). 2021;12(11):1793.
219. Das B, Pal B, Bhuyan R, Li H, Sarma A, Gayan S, et al. MYC regulates the HIF-2α stemness pathway via Nanog and Sox2 to maintain self-renewal in cancer stem cells versus non-stem cancer cells. Cancer Res.

2019;79(16):415–4025.
220. D'Ignazio L, Batie M, Rocha S. TNFSF14/LIGHT, a non-canonical NF-κB stimulus, induces the HIF pathway. Cells. 2018;7(8):102.
221. Hamidian A, Vaapil M, von Stedingk K, Fujita T, Persson CU, Eriksson P, et al. Promoter-associated proteins of EPAS1 identified by enChIP-MS – A putative role of HDX as a negative regulator. Biochem Biophys Res Commun. 2018;499(2):291–8.
222. Ho JJD, Metcalf JL, Yan MS, Turgeon PJ, Wang JJ, Chalsev M, et al. Functional importance of dicer protein in the adaptive cellular response to hypoxia. J Biol Chem [Internet]. 2012;287(34):29003–20. Available from: http://dx.doi.org/10.1074/jbc.M112.373365
223. Zhang H, Pu J, Qi T, Qi M, Yang C, Li S, et al. MicroRNA-145 inhibits the growth, invasion, metastasis and angiogenesis of neuroblastoma cells through targeting hypoxia-inducible factor 2 alpha. Oncogene. 2014;33(3):387–97.
224. Xu Z, Zhao L, Zhu LY, He M, Zheng L, Wu Y. MicroRNA-17, 20a Regulates the Proangiogenic Function of Tumor-Associated Macrophages via Targeting Hypoxia-Inducible Factor 2α. PLoS One. 2013;8(10):2–10.
225. Sanchez M, Galy B, Muckenthaler MU, Hentze MW. Iron-regulatory proteins limit hypoxia-inducible factor-2α expression in iron deficiency. Nat Struct Mol Biol. 2007;14(5):420–6.
226. Zimmer M, Ebert BL, Neil C, Brenner K, Papaioannou I, Melas A, et al. Small-Molecule Inhibitors of HIF-2a Translation Link Its 5′UTR Iron-Responsive Element to Oxygen Sensing. Mol Cell. 2008;32(6):838–48.
227. Zhu T, Wang Z, Wang G, Hu Z, Ding H, Li R, et al. Long non-coding RNA ZFAS1 promotes the expression of EPAS1 in gastric cardia adenocarcinoma. J Adv Res. 2021;28(1):7–15.
228. Nakayama K, Frew IJ, Hagensen M, Skals M, Habelhah H, Bhoumik A, et al. Siah2 Regulates Stability of Prolyl-Hydroxylases , Controls HIF1 ⎵ Abundance , and Modulates Physiological Responses to Hypoxia. 2004;117:941–52.
229. Xu Z, Wu Y, Yang M, Wei H, Pu J. CBX2-mediated suppression of SIAH2 triggers WNK1 accumulations to promote glycolysis in hepatocellular carcinoma. Exp Cell Res. 2023;426(1):113513.
230. Schito L, Semenza GL. Hypoxia-Inducible Factors: Master Regulators of Cancer Progression. Trends in Cancer. 2016;2(12):758–70.

231. Yu J, Cao Q, Mehra R, Laxman B, Yu J, Tomlins SA, et al. Integrative Genomics Analysis Reveals Silencing of β-Adrenergic Signaling by Polycomb in Prostate Cancer. Cancer Cell. 2007;12(5):419–31.
232. Brooun A, Gajiwala KS, Deng YL, Liu W, Bolaños B, Bingham P, et al. Polycomb repressive complex 2 structure with inhibitor reveals a mechanism of activation and drug resistance. Nat Commun. 2016;7:11384.
233. Margueron R, Li G, Sarma K, Blais A, Zavadil J, Woodcock CL, et al. Ezh1 and Ezh2 Maintain Repressive Chromatin through Different Mechanisms. Mol Cell. 2008;32(4):503–18.
234. Xu J, Shao Z, L D, Xie H, Kim W, Huang J, et al. Developmental control of Polycomb subunit composition by GATA factors mediates a switch to non-canonical functions. Mol Cell. 2015;57(2):304–316.
235. Kopan R, Ilagan MXG. The Canonical Notch Signaling Pathway: Unfolding the Activation Mechanism. Cell. 2009;137(2):216–33.
236. Mutvei AP, Landor SKJ, Fox R, Braune EB, Tsoi YL, Phoon YP, et al. Notch signaling promotes a HIF2α-driven hypoxic response in multiple tumor cell types. Oncogene. 2018;37(46):6083–95.
237. Dovey HF, John V, Anderson JP, Chen LZ, De Saint Andrieu P, Fang LY, et al. Functional gamma-secretase inhibitors reduce beta-amyloid peptide levels in brain. J Neurochem. 2001;76(1):173–81.
238. Jarriault S, Brou C, Logeat F, Schroeter Eh, Kopan R, Israel A. Signalling downstream of activated mammalian Notch. Nature. 1995;377(6547):355–8.
239. Zovoilis A, Cifuentes-Rojas C, Chu H-P, Hernandez AJ, Lee JT. Destabilization of B2 RNA by EZH2 activates the stress response. Cell. 2016;167(7):1788–1802.
240. Hennequin LF, Allen J, Breed J, Curwen J, Fennell M, Green TP, et al. N-(5-Chloro-1,3-benzodioxol-4-yl)-7-[2-(4-methylpiperazin-1-yl)ethoxy]-5-(tetrahydro-2H-pyran-4-yloxy)quinazolin-4-amine, a Novel, Highly Selective, Orally Available, Dual-Specific c-Src/Abl Kinase Inhibitor. J Med Chem. 2006;49:6465–88.
241. Hamburger AW, Salmon SE. Primary Bioassay of Human Tumor Stem Cells. Science. 1977;197:461–3.
242. Colburn NH, Bruegge WF, Bates JR, Gray RH, Rossen JD, Kelsey WH, et al. Correlation of anchorage-independent growth with tumorigenicity of chemically

transformed mouse epidermal cells. Cancer Res. 1978;38(3):624–34.
243. Uroz M, Stoddard AE, Sutherland BP, Courbot O, Oria R, Li L, et al. Differential stiffness between brain vasculature and parenchyma promotes metastatic infiltration through vessel co-option. Nat Cell Biol. 2024;26(12):2144–53.
244. Győrffy B. Survival analysis across the entire transcriptome identifies biomarkers with the highest prognostic power in breast cancer Balázs Gy o. Comput Struct Biotechnol J. 2021;19:4101–9.
245. Trompak O. The role of hypoxic signaling in evasive tumor resistance against anti-angiogenic therapy. Justus Liebig University Giessen; 2019.
246. Safran M, Kim WY, O'Connell F, Flippin L, Günzler V, Horner JW, et al. Mouse model for noninvasive imaging of HIF prolyl hydroxylase activity: Assessment of an oral agent that stimulates erythropoietin production. Proc Natl Acad Sci U S A. 2006;103(1):105–10.
247. Schröter I. Die Regulation des Hypoxie-Signalwegs durch Enhancer of Zeste Homolog 2 in Brust- , Gliom- und Lungenkrebszellen. Justus Liebig University; 2023.
248. Westermann L, Li Y, Göcmen B, Niedermoser M, Rhein K, Jahn J, et al. Wildtype heterogeneity contributes to clonal variability in genome edited cells. Sci Rep. 2022;12(1):18211.
249. Saxena K, Jolly MK. Acute vs. Chronic vs. cyclic hypoxia: Their differential dynamics, molecular mechanisms, and effects on tumor progression. Biomolecules. 2019;9(8):339.
250. Liu Q, Palmgren VAC, Danen EH, Le Dévédec SE. Acute vs. chronic vs. intermittent hypoxia in breast Cancer: a review on its application in in vitro research. Mol Biol Rep. 2022;49(11):10961–73.
251. Rao DD, Vorhies JS, Senzer N, Nemunaitis J. siRNA vs. shRNA: Similarities and differences. Adv Drug Deliv Rev. 2009;61(9):746–59.
252. Xue C, Greene EC. DNA repair pathway choices in CRISPR-Cas9 mediated genome editing. Trends Genet. 2021;37(7):639–56.
253. Uddin F, Rudin CM, Sen T. CRISPR Gene Therapy: Applications, Limitations, and Implications for the Future. Front Oncol. 2020;10:1387.
254. Gilbert LA, Horlbeck MA, Adamson B, Jacqueline E, Chen Y, Whitehead EH, et al. Genome-Scale CRISPR-Mediated Control of Gene Repression and Activation. Cell. 2014;159(3):647–61.

255. Wang Y, Zhai Y, Zhang M, Song C, Zhang Y, Zhang G. Escaping from CRISPR–Cas-mediated knockout: the facts, mechanisms, and applications. Cell Mol Biol Lett. 2024;29(1):48.
256. Henze A, T A. Feedback regulators of hypoxia-inducible factors and their role in cancer biology. Cell Cycle. 2010;9(14):2749–63.
257. Yu Y, Qi J, Xiong J, Jiang L, Cui D, He J, et al. Epigenetic co-deregulation of EZH2/TET1 is a senescence-countering, actionable vulnerability in triple-negative breast cancer. Theranostics. 2019;9(3):761–77.
258. Wang L, Zeng D, Wang Q, Liu L, Lu T, Gao Y. Screening and Identification of Novel Potential Biomarkers for Breast Cancer Brain Metastases. Front Oncol. 2022;11:784096.
259. Arafeh R, Shibue T, Dempster JM, Hahn WC, Vazquez F. The present and future of the Cancer Dependency Map. Nat Rev Cancer. 2025;25(1):59–73.
260. Q15910 · EZH2_HUMAN [Internet]. UniProt. 2025. Available from: https://www.uniprot.org/uniprotkb/Q15910/entry
261. Kim W, Bird GH, Neff T, Guo G, Kerenyi MA, Walensky LD, et al. Targeted disruption of the EZH2-EED complex inhibits EZH2-dependent cancer. Nat Chem Biol. 2013;9(10):643–50.
262. Grau D, Zhang Y, Lee CH, Valencia-Sánchez M, Zhang J, Wang M, et al. Structures of monomeric and dimeric PRC2:EZH1 reveal flexible modules involved in chromatin compaction. Nat Commun. 2021;12(1):714.
263. Calebiro D, Grassi ES, Eszlinger M, Ronchi CL, Godbole A, Bathon K, et al. Recurrent EZH1 mutations are a second hit in autonomous thyroid adenomas. J Clin Invest. 2016;126(9):3383–8.
264. Feng X, Wang AH, Juan AH, Ko KD, Jiang K, Ciuffoli V, et al. Polycomb Ezh1 maintains murine muscle stem cell quiescence through non-canonical regulation of Notch signaling. 2023;58(12):1052–70.
265. ChIP Analysis [Internet]. Thermo Fisher Scientific. 2025. Available from: https://www.thermofisher.com/de/de/home/life-science/epigenetics-noncoding-rna-research/chromatin-remodeling/chromatin-immunoprecipitation-chip/chip-analysis.html#:~:text=Here we discuss two common,and standard error when possible.
266. Mousavi K, Zare H, Wang AH, Sartorelli V. Polycomb Protein Ezh1 Promotes RNA Polymerase II Elongation. Mol Cell. 2012;45(2):255–62.

267. Bao B, Ali S, Banerjee S, Wang Z, Logna F, Azmi AS, et al. Curcumin analogue CDF inhibits pancreatic tumor growth by switching on suppressor microRNAs and attenuating EZH2 expression. Cancer Res. 2012;72(1):335–45.
268. Kwon H, Song K, Han C, Zhang J, Lu L, Chen W, et al. Epigenetic Silencing of miRNA-34a in Human Cholangiocarcinoma via EZH2 and DNA Methylation: Impact on Regulation of Notch Pathway. Am J Pathol. 2017;187(10):2288–99.
269. Zhao G, Deng Z, Li X, Wang H, Chen G, Feng M, et al. Targeting EZH2 regulates the biological characteristics of glioma stem cells via the Notch1 pathway. Exp Brain Res. 2023;241(10):2409–18.
270. Hu YY, Fu LA, Li SZ, Chen Y, Li JC, Han J, et al. Hif-1α and Hif-2α differentially regulate Notch signaling through competitive interaction with the intracellular domain of Notch receptors in glioma stem cells. Cancer Lett. 2014;349(1):67–76.
271. Bolognesi B, Lehner B. Reaching the limit. Elife. 2018;7:e39804.
272. Gordan JD, Bertout JA, Hu CJ, Diehl JA, Simon MC. HIF-2α Promotes Hypoxic Cell Proliferation by Enhancing c-Myc Transcriptional Activity. Cancer Cell. 2007;11(4):335–47.
273. Florczyk U, Czauderna S, Stachurska A, Tertil M, Nowak W, Kozakowska M, et al. Opposite effects of HIF-1α and HIF-2α on the regulation of IL-8 expression in endothelial cells. Free Radic Biol Med. 2011;51(10):1882–92.
274. Hoefflin R, Harlander S, Schäfer S, Metzger P, Kuo F, Schönenberger D, et al. HIF-1α and HIF-2α differently regulate tumour development and inflammation of clear cell renal cell carcinoma in mice. Nat Commun. 2020;11(1):4111.
275. Xue G, Yan HL, Zhang Y, Hao LQ, Zhu XT, Mei Q, et al. C-Myc-mediated repression of miR-15-16 in hypoxia is induced by increased HIF-2α and promotes tumor angiogenesis and metastasis by upregulating FGF2. Oncogene. 2015;34(11):1393–406.
276. Harlen KM, Churchman LS. The code and beyond: Transcription regulation by the RNA polymerase II carboxy-terminal domain. Nat Rev Mol Cell Biol. 2017;18(4):263–73.
277. Perez G, Barber GP, Benet-Pages A, Casper J, Clawson H, Diekhans M, et al. The UCSC Genome Browser database: 2025 update. Nucleic Acids Res. 2025;53(D1):D1243–9.

278. Chile T, Fortes MAHZ, Corrêa-Giannella MLC, Brentani HP, Maria DA, Puga RD, et al. HOXB7 mRNA is overexpressed in pancreatic ductal adenocarcinomas and its knockdown induces cell cycle arrest and apoptosis. BMC Cancer. 2013;13:451.
279. Roy B, Granas D, Bragg F, Cher JAY, White MA, Stormo GD. Autoregulation of yeast ribosomal proteins discovered by efficient search for feedback regulation. Commun Biol. 2020;3(1):761.
280. Kirmizis A, Bartley SM, Kuzmichev A, Margueron R, Reinberg D, Green R, et al. Silencing of human polycomb target genes is associated with methylation of histone H3 Lys 27. Genes Dev. 2004;18(13):1592–605.
281. Yan J, Ng SB, Tay JLS, Lin B, Koh TL, Tan J, et al. EZH2 overexpression in natural killer/T-cell lymphoma confers growth advantage independently of histone methyltransferase activity. Blood. 2013;121(22):4512–20.
282. Cao Q, Wang X, Zhao M, Yang R, Malik R, Qiao Y, et al. The central role of EED in the orchestration of polycomb group complexes. Nat Commun. 2014;5:3127.
283. Li Z, Li M, Wang D, Hou P, Chen X, Chu S, et al. Post-translational modifications of EZH2 in cancer. Cell Biosci. 2020;10(1):143.
284. Smith HW, Hirukawa A, Sanguin-Gendreau V, Nandi I, Dufour CR, Zuo D, et al. An ErbB2/c-Src axis links bioenergetics with PRC2 translation to drive epigenetic reprogramming and mammary tumorigenesis. Nat Commun. 2019;10(1):2901.
285. Hu C-J, Sataur A, Wang L, Chen H, Simon MC. The N-Terminal Transactivation Domain Confers Target Gene Specificity of Hypoxia-inducible Factors HIF-1α and HIF-2α. Mol Biol Cell. 2007;18:4528–4542.
286. Wehn PM, Rizzi JP, Dixon DD, Grina JA, Schlachter ST, Wang B, et al. Design and Activity of Specific Hypoxia-Inducible Factor-2α (HIF-2α) Inhibitors for the Treatment of Clear Cell Renal Cell Carcinoma: Discovery of Clinical Candidate (S)-3-((2,2-Difluoro-1-hydroxy-7-(methylsulfonyl)-2,3-dihydro-1 H-inden-4-yl)oxy)-5-fluor. J Med Chem. 2018;61(21):9691–721.
287. Wallace EM, Rizzi JP, Han G, Wehn PM, Cao Z, Du X, et al. A small-molecule antagonist of HIF2α is efficacious in preclinical models of renal cell carcinoma. Cancer Res. 2016;76(18):5491–500.
288. Arnaiz E, Miar A, Bridges E, Prasad N, Hatch SB, Ebner D, et al. Differential

effects of HIF2α antagonist and HIF2α silencing in renal cancer and sensitivity to repurposed drugs. BMC Cancer. 2021;21(1):896.

289. Covello KL, Kehler J, Yu H, Gordan JD, Arsham AM, Hu C, et al. HIF-2regulates Oct-4: effects of hypoxia on stem cell function, embryonic development, and tumor growth. Genes Dev. 2006;20(5):557–70.
290. Aprelikova O, Wood M, Tackett S, Chandramouli GVR, Barrett JC. Role of ETS transcription factors in the hypoxia-inducible factor-2 target gene selection. Cancer Res. 2006;66(11):5641–7.
291. Gonzalez ME, Li X, Toy K, Duprie M, Ventura AC, Banerjee M, et al. Down-regulation of Enhancer of Zeste-2 decreases growth of estrogen receptor negative invasive breast carcinoma and requires BRCA1. Oncogene. 2009;28(6):843–53.
292. Chen KC, Nicholson C. Changes in brain cell shape create residual extracellular space volume and explain tortuosity behavior during osmotic challenge. Proc Natl Acad Sci U S A. 2000;97(15):8306–11.
293. Spennati G, Horowitz LF, McGarry DJ, Rudzka DA, Armstrong G, Olson MF, et al. Organotypic platform for studying cancer cell metastasis. Exp Cell Res. 2021;401(2):112527.
294. Lehmann S, te Boekhorst V, Odenthal J, Bianchi R, van Helvert S, Ikenberg K, et al. Hypoxia Induces a HIF-1-Dependent Transition from Collective-to-Amoeboid Dissemination in Epithelial Cancer Cells. Curr Biol. 2017;27(3):392–400.
295. te Boekhorst V, Jiang L, Mähler M, Meerlo M, Dunkel G, Durst FC, et al. Calpain-2 regulates hypoxia/HIF-induced plasticity toward amoeboid cancer cell migration and metastasis. Curr Biol. 2022;32(2):412-427.e8.
296. Paňková K, Rösel D, Novotný M, Brábek J. The molecular mechanisms of transition between mesenchymal and amoeboid invasiveness in tumor cells. Cell Mol Life Sci. 2010;67(1):63–71.
297. Li Y, Zhang H, Merkher Y, Chen L, Liu N, Leonov S, et al. Recent advances in therapeutic strategies for triple-negative breast cancer. J Hematol Oncol. 2022;15(1):121.
298. Shin KJ, Wall EA, Zavzavadjian JR, Santat LA, Liu J, Hwang JI, et al. A single lentiviral vector platform for microRNA-based conditional RNA interference and coordinated transgene expression. Proc Natl Acad Sci U S A.

2006;103(37):13759–64.
299. Ye J, Coulouris G, Zaretskaya I, Cutcutache I, Rozen S, Madden TL. Primer-BLAST: a tool to design target-specific primers for polymerase chain reaction. BMC Bioinformatics. 2012;13:134.
300. Koressaar T, Remm M. Enhancements and modifications of primer design program Primer3. Bioinformatics. 2007;23(10):1289–91.
301. Untergasser A, Cutcutache I, Koressaar T, Ye J, Faircloth BC, Remm M, et al. Primer3-new capabilities and interfaces. Nucleic Acids Res. 2012;40(15):e115.
302. Kõressaar T, Lepamets M, Kaplinski L, Raime K, Andreson R, Remm M. Primer3-masker: Integrating masking of template sequence with primer design software. Bioinformatics. 2018;34(11):1937–8.
303. Guarani V, Deflorian G, Franco CA, Bentley K, Toussaint L, Dequiedt F, et al. Acetylation-dependent regulation of endothelial Notch signalling by the SIRT1 deacetylase. Nature. 2011;473(7346):234–8.
304. Schindelin J, Arganda-Carrera I, Frise E, Verena K, Mark L, Tobias P, et al. Fiji - an Open platform for biological image analysis. Nat Methods. 2012;9(7):676–82.
305. Pisal R V., Hrebíková H, Chvátalová J, Kunke D, Filip S, Mokrý J. Detection of mycoplasma contamination directly from culture supernatant using polymerase chain reaction. Folia Biol (Czech Republic). 2016;62(5):203–6.
306. Uphoff CC, Drexler HG. Comparative PCR analysis for detection of mycoplasma infections in continuous cell lines. Vitr Cell Dev Biol - Anim. 2002;38(2):79–85.
307. Lowry OH, Rosebrough NJ, Farr AL, Randall RJ. Protein measurement with the Folin phenol reagent. J Biol Chem. 1951;193(1):265–75.
308. Laemmli U. Cleavage of structural proteins during the assembly of the head of bacteriophage T4. Nature. 1970;227:680–5.
309. Walker J. Gradient SDS Polyacrylamide Gel Electrophoresis. Methods Mol Biol. 1984;1:57–61.

Acknowledgements

First of all, I would like to thank Prof. Dr. med. Till Acker and Prof. Dr. Attila Németh for giving me the opportunity to pursue my PhD at the Giessen Institute of Neuropathology and for their supervision. Special thanks to Prof. Dr. Attila Németh for the excellent and constant guidance, helpful discussions, and overall support.

I would also like to thank the colleagues who performed preliminary work for my thesis project: Isabel, Sabine, Sandra, and Sarah. In addition, I would like to thank Prof. Dr. Gergana Dobreva for her valuable advice on my thesis project, and Prof. Dr. Tilman Borggrefe for suggesting the exploration of the link between EZH2, Notch1 and HIF2α.

Furthermore, I am grateful to my previous and current colleagues for their help and feedback: Abdelrahman, Angelina, Annika, Aya, Carmen, Claudia, Declan, Julia, Lili, Moritz, Nuray, Sasha, Weam, Yasmine, and Zoe. Special thanks to Nadja, Nazli, and Sabine for their patience and kindness in training me.

Finally, I would like to thank my lab friends, my friends outside the lab, and my family for their continuous support.

Thank you! Bedankt! Vielen Dank!